The results of the calculations of the PARAMETER-SF experiments

2007

Contents

1 Introduction

The most serious accident at VVER NPP, as to its consequences, is the beyond design basis accident with loss of coolant. The initiating event is the primary leak with superimposing of additional failures, for instance, in case of complete failure of the emergency core cooling system active part, could result in the core drying, its melting, damage of the reactor vessel, release of hydrogen, radioactive fission products and corium into the containment. The main method of the analysis of severe accidents is the numerical simulation with the use of computer codes. Complexity and mutual relation of physical processes and phenomena, accompanying the accident process, including the stage of temperature rise and the stage of the core reflooding, require the comprehensive verification of the models. Besides, to take the justified solutions on accident management and bringing the reactor into safe state it is necessary to have a rather clear concept of the change in the core state in the course of accident and of possible methods of its cooling down. In this connection the special significant is taken for the studying of the initial stage of severe accident wherein a possibility of the overheated core cooling is investigated as a possible measure on managing the accident process. The detailed information on the behaviour of fuel rods under the reflooding conditions is necessary both at the stage of developing the Symptom-oriented Emergency Instructions, Manual on BDBA management, Manual on severe accident management, and verification of the procedures proposed. Obtaining of such information requires, in its turn, the detailed experimental study of the behaviour of fuel rod assemblies, including the ex-pile test facilities.

One of the specific features of VVER reactor plant is a possibility of the core reflooding from top and bottom in case of restoration of ECCS active part. Under "bottom" flooding the pressure chamber is filled first, and only after its filling the boiling starts. The core is cooled down with steam first and with water after wetting of fuel rods. Under "top" flooding the water enters the reactor collection chamber, then it is distributed through the core section, moves downwards cooling the core, therefore the core cooling under "top" flooding can be implemented somewhat earlier than under "bottom" flooding. Considering the core height it can be supposed that the core upper part will remain under the top flooding conditions for some time, the lower part – under bottom flooding conditions, the middle part – under the conditions of combined flooding (from top and bottom).

In this connection the experimental study of FA behaviour under the severe accident conditions, including the stage of the reflooding from top, bottom, from top and bottom simultaneously is of scientific interest.

Behaviour of the overheated assembly of PWR and VVER (test QUENCH-12) under bottom reflooding was studied in the experiments QUENCH and the corresponding data are widely used for verification of computer codes. However the conditions of the experiment of QUENCH program (bottom flooding) model the prototype reactor conditions only partially.

The PARAMETER-SF experiments performed recently in the test facility complex PARAMETER in FSUE SRI SIA "Luch" became the essential supplement to the verification base of computer codes. In the PARAMETER-SF1 experiment the behaviour of VVER-1000 assembly overheated to 2000ºC was studied for the first time under top flooding conditions. The obtained experimental data are indicative of formation of considerable amount of melt and considerable damage of fuel rods and structures surrounding the assembly (shroud, thermal insulation). In the other experiment PARAMETER-SF2 the efficiency of simultaneous top and bottom flooding of VVER-1000 assembly overheated to 1500ºC was studied. The rate of top and bottom flooding corresponded to the prototype (by water mass per fuel rod) under the LOCA conditions at VVER NPP.

In the present report the results of the pre-test calculations of the experiments PARAMETER-SF1, SF2, as well as of the post-test calculation of PARAMETER-SF1 are discussed. On the basis of the developed models the assessment on reliability and self-consistency of the PARAMETER-SF1 experimental results was made by different computer code.

2 Pre-test calculations of the PARAMETER-SF1 experiment

Experiments performed in Joule heated test facilities with flooding the assemblies overheated to high temperatures require the thorough preparation including the preliminary numerical modelling of the planned experiment. Such numerical analysis is required for evaluation of contribution of physical processes at different stages of the experiment. This allows to justify the experiment scenario and to establish the main requirements for the monitoring and measuring systems.

The experiment PARAMETER-SF1 included the following main stages:

- Preparatory stage for the assembly heating-up to temperature of 1200 °C in the hottest section;
- Annealing at temperature of 1200°C for peroxidising the assembly in the hottest section to the degree of oxidization of ~200 mμ (argon/steam flow rate– 2/3 g/s)
- Heating-up of the assembly to temperature of 1850°C (transient stage)
- The model assembly top flooding to complete cooling

The pre-test calculations have been performed using the computer codes SOCRAT/B1 (RATEG/SVECHA), PARAM-TG, RELAP5/MOD3.3, MELCOR, ICARE/CATHAR, ATHLET-CD. The analytical support was made by the following organizations:

- SOCRAT – IBRAE RAS
- PARAM-TG – FSUE SRI SIA "Luch"
- RELAP5/MOD3.3 – FSUE OKB "Gidropress", RRC KI
- MELCOR – FSUE OKB "Gidropress"
- ICARE/CATHARE V1 – RRC KI
- MAAP4.04d4 – EdF [1]
- ATHLET – GRS [2].

Below the main characteristics of computer codes used for pre-test calculations, their nodalizations for simulation of the experiments with 19-rod assembly at the facility PARAMETER, as well as the results of numerical analysis of the experiment PARAMETER-SF1 (hereinafter referred to as SF1) are presented.

2.1 Brief characteristics of the computer codes

2.1.1 The RATEG/SVECHA computer code

Computer code RATEG/SVECHA is the best estimate code intended, in the first turn, for detailed numerical simulation of physical processes and phenomena at the in-vessel stage of beyond design basis accidents at VVER NPPs. In addition to the main purpose the code can be applied for simulation of the operating and accident conditions of operation of other nuclear power facilities and for simulation of other complicated thermohydraulic systems, experimental facilities, test benches, etc.

The developed code allows simulating a wide spectrum of physical-and-chemical phenomena and processes. This spectrum of phenomena and processes includes various thermohydraulic processes, as well as the processes of oxidation, hydrogen generation, damage of the core and internals structural components and other processes essential for realistic description of core heating-up and change in geometry. The displacement of materials within the core together with their displacement from the core into the lower mixing chamber are treated as well.

The computer code RATEG/SVECHA consists of two large program modules, and namely:

- computer code RATEG [3], [4] − simulation of the full-circuit two-liquid thermohydraulics;
- computer code SVECHA [5], [6] − simulation of physical processes in reactor structural components in the case of the core damage in the severe accidents.

The structure of code includes the following basic modules:

- control module,
- module of preparing the input data;

– module of operation with the archive of calculations and sections;
– module of thermohydraulics;
– module SVECHA;
– 2D (1D) heat conduction;
– radiative heat transfer;
– equations of state and thermophysical properties;
– control and monitoring system;
– check of accuracy and choice of time step;
– data output.

2.1.2 The PARAM-TG computer code

PARAM-TG computer code has been developed since the beginning of tests of the model assemblies in the test facility PARAMETER, simulating the accidents of LB LOCA type for predicting the electric energy supply mode to achieve the target temperature of the model fuel rods at the assigned rate , as well as for maintaining the temperature at a definite level. The code PARAM-TG was verified against all tests performed in the test facility PARAMETER with 37-rod, 19-rod and one-rod assemblies.

The gas flow and temperature field in the test section of the test facility PARAMETER are calculated by thermohydraulic code PARAM-TG. Test section is schematically represented as a system of separate cylindrical bodies divided by paths (channels) wherein the coolant flow (water, steam, gas mixtures). In the code the system of equations of heat conduction is solved for solid bodies and the equations of hydraulics and heat transfer is solved for liquids. The temperature field in the test section is described using unsteady two-dimensional assumption, flow of liquids in paths – using unsteady one-dimensional assumption.

The code consists of five interrelated blocks:
– the block of input data preparation;
– the main block of thermohydraulics;
– the additional block of thermohydraulics;
– the block of calculation of angular coefficients;
– the block of output of results.

In the block of input data preparation the whole structure of the test section is considered: fuel rods, thermocouples, insulation with the shroud, tests section body, spacing grids. The bodies in the plane normal to test section axis are assigned by their limiting curves, and along the length – by their reference to the longitudinal coordinate. The following types of curves are used: straight line, circumference and hexahedron. Each curve is described by the number of the curve type and the three characterizing digits. The surrounding components of the test facility and the room can be modelled also to consider the heat losses from test section surface. All the structure components are assigned without regard for the symmetry, i.e. consideration of random deviations of each structure component is possible.

The cross section is devided into separate channels by physical boundaries or fictitious lines. Coupling between neighbour paths in radial direction is described by isobaric assumption approach. The radiative heat transfer is considered in each section.

2.1.3 The RELAP5/MOD3.3 computer code

The calculations were performed using the computer code RELAP5/MOD3.3 [7], that is based on two-liquid model of two-phase flow described by six conservation equations for steam and liquid phases. Additional equations are used for considering the presence of noncondensable gas and boron solution. Numerical scheme used in the code is based on partial-implicit approximation of the conservation equations. Multidimensionality of actual flow can be considered at the expense of application of the so-called cross junctions. The code allows to calculate various accident situations at

NPP including the situations related to reflooding: from the bottom, from the top and combined flooding.

2.1.4 The MELCOR computer code

Computer code MELCOR [8] is widely used for the analysis of severe accidents at NPP with light water reactors, including VVER, at all stages of accident scenario.

Computer code MELCOR represents a set of mechanistic and parametric models describing different phenomena in the course of sever accident both in the reactor plant, and in the containment. The subroutines of the code MELCOR, referred to one structural component or to one type of phenomena, are combined into packages. In case of necessity the desired package is called at each calculation iteration.

A brief description of the most important characteristics of the specific features of the computer code MELCOR, related to the simulation of the experiments in the test facility PARAMETER is presented below.

The computer code MELCOR has a flexible topology that allows developing practically any nodalization of the facility simulated. The basis of this is the idea of "–control volume" – the elementary calculated volume. From the set of test volumes the real structure is modelled. Up to 999 control volumes is allowed. Each control volume may contain a gas (atmosphere) and liquid parts being, in general case in non-equilibrium state between themselves (different temperature of the parts). The atmosphere is multi-component (steam, moisture droplets, noncondensable gases, aerosols), the liquid part is one-component (water and steam bubbles). Some portion (in the course of the calculation can vary) of the test volume is inaccessible for hydrodynamics and is allocated to heat structures (up to 99999 heat structures – heat sources and sinks – is allowed), the core structures (sources and sinks of energy, mass and volume), etc. according to the applied package (HS, COR, BUR, CAV, FD, RN, etc.). A great contribution into the flexibility of nodalization is made also by the idea of "flow path") – the hydrodynamic junction between test volumes and the length of the coolant flow path. Up to 999 hydrodynamic junctions is allowed. Using of various flow models and the dependence of parameters on time or any other parameter (conditional hydrodynamic junction) allows to simulate practically any equipment of the reactor plant and containment including the systems of normal operation and safety systems.

The core is represented by the calculated volumes obtained by its meshing along the height (99 layers maximum) and radius (9 rings maximum). The core calculated volumes shall be considerably smaller than the test volumes simulating the core and the space under it. Inside each calculated volume of the core the detailed description is given for the fuel, fuel rod cladding, material of CPS control rods (B_4C also is allowed), the structural material. The energy of fission products radioactive decay is considered as well as zirconium and steel oxidation, convective and radiactive heat transfer and axial heat conduction. The presence of noncondensable gases, aerosols and gaseous fission products is considered. The clear opening blockage is considered as a result of fuel rod leakiness and their subsequent melting and relocation of the core materials. The options of the model of fuel rod cladding oxidization and of the damage criteria for the core, core barrel and reactor vessel bottom are provided.

2.1.5 The MAAP4.04d4 computer code

The MAAP4.04d4 code has been developed for reactor calculations but verification and validation need more versatility so as take some peculiarities of experiments: surrounding structure with imposed boundary conditions, experimental specific geometry, etc .

An electrical heater rod model is used for this out-of-pile test facility. The electric heater model computes the local heat release in the heated zone as well as in the electrodes zones (molybdenum and copper). The resistance of each node is calculated at each time step as a function of the fuel pellet temperature, the cross section, the height and the number of rods of each row. Resistivities are those recommended in the specification document for ISP-45 (with T in Kelvin).

$\rho tungsten\ (\Omega \cdot mm^2 \cdot m^{-1}) = -2{,}610 \cdot 10^{-2} + 2{,}630 \cdot 10^{-4} \cdot T + 2{,}200 \cdot 10^{-8} \cdot T^2$

ρ copper ($\Omega \cdot mm^2 \cdot m^{-1}$)= $-7{,}890 \cdot 10^{-3} + 9{,}900 \cdot 10^{-5} \cdot T - 5{,}490 \cdot 10^{-8} \cdot T^2 + 3{,}160 \cdot 10^{-11} \cdot T^3$

ρ molybdenum ($\Omega \cdot mm^2 \cdot m^{-1}$)= $-2{,}290 \cdot 10^{-2} + 5{,}360 \cdot 10^{-5} \cdot T - 1{,}380 \cdot 10^{-7} \cdot T^2 - 2{,}220 \cdot 10^{-11} \cdot T^3$

Along its whole height, the core region is surrounded by a cylinder which is called core barrel in MAAP4.04d4. To model the PARAMETER facility, the core barrel is supposed to be made of ZrO2 using the same mass of ZrO2 insulation as in the experiment. Axial heat conduction through the core barrel is considered. But the insulation geometry has to be interpreted as regards as heat transfers. In MAAP4.04d4, the thickness of the core barrel is supposed to be small compared to its radius. As a consequence, the inside surface is supposed to be approximately the same as the outside surface, so that in terms of conductive heat transfers, the core barrel behaves as a plane wall. For PARAMETER, the equivalent area used for conductive heat transfer calculations trough the wall is an average value of the inner and outer area.

Modeling of Zr1%Nb shroud liner: шn MAAP4.04d4, the oxidation of the shroud is not possible when the shroud is located in the core barrel. To take into account the shroud oxidation, the mass shroud is redistributed in the most outer radial ring from axial elevation -300 mm to 1447 mm. This way, the whole shroud mass can potentially contribute to the oxidation process.

2.1.6. The ICARE/CATHARE V1 computer code

Computer code ICARE/CATHARE V1 [9], developed in IRSN Institute (France), is the code of the best estimate for simulation of transient and accident processes at NPP with light water reactors, including the conditions with severe core damage. Both parts of the code, ICARE2 and CATHARE2, were developed separately during last decades both for the detailed analysis of the wide spectrum of high-temperature phenomena in the core (ICARE2), and for realistic calculations of thermohydraulics of all reactor components (CATHARE2). The recent broadened verification of ICARE/CATHARE V1 (2002 – 2004) in rather large number of integral experiments and scenarios of severe accident showed the applicability and high predictive capability of the code, in particular to VVER reactors and experimental facilities, considering the VVER specific features.

The architecture of computer code ICARE2 is of clearly expressed modular structure with the orientation of the base modules towards description of separate physical phenomena occurring with "components" – the analogs of the core physical objects. The base modules of the code ICARE2 are the module of thermohydraulics, the module describing heat transfer, the module describing power, the module of mechanical behaviour, the module of chemical interactions, the module of relocation of melted materials, the module of fission products release.

For numerical analysis of the experiment SF1 the following code models were used: two-phase model for description of thermohydraulics, the model of water cooling, the models of convection, heat conduction, radiant heat conduction, the model of electric heating, the model of thermal expansion, the model of fuel rod cladding behaviour, the model of oxidization of cladding and jacket of Zr, the model of fuel-clad interaction.

Selection of the given models from a number of alternative models is explained by the experience of their successful verification in the experiments performed at the facilities PHEBUS (France), CORA and QUENCH (Germany), CODEX (Hungary).

2.1.7. The ATHLET-CD computer code

The system code ATHLET-CD is developed by the GRS in cooperation with the Institut fur Kernenergetik und Energiesysteme (IKE) of the University at Stuttgart. The code can be used for investigations of beyond design basis accidents like core heat-up with core melting including the release of fission products as well as their transport and deposition at structures. ATHLET-CD is validated by analyzing single effects, integral experiments and accident sequences in nuclear power plants. This includes for example analytical investigations of experiments in several facilities such as CORA, QUENCH, PHEBUS, or PBF. In the frame of investigations for accident management measures for light water reactors like the German KONVOI - type reactor ATHLET-CD was also used for beyond design basis accident calculations with core damage.

The development of the different models results from the requirements according to the simulation of the processes in a nuclear power plant. The main parts of the code are combined in five modules: thermo-hydraulic of the cooling system (ATHLET), fuel behavior during heat up and

degradation (ECORE), formation of a molten pool (MESOCO), release of fission products (FIPREM), transport and deposition of fission products and aerosols (SOPHAEROS) which is developed in cooperation with the IRSN.

The thermo-fluid-dynamics can be analyzed in two ways. First possible way is using a 5-equation system which is based on the conservation of mass and energy separately for water and gas (vapor and up to 5 non-condensable gases) together with one momentum equation for the two phase mixture and a drift-flux model to calculate the relative flow velocity between the liquid and gas phase. The second possibility is to use a | 6-equation system with separated balance equations for the two phases.

For the description of the movement of the coolant level within the bundle a special model allows determining the proceeding of the swell as well as the collapsed level.

The model describing the fuel and absorber elements allows investigating the mechanical behavior like ballooning and failure of the cladding. Furthermore, the oxidation of the cladding during the heat up phase together with the resulting hydrogen generation and the escalation of the temperature caused by this exothermic reaction are also modeled. The processes leading to the melting of core material are analytically treated, too as well as the relocation of the molten material which includes the possible forming of blockages.

At the present stage it is not possible to calculate the melting of other structures within the reactor vessel as, e. g., spacer grids or the core shroud. But if the material of these other structures is made of Zircaloy oxidation reactions can be taken into account, too.

Besides the convective heat transfer energy can also be exchanged by thermal radiation. This is taken into account between fuel rods and surrounding structures as well as from structure to structure.

All phenomena are modeled with respect to their feed-back to the system.

The modules MESOCO, FIPREM and SOPHAEROS have not been used for the analyses of this experiment SF1.

2.2 Description of the test section nodalizations in the codes applied

2.2.1 Description of the test section nodalization for the code RATEG/SVECHA

Nodalization (Fig. 2.1) for numerical analysis of the experiments, performed at the test facility PARAMETER, is based on the assembly design.

The FA hydraulic channel can be divided into three parts:

- the lower part of the hydraulic channel (the simulated length is 167 mm from the level of coolant inlet to the elevation of 0 mm);
- the central part of the hydraulic channel (the assembly heated part, the simulated length is 1275 mm);
- the upper part of the hydraulic channel (at the level of the upper molybdenum lead, the simulated length is 400 mm).

Heights of hydraulic volumes are indicated in Table 2.1.

Table 2.1 Heights of hydraulic volumes in nodalization scheme for the code RATEG/SVECHA

Name of hydraulic volume	Height, mm
Bundle_m1	72
Bundle_m2	95
Bundle_ 1 ÷ Bundle_ 15	80
Bundle_ 16	75
Bundle_ 17	113
Bundle_ 18a	45
Bundle_ 18b	42
Bundle_ 19, Bundle_ 20	100

The FAis simulated by four thermal elements:

HEAT_1 - central rod,

HEAT_2 - 6 heated simulators of fuel rods of the internal row,
HEAT_3 -12 heated simulators of fuel rods of the external row,
SHROUD – assembly shroud and surrounding structures.

The scheme of the shroud and surrounding structures is presented in Fig. 2.2.

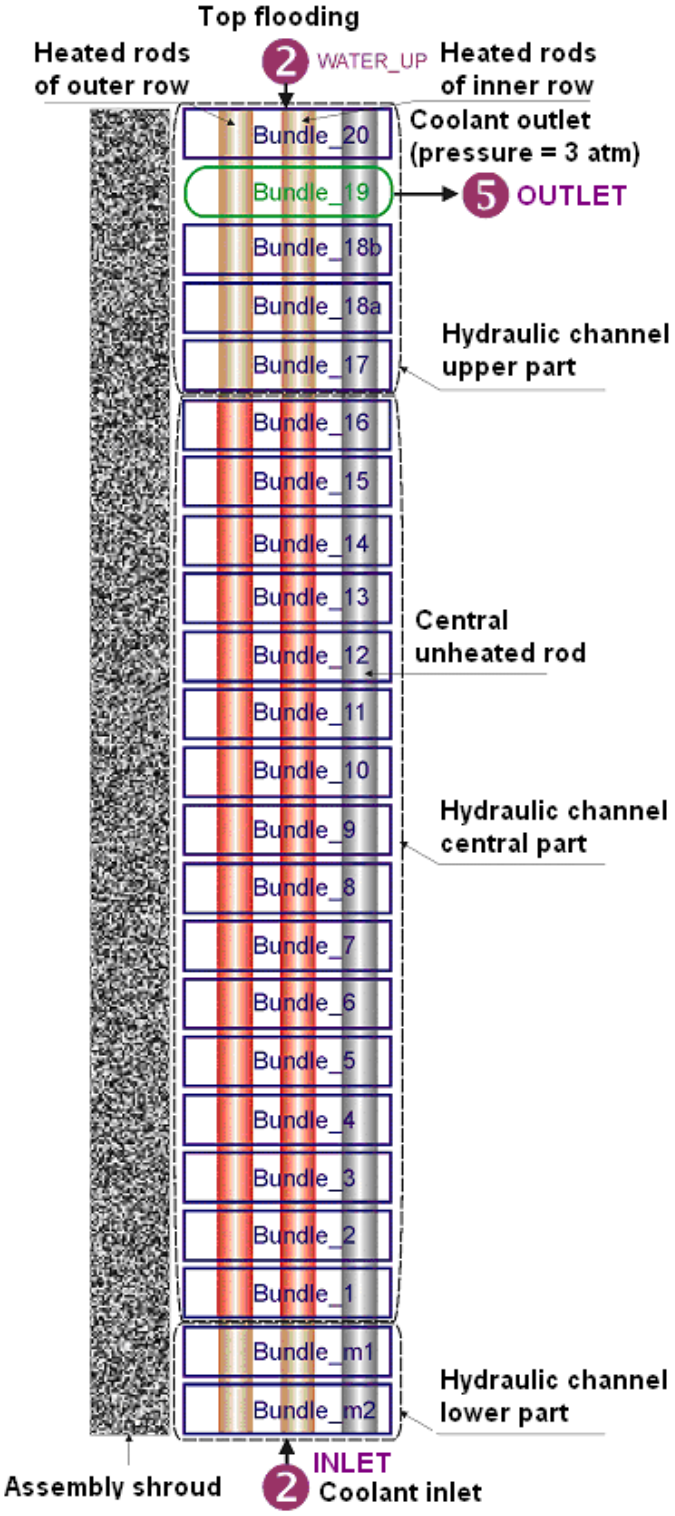

Figure 2.1 Nodalization of the test section PARAMETER for the code RATEG/SVECHA

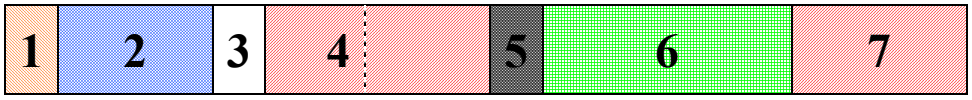

1 - shroud (zirconium);
2 - heat insulation;
3 - gap;
4 - heat insulation shroud and steel body;
5 - water cooling jacket (steel tubes coiled on body);
6 - insulation;
7 - steel shroud

Figure 2.2 Schematic view of the assembly shroud and surrounding structures

2.2.2 Description of the test section nodalization for the code PARAM-TG

The version of the test section nodalization for the numerical analysis of the experiment SF1 is shown in Fig. 2.3

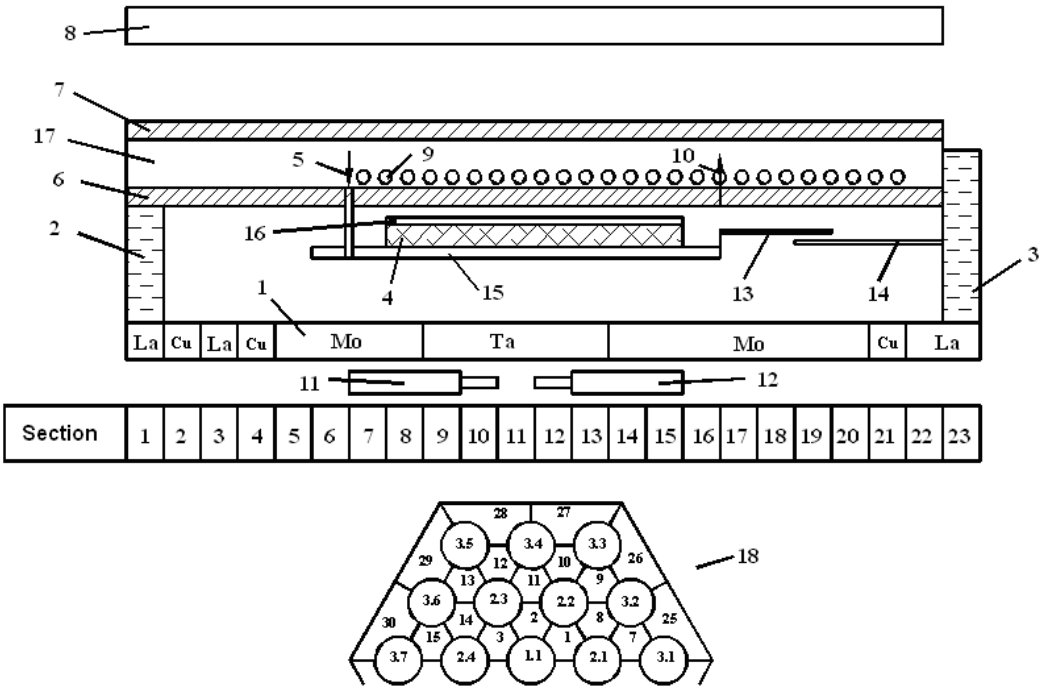

Figure 2.3 Nodalization of the PARAMETER test facility for the code PARAM-TG

1 – fuel rod heater, 2, 3 – bottom and top water, 4 – model assembly thermal insulation, 5 – steam and argon inlet section, 6 – steel body of test section, 7 – steel shroud of the test section, 8- room walls, 9 – tubes of cooling jacket, 10 – steam and argon outlet section, 11, 12 – lower and upper thermocouples, 13 – collecting cylinder, 14 –guide tube, 15 – shroud, 16 – thermal insulation shroud, 17 – outside thermal insulation, 18 – assembly cross-section (without thermal insulation) without thermocouples.

In the nodalization presented in Fig. 2.3 the test section is divided into 23 section with different geometry and composition of materials. The bottom view ~~if~~ is presented for the cross-section. A half of cross-section is given. In section 11 in which thermocouples are absent the cross-section ~~if~~ is divided into 36 paths: 24 paths are formed with three adjacent fuel rods, and 12 peripheral ones– with two fuel rods and the shroud.

The test section is devided into 23 section along the length, with different geometry and composition of materials. Their description is given in Table 2.2. The sections are defined by typical features: materials of heaters, structural elements, etc.

Table 2.2 Structure of nodalization along the length

No. and description of a section	Section length, and total, mm	Number of nodes along the length: of the section and total
1. Bottom water, brass lead	230	5
2. Copper cable, stagnant argon	150; 380	3; 8
3 Brass lead, stagnant argon	132; 512	2; 11
4. Copper, stagnant argon	20; 532	1; 12
5. Molybdenum lead, stagnant argon	48; 580	1; 13
6. Molybdenum lead, shroud without insulation, stagnant argon	85; 645	2; 15
7. Molybdenum lead, shroud without insulation, main flow, lower thermocouples	65; 730	2; 17
8. Molybdenum lead, insulation, lower thermocouples	102; 832	2; 19
9 Tantalum heater, insulation, lower thermocouples (core beginning)	394; 1226	8; 27
10. Tantalum heater, insulation, tacking of lower thermocouples	6; 1232	1; 18
11. Tantalum heater, insulation, without thermocouples	600; 1832	12; 40
12. Tantalum heater, insulation, tacking of upper thermocouples	6; 1838	1; 41
13. Tantalum heater, insulation, upper thermocouples, band No.2	269; 2107	6; 47
14. Molybdenum lead, insulation, upper thermocouples, band No.2	113; 2200	3; 50
15. Molybdenum lead, insulation, upper thermocouples, band No.2, steam outlet tube	15; 2235	1; 51
16. Molybdenum lead, shroud without insulation, steam outlet tube	30; 2265	1; 52
17. Molybdenum lead, Zr1%Nb cylinder	30; 2295	1; 53
18. Molybdenum lead, Zr1%Nb cylinder, band No.1	12; 2307	1; 54
19. Molybdenum lead, Zr1%Nb cylinder, jacket, band No.1	158; 2465	3; 57
20. Molybdenum lead, jacket, band No.1	42; 2507	1; 58
21. Copper sleeve, jacket, band No.1	20; 2527	1; 59
22. Brass lead, jacket	260; 2787	6; 65
23. Brass lead, tank with water	325; 3112	6; 71

2.2.3 Description of the test section nodalization for the code RELAP5/MOD3.3

Nodalization of the facility is presented in Fig. 2.4. It includes two channels of “PIPE” type that simulate the flow path of the assembly: one channel - for a part of the assembly with the groups of the inner rows of simulators (10), another channel - for that part of the assembly that contains the outer row of simulators and contacts the body (8).

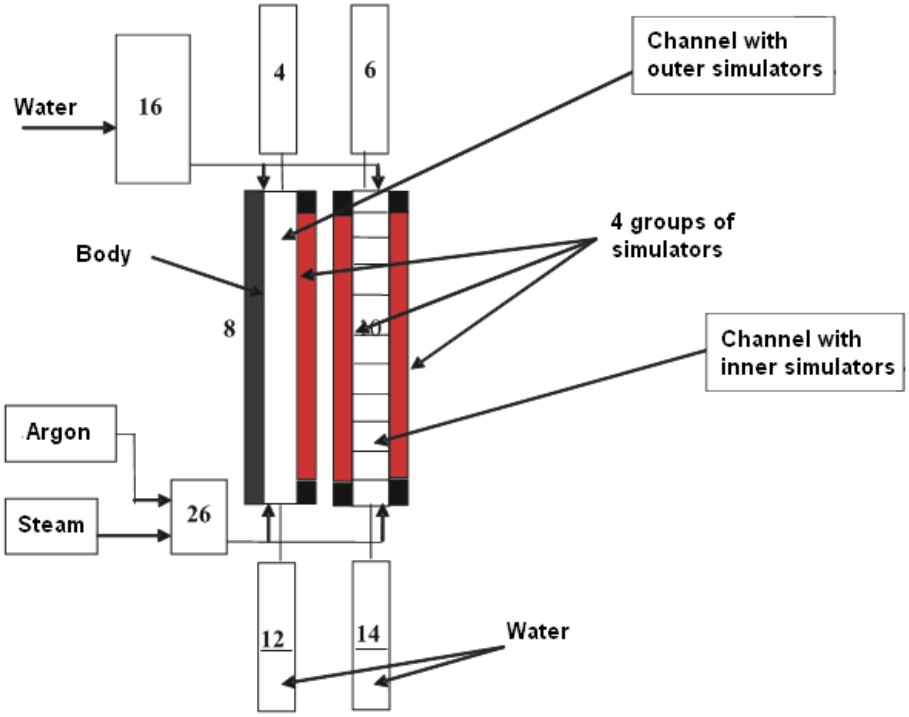

Figure 2.4 Nodalization of the test facility PARAMETER for the code RELAP5

Elements 4,6,12 and 14 of "PIPE" type simulate a space above and under the assembly, with this, the water is available in the lower part of elements 12 and 14. Through the elements of "BRANCH" 26 type the steam or argon enters the assembly from elements of "TMDPVOL" and "TMDPJUN" type, wherein the parameters and flow rates of steam and gas are assigned. Through the element of "BRANCH" 16 type the water from elements of "TMDPVOL" and "TMDPJUN" type, wherein the parameters and flow rates of cooling water are assigned, enters the assembly – elements 8 and 10. Elements 10 and 12 were broken down into 12 sections along the length. Each of 12 subelements were connected between themselves with the so-called "crossflow" – the nodes accounting for the cross overflows between these subelements. Similar breakdown was made for heat structures modelling the simulators. With this, the upper and lower subelement were non-heated. The rest of them had the uniform axial power profile. According to the breakdown into three groups with equal number of simulators, the total power, supplied to the section, was divided into three equal parts. Modelling of the simulator was made by two methods: exact reproduction of all simulator layers, including gas plenums, or as a fuel rod with the same geometrical dimensions as the simulator, but with the only three layers over radius – UO_2 , the gas plenum and zirconium cladding. The last method was used for considering the steam-zirconium reaction because with other modelling of the simulator it is impossible to consider this process with the use of RELAP5/MOD3.3 code. The performed calculations showed that the stage of heating-up for the model test using these two methods of modelling of the simulator gives similar results. The inner non-heated simulator was modelled as well. On the outer boundary of the vessel the constant temperature, equal to 300 K, was assigned, or the heat transfer coefficient typical for the process of convective heat transfer with air.

In modelling the process of heating-up and flooding the process of radiation and change in electric resistance of tantalum heater from temperature were not considered as well as power in the upper and lower leads.

2.2.4 Description of the nodalization for the code MELCOR

Nodalization of the test facility PARAMETER for the code MELCOR is shown in Fig. 2.5.
The FA hydraulic channel if represented with the system of control volumes (package CVH):

- CV001 – FA inlet section;
- CV002, CV004, CV006, CV008, CV010 – FA heated section;
- CV012 – FA outlet section.

Hydraulic relations between the test volumes are governed by the capabilities of package FL and designated in the figure as FL001, FL002, FL004, etc.

FA fuel rod simulators are modelled with the means of package COR as usual fuel rods. In the axial direction the assembly is divided into 15 layers, and in radial direction two rings are picked out.

- COR101 – COR115 – 6 fuel rods of the inner row and the central channel;
- COR201 – COR215 – 12 fuel rods of the outer row.

Thermal insulation is modelled with the capabilities of package HS, totally 15 heat elements. Each of the heat elements presents a ring divided in radial direction into 10 layers with indication of boundaries and material. Thermal-physical properties of materials are applied in the form of tabular dependences on temperature. The inner surface of thermal insulation is within the control volumes of FA hydraulic channel. The outer surface of thermal insulation has the boundary with water volume at constant temperature of 300 K.

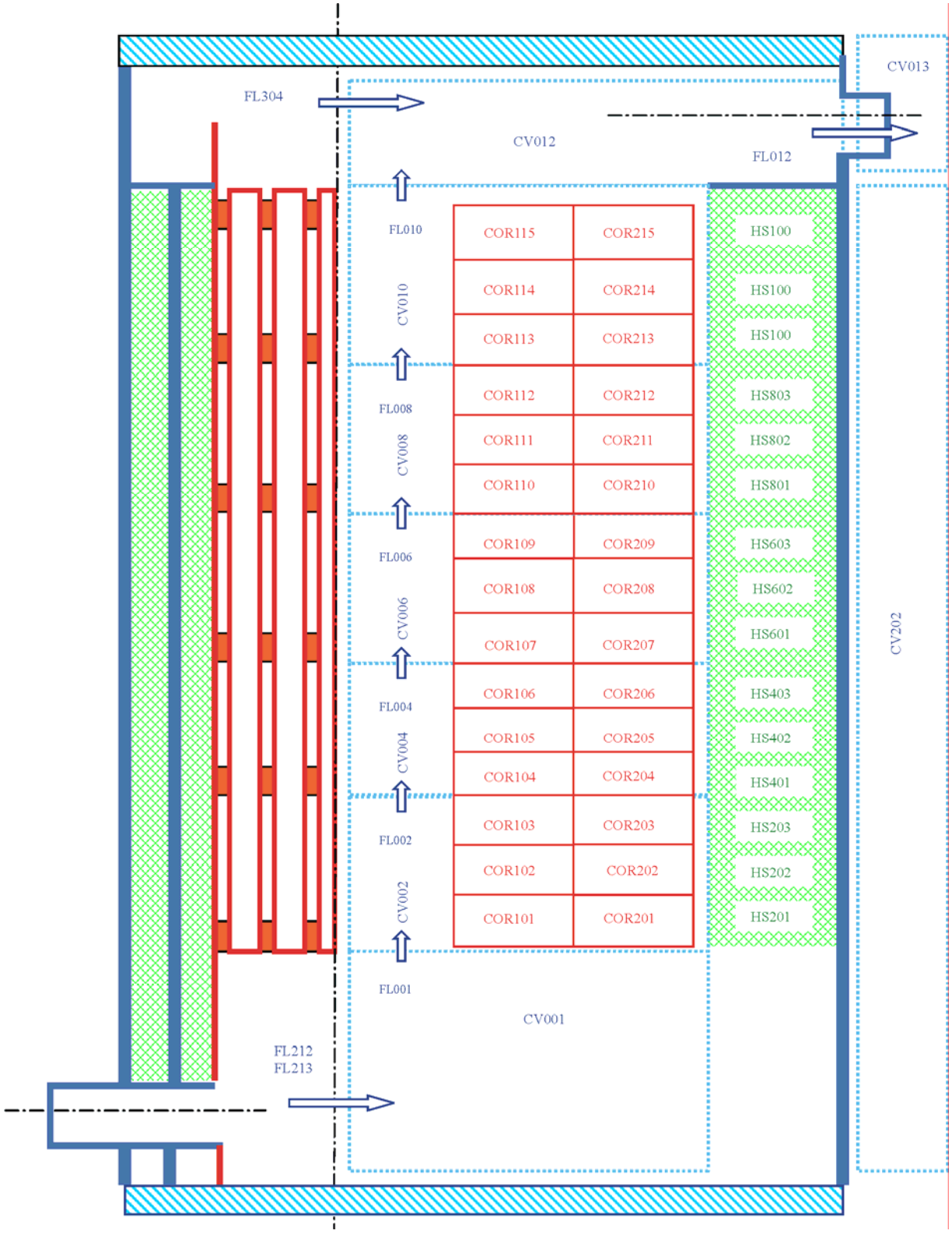

Figure 2.5 Nodalization of the test facility PARAMETER for the code MELCOR

As the boundary conditions the flow rates of steam and argon at the inlet to volume CV001 are applied. The values of flow rates and temperature of gases, supplied to the assembly, are defined as a functions of time for hydraulic bonds FL212, FL213. As the boundary condition at the FA outlet the boundary volume CV013 is applied with a constant pressure of 0,1 MPa.

The assembly flooding with water is initiated after the value of 2000ºC (2273 K) is exceeded for the maximum temperature of fuel rod cladding. The mass flow rate of the supplied water is 40 g/s. Water at temperature of 300 K is supplied to volume CV012 by the hydraulic junction FL304.

2.2.5 Description of the nodalization for the code MAAP4.04d4

In MAAP4.04d4, the core zone is modeled in two dimensions and the nodalization is symmetrical compared to the center of the bundle, and is divided in coaxial rings (Fig. 2.6, right). That's why the nodalization is composed of 3 channels and 58 rows. The first channel in pink on Fig. 2.6 contains the five central fuel rods represented on Fig. 2.6 on the left, the second channel in green contains the eight fuel rods represented in the green zone on Fig. 2.6, and the third channel in gray contains the six fuel rods in the gray zone and the shroud. The five upper rows and the five lower rows are unheated nodes. The forty eight central rows represent the heated zone of the PARAMETER test facility. All these 48 rows are equidistant.

The bundle zone which corresponds in MAAP4.04d4 to the core region is modeled from elevation - 460 mm to 1761 mm (Fig. 2.7, left).The heater section plus the molybdenum and copper electrodes zones are modeled. In MAAP4.04d4, the nodes which represent the active core are equidistant. Above and below the active core, ten nodes allow to model the non-active parts of the rods. The inactive nodes represent the molybdenum and copper electrode zones above and below the heated region. The nodalization of the bundle is detailed on Fig. 2.7 on the right.

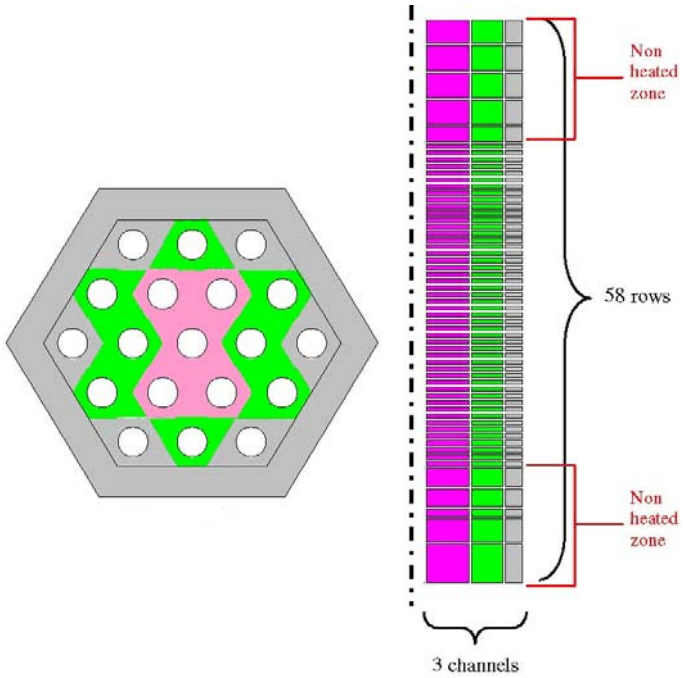

Figure 2.6 Radial nodalization of the test facility PARAMETER for the code MAAP4.04d4

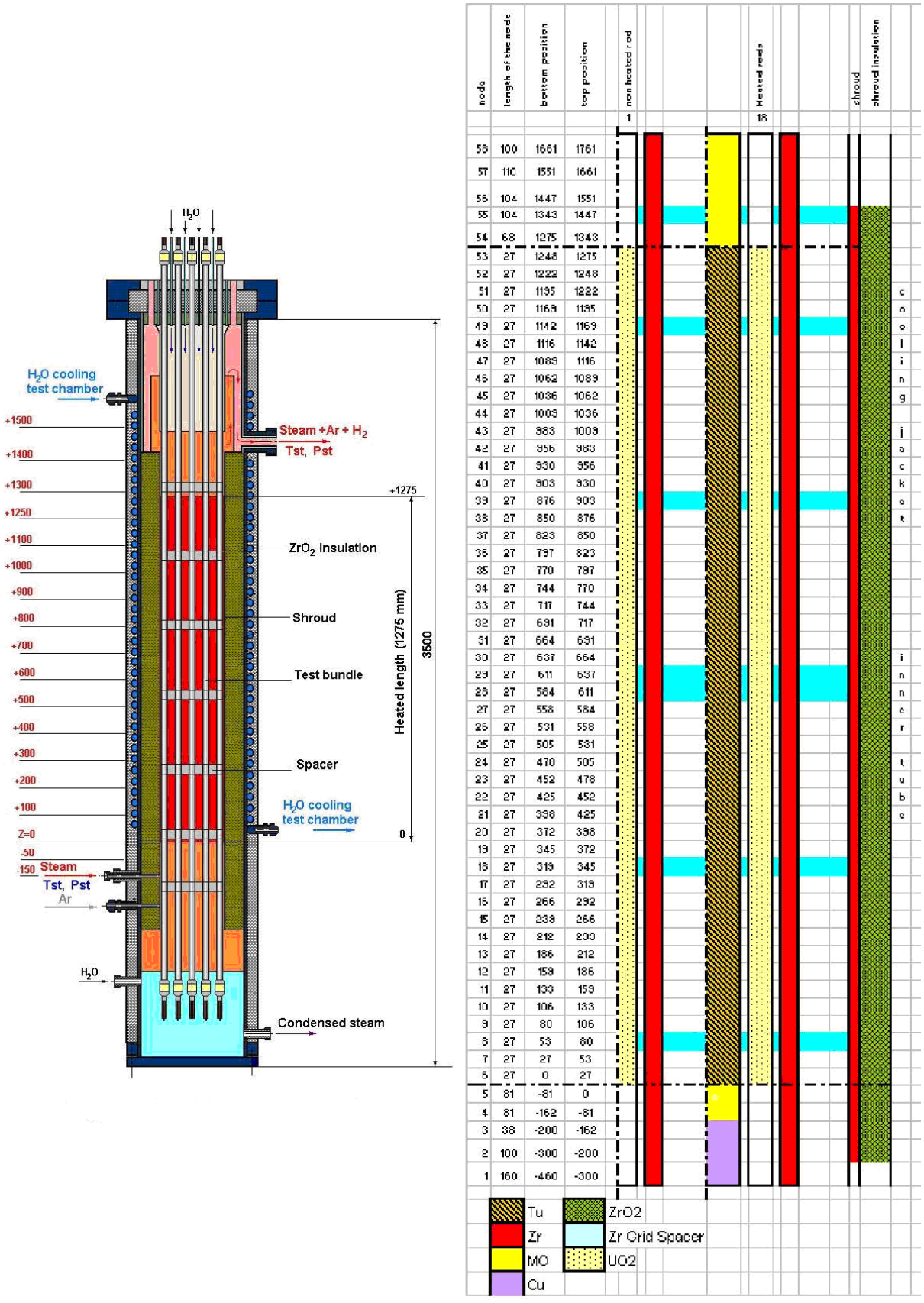

Figure 2.7 Axial nodalization of the test facility PARAMETER for the code MAAP4.04d4

2.2.6 Description of the nodalization for the code ICARE/CATHARE V1

For modelling in the code ICARE/CATHARE V1 the detailed nodalization is applied with reference of separate physical FA elements to the geometry of nodalization with radial and vertical meshes. In Figs. 2.8, 2.9 the nodalization scheme is shown for the test section.

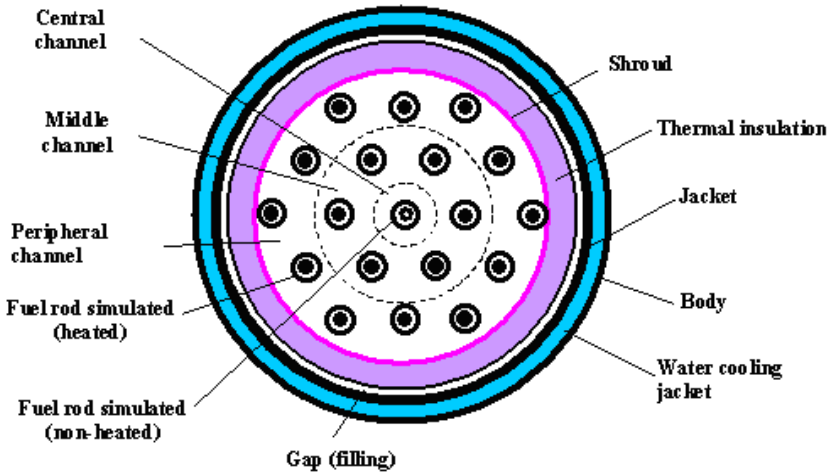

Figure 2.8 Scheme of FA model arrangement in radial section

Figure 2.8. shows the radial nodalization of FA hydraulic channel of the test facility PARAMETER into three parts (meshes) including the central fuel rod simulator, six middle fuel rod simulators and 12 outer fuel rod simulators, respectively. With this, among the outer simulators two groups of six fuel rod simulators each with different distance to the center are considered for detailed description of radiative heat transfer.

The shroud and thermal insulation in the model (Fig. 2.8) are represented by the cylindrical rings instead of actual hexahedrons that is caused by capabilities of the code ICARE2). The heat transfer by heat conduction is treated in all radial concentric structures including water cooling jacket. The model of radiative heat transfer is used for the gap.

As shown in Fig. 2.9, in the vertical direction the FA hydraulic channel of the test facility PARAMETER is divided into 28 meshes and has three characteristic parts:

- lower part – below the heated zone;
- central part including the heated zone;
- upper part – above the heated zone.

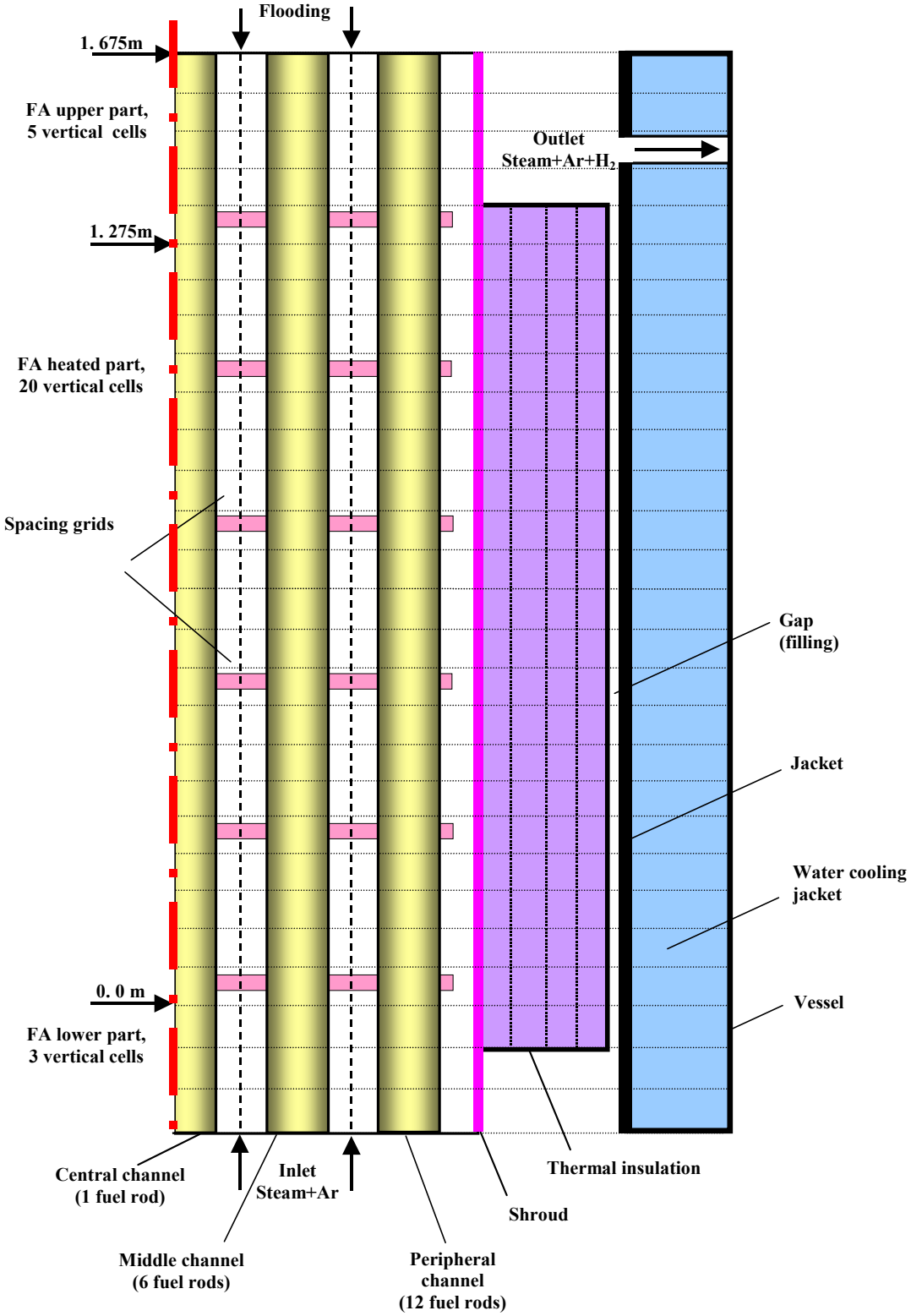

Figure 2.9 Scheme of the model FA arrangement in vertical section for the code ICARE

In modelling the nodalization is used with small axial mesh (to 6 cm in the heated zone). Expirience of quench experiments modelling by ICARE/CATHARE V1 code shows that such meshing provides satisfactory accuracy of the flooding front motion modelling.

2.2.7 Description of the test section nodalization for the code ATHLET-CD

The nodalization scheme is shown in Fig 2.10. The flow path area was radial divided into three concentric flow channels containing the fuel rod simulators: CORE1 includes the unheated rod ROD1, CORE2 six heated rods represented by ROD2 and CORE3 the remaining twelve heated rods represented by ROD3. The areas of the three sections are related to each other in the following way: 0.045, 0.270 and 0.685. The flow channels were axially subdivided into nineteen zones. The lowest

two and the uppermost three zones represent the unheated parts of the rods (plugs and electrodes), the other zones the heated part of the fuel rods. The three channels were radial cross connected at each level. The outer channel CORE3 was surrounded by heat structures from the bottom to the top: H-LPWALL, SHRLP, SHROUD, H-UPWALL. The lower three heat structures were modeled with three materials as given in the specification: 1.) a thin Zr-layer on the inner side to the flow area CORE3, 2.) a thick insulation of ZrO_2 and 3.) a tube on the outer side to the cooling jacket made of stainless steel. Each of these materials was divided into several layers (3, 7, 3). Argon and steam enter the three channels through the INPIPE and leave the test section together with the generated hydrogen through the OUTPIPE. Flooding from the top is modeled by the injection of H_2O through TOPH2OINJ only into the second channel CORE2. The OUTPIPE is connected only to the channel CORE3. In this way it is avoided that there exists a direct connection between the injected cold water and the outlet of the test section. The insulation of INPIPE and OUTPIPE is modeled with heat structures H-INPIPE and H-OUTPIPE, respectively. The grid spacers (material Zr-1%Nb) are also modeled (GRID1…GRID6). The pressure boundary condition of the test section is simulated with the time dependent object PHCOROUT. The test section is cooled from the outside where cooling water flows from the top (JACKETIN) to the bottom (JACKETOUT) through the JACKETTUBE. These pipes are also insulated to the environment with heat structures (H-…).
The steam / Zircaloy reaction is considered in this problem for the outside of the cladding, the inner side of the structures around channel CORE3 and the grids.

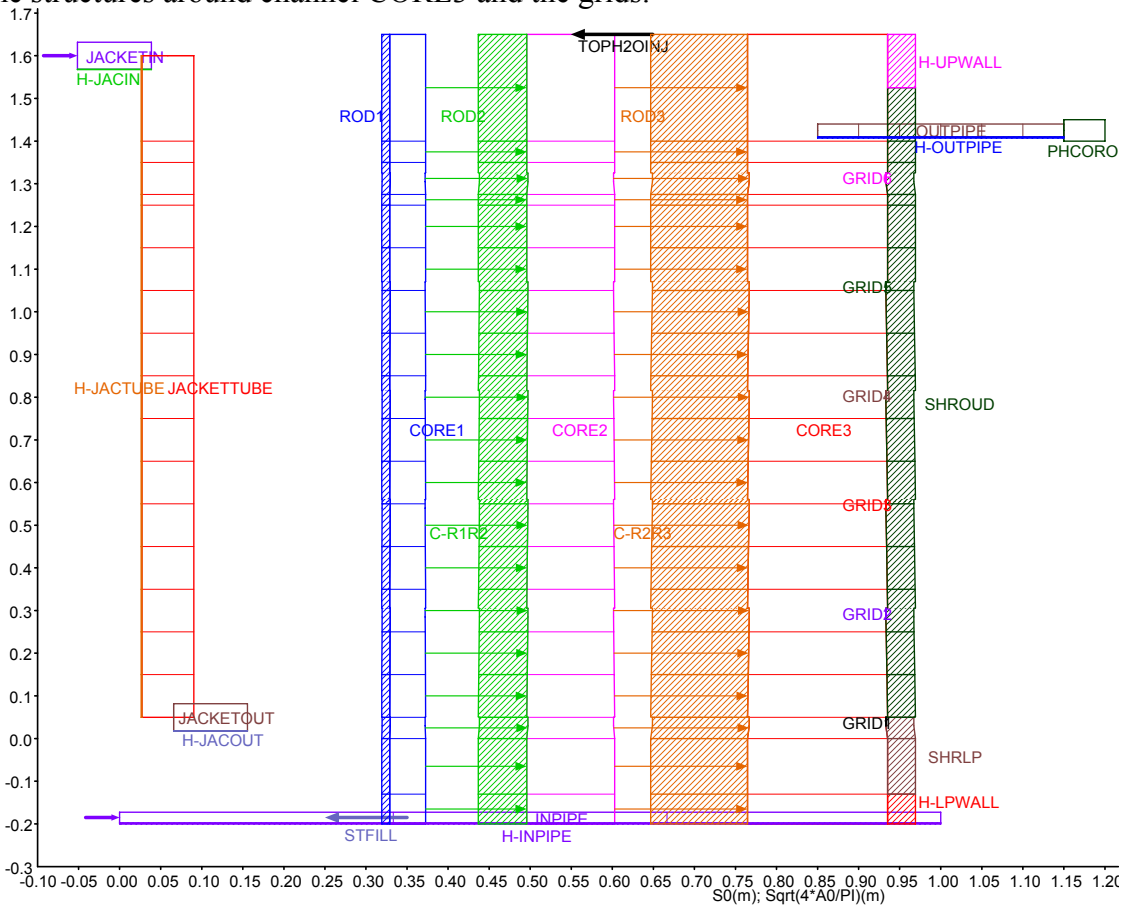

Figure 2.10 Nodalization of the test section for the code ATHLET-CD

2.2.8. Experiment scenario

The main stages of the SF1experiment scenario are presented in Table 2.3. During all stages of the experiment, except for the flooding stage, the pressure inside the test section is equal to 0.3 MPa.

Table 2.3 Assumed scenario of the SF1experiment

No.	Stage	Main parameters			
		FA temperature,^{o}C	Environment	Heating rate	Time, s
1	FA heating within argon flow	20 - 100	Argon with flow rate of 2 g/s and temperature ut to 160 ^{o}C	-	0-500
2	Joule heating of the bundle in the flow of steam-argon mixture	100-500	Steam/argon with flow rates of 3/2 g/s	0.1-0.3 K/s	500-1600
3	Stabilization of the main parameters	~ 500	Steam/argon with flow rates of 3/2 g/s	-	1600-2500
4	FA heating to 1200^{o}C	500-1200	Steam/argon with flow rates of 3/2 g/s	~0.25 K/s	2500-5000
5	FA pre-oxidation	~ 1200	Steam/argon with flow rates of 3/2 g/s	-	5000-9000
6	Assembly heating to maximum temperature (transient phase)	1200-1850	Steam/argon with flow rates of 3/2 g/s		Determined experimentally as the assembly reached the required temperature
7	Top flooding of the assembly (in 10 s after the assembly reached T_{FA}max=1850^{O}C)	Till bundle cooling	Water flow rate of 40 g/s per assembly		~300 (duration)

2.3 Results of pre-test numerical analysis of the PARAMETER-SF1 experiment

2.3.1 Results of pre-test calculations of the PARAMETER-SF1 experiment at the heating stage

For the analysis of the effect of the processes on the assembly behaviour, as well as for specifying the electric power mode according to the experiment scenario the pre-test numerical analyses have been performed for the PARAMETER-SF1 using various computer codes.

Initial and boundary conditions, used by the users of codes, are presented in Figs. 2.11-2.15.

In Figs. 2.16-2.19 the calculated data of cooling (heating) capacity of the assembly with steam-gas mixture, of radial heat loss (per unit time) into insulation; of heat release due to steam-zirconium reaction are presented. These processes together with the Joule heating govern the assembly temperature behaviour. The coolant temperature behaviour at different elevations (0, 600, 1000, 1250 mm) is presented in Figs. 2.20-2.23. In Figs. 2.24 – 2.34 we can see the temperature behaviour of claddings of fuel rods of the 2nd row at elevations 200, 600, 1000, 1100 mm) and of claddings of fuel rods of the 3rd row at elevations 0, 200, 700, 1000, 1250, 1300, 1400 mm. In Figs. 2.35-2.39 the

calculated data on the shroud temperature at elevations 200, 700, 900, 1100, 1300 mm are given. On the whole, the codes predict close values of maximum temperatures of fuel rod claddings at the preheating, pre-oxidation and transient phases. The numerical analysis by various computer codes shows that the maximum temperatures in the assembly will be reached at the elevations of 1250-1350 mm. Oxide scale thicknesses , predicted by the codes for the claddings of fuel rods of 2nd row at elevations 200, 600, 1000, 1200, 1300 mm are presented in Figs. 2.40 - 2.44. Difference in thickness is caused by difference in calculated values of temperatures and different oxidation models applied in the codes. The total hydrogen release is shown in Fig.2.45.

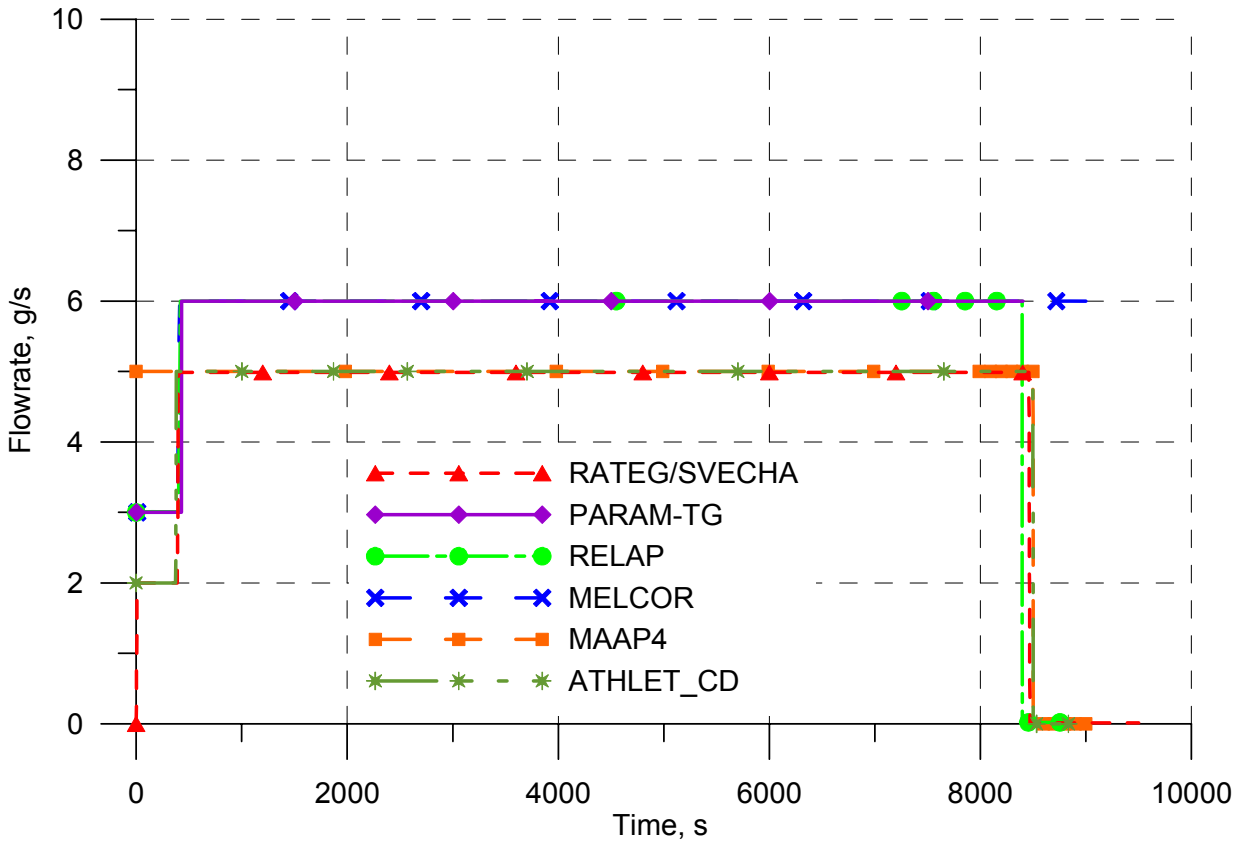

Figure 2.11 Coolant flow rate at the assembly inlet

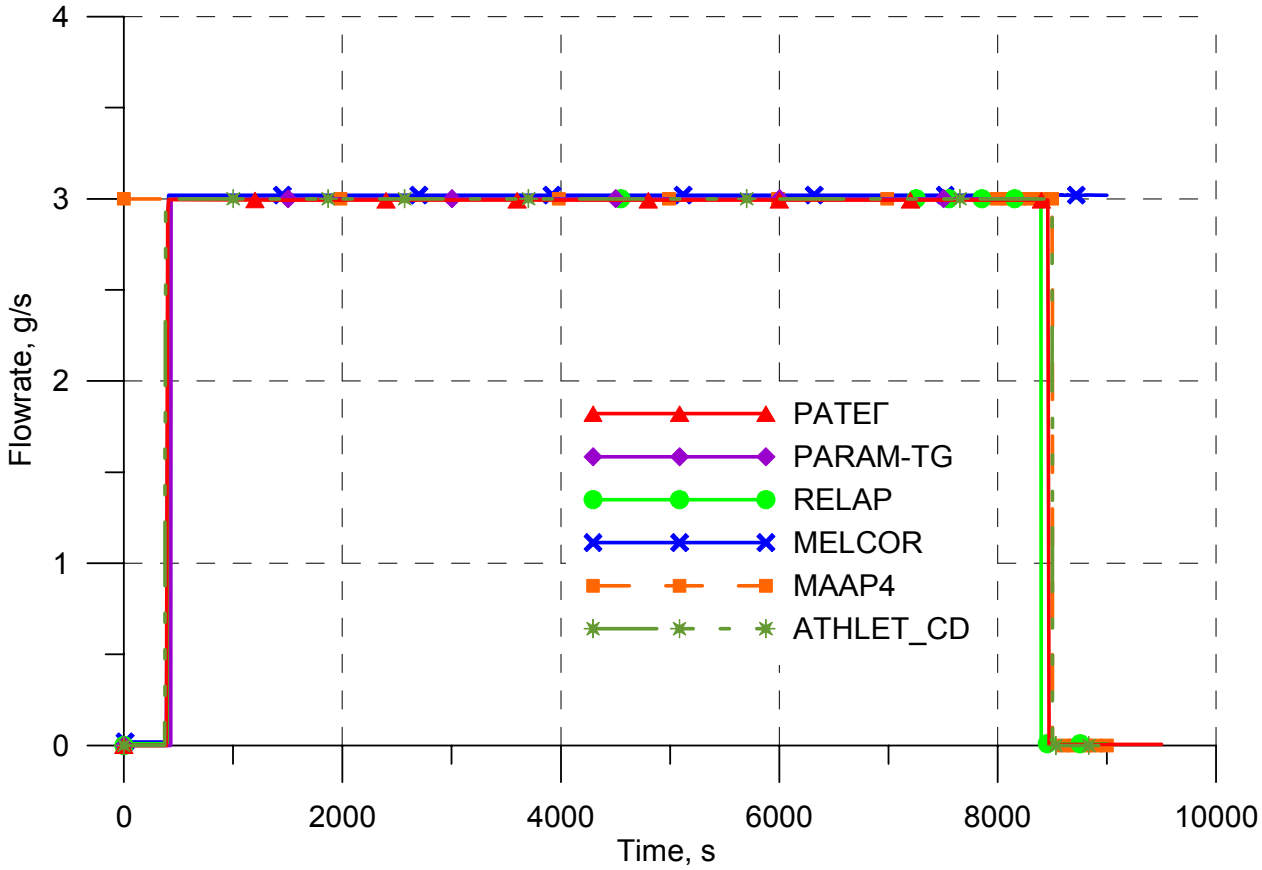

Figure 2.12 Steam flow rate at the assembly inlet

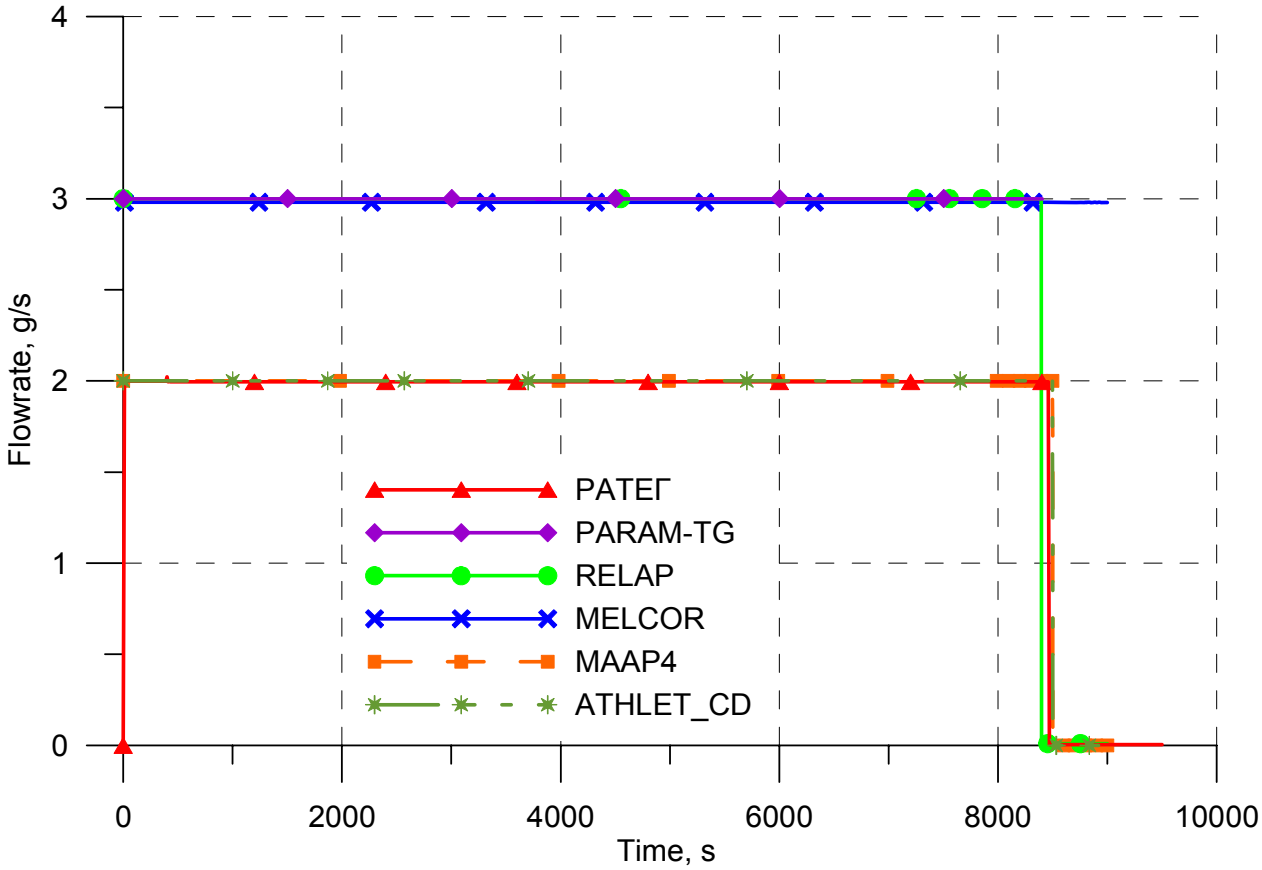

Figure 2.13 Argon flow rate at the assembly inlet

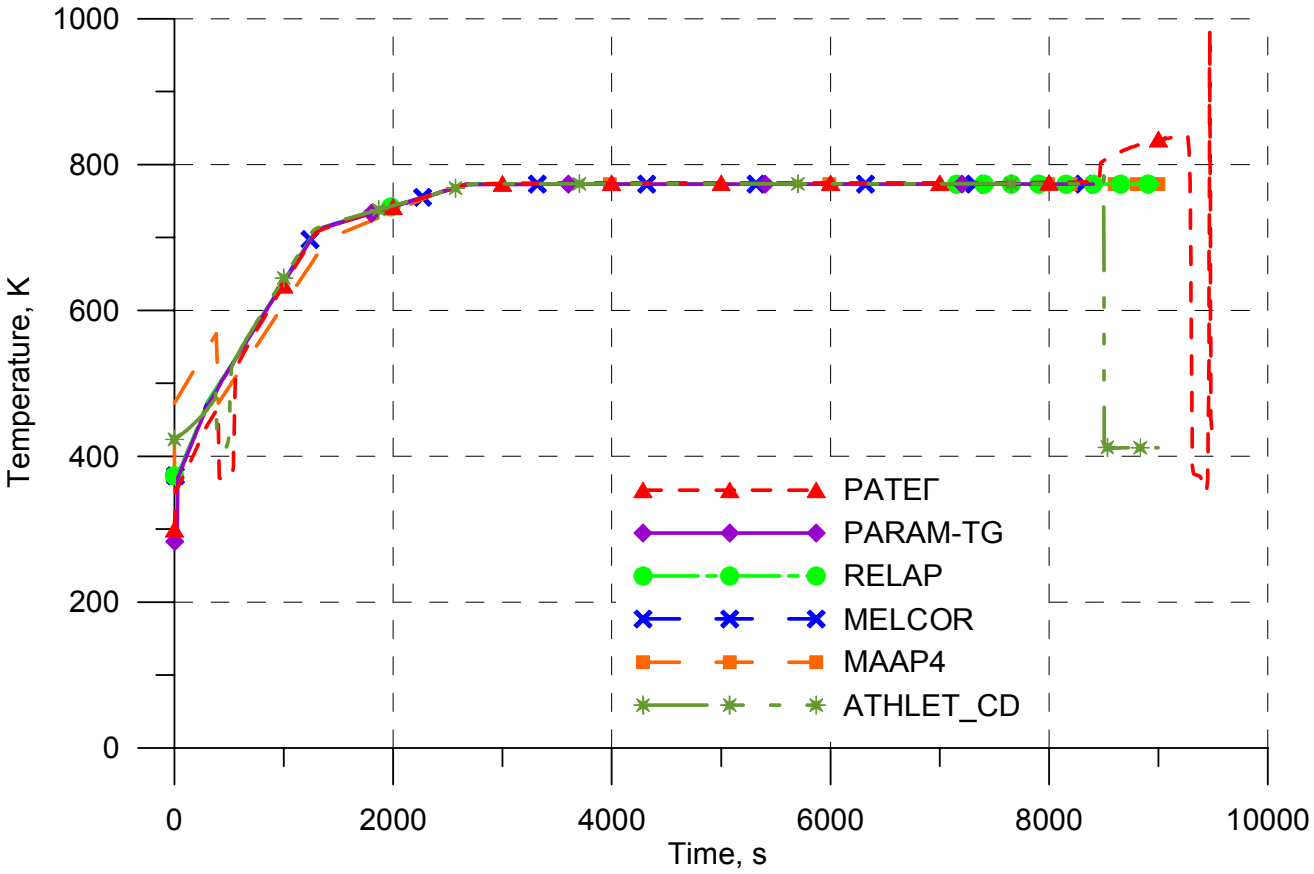

Figure 2.14 Coolant temperature at the assembly inlet

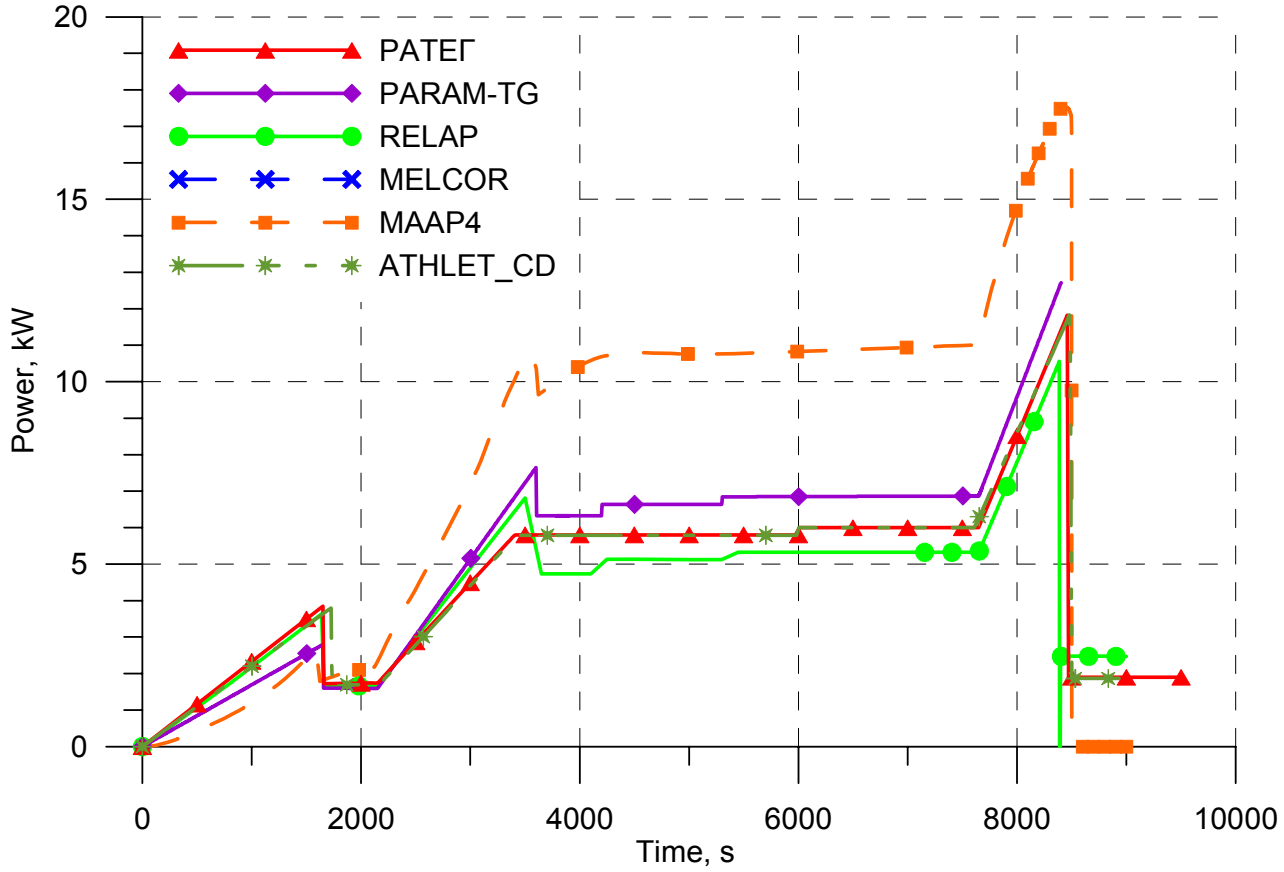

Figure 2.15 Electric power supply

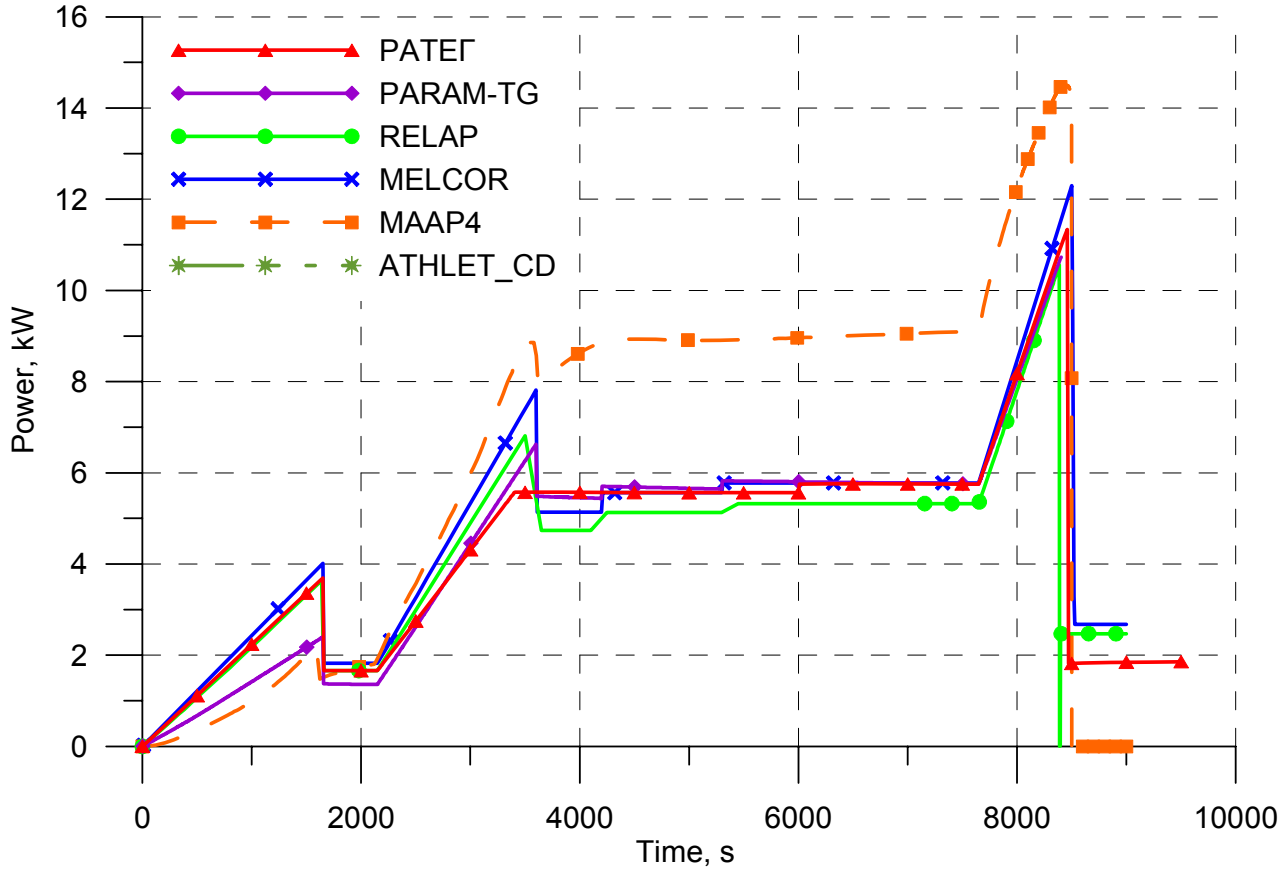

Figure 2.16 Joule heating power

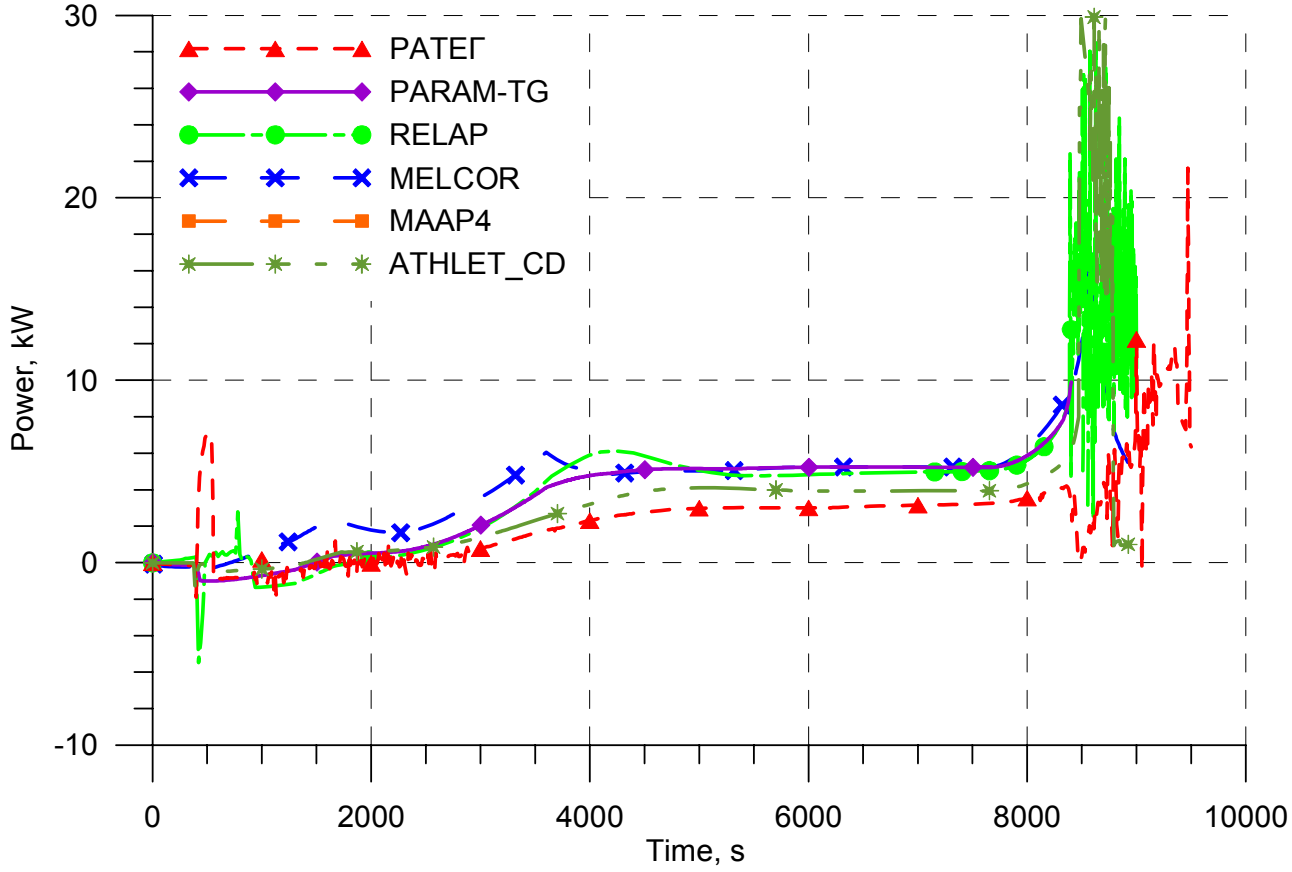

Figure 2.17 Power to coolant

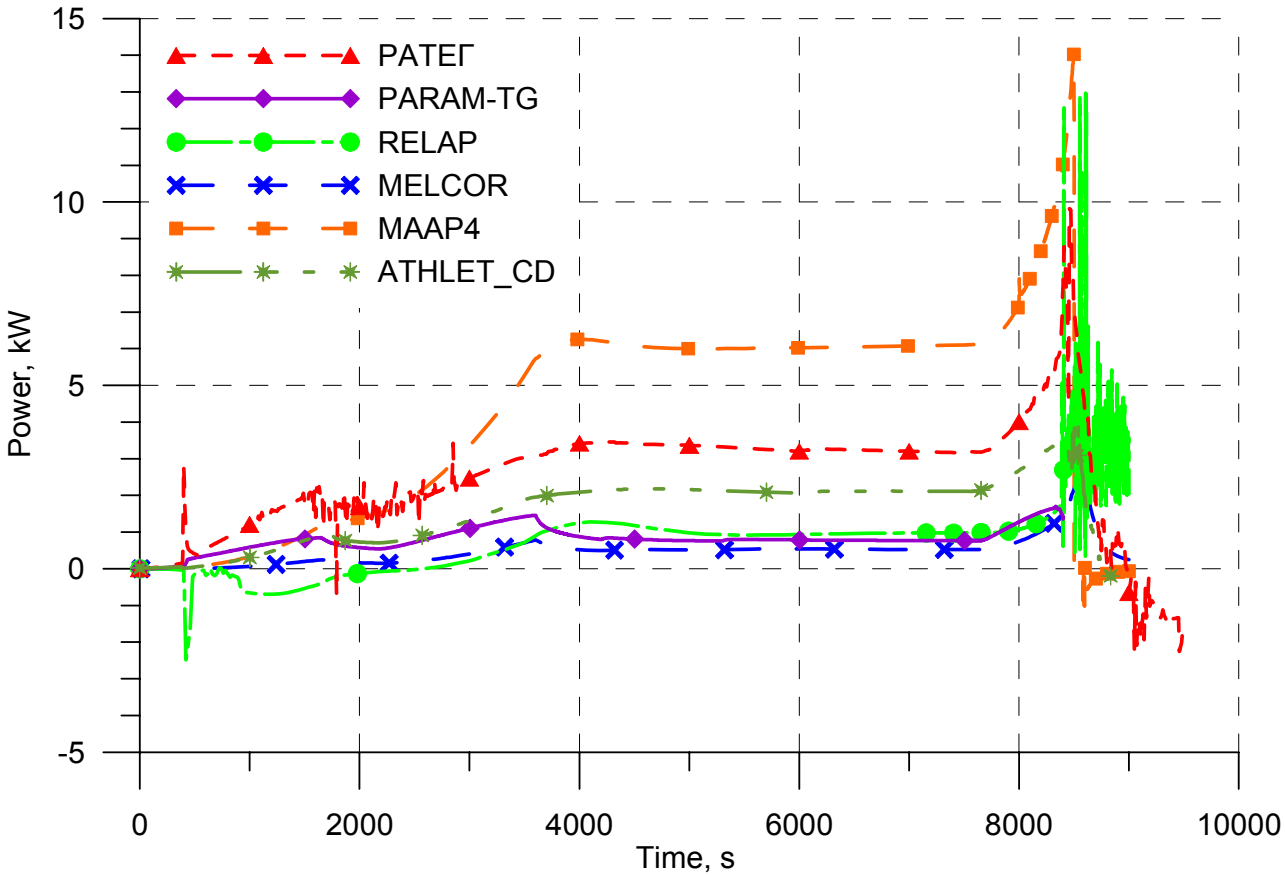

Figure 2.18 Power to shroud

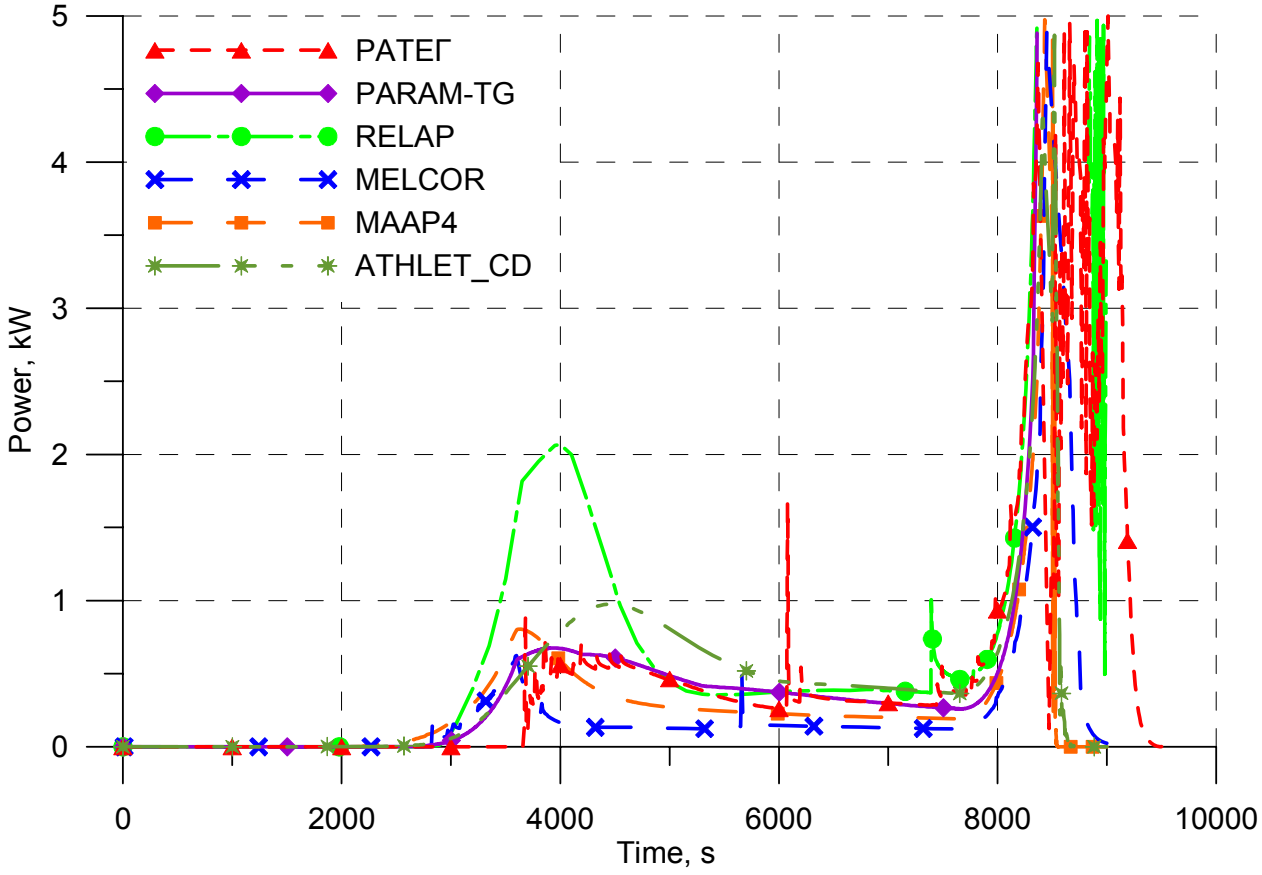

Figure 2.19 Oxidation reaction power

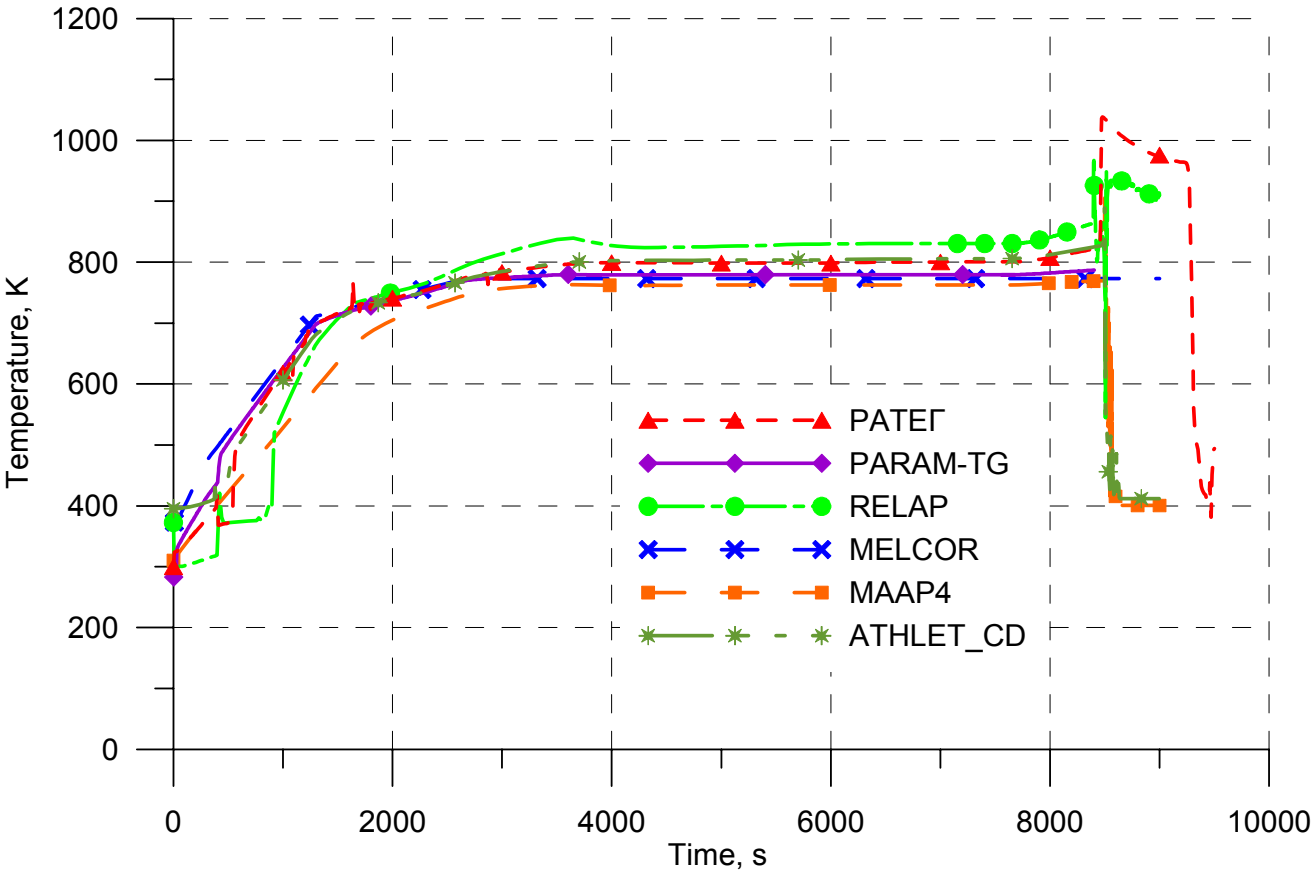

Figure 2.20 Coolant temperature at the elevation of 0 mm

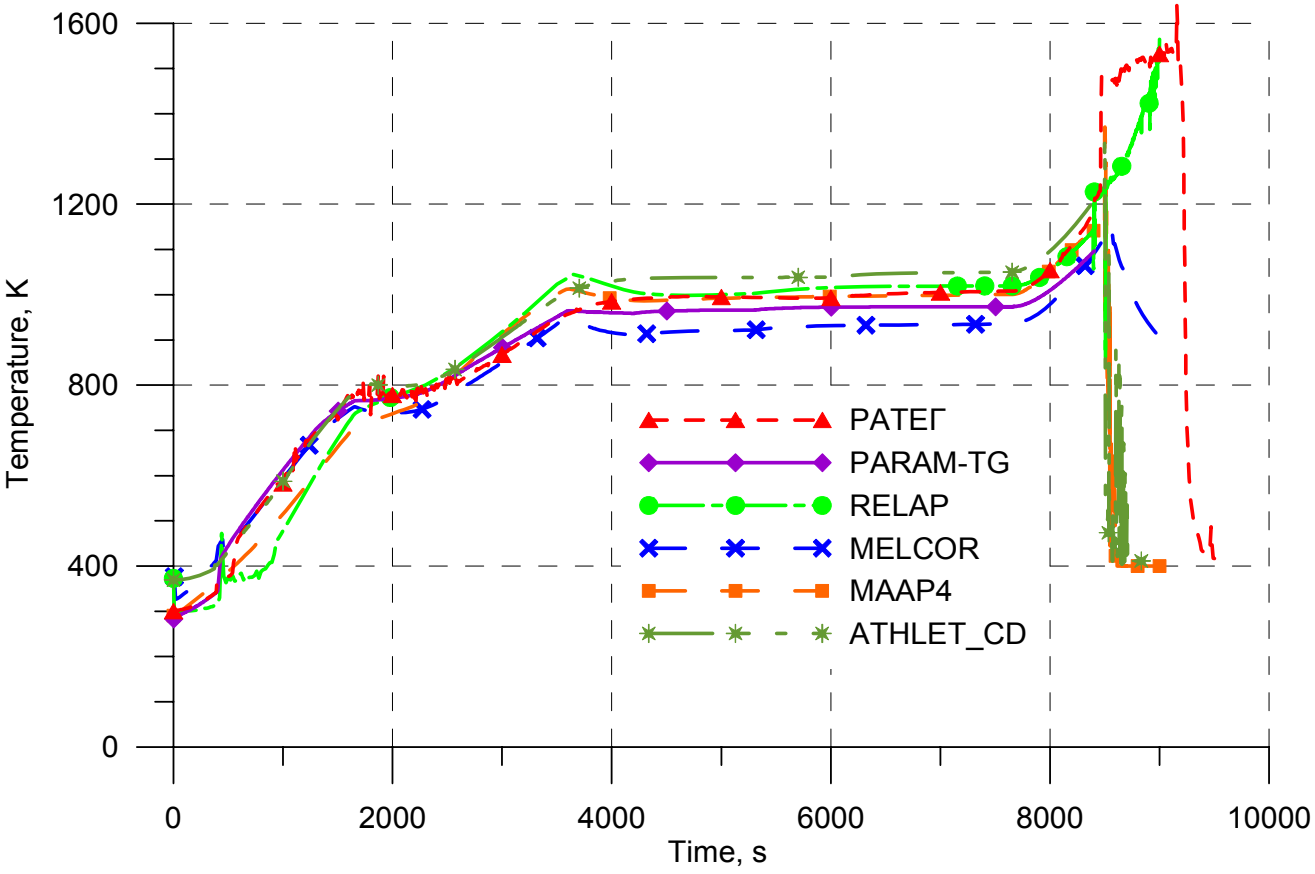

Figure 2.21 Coolant temperature at the elevation of 600 mm

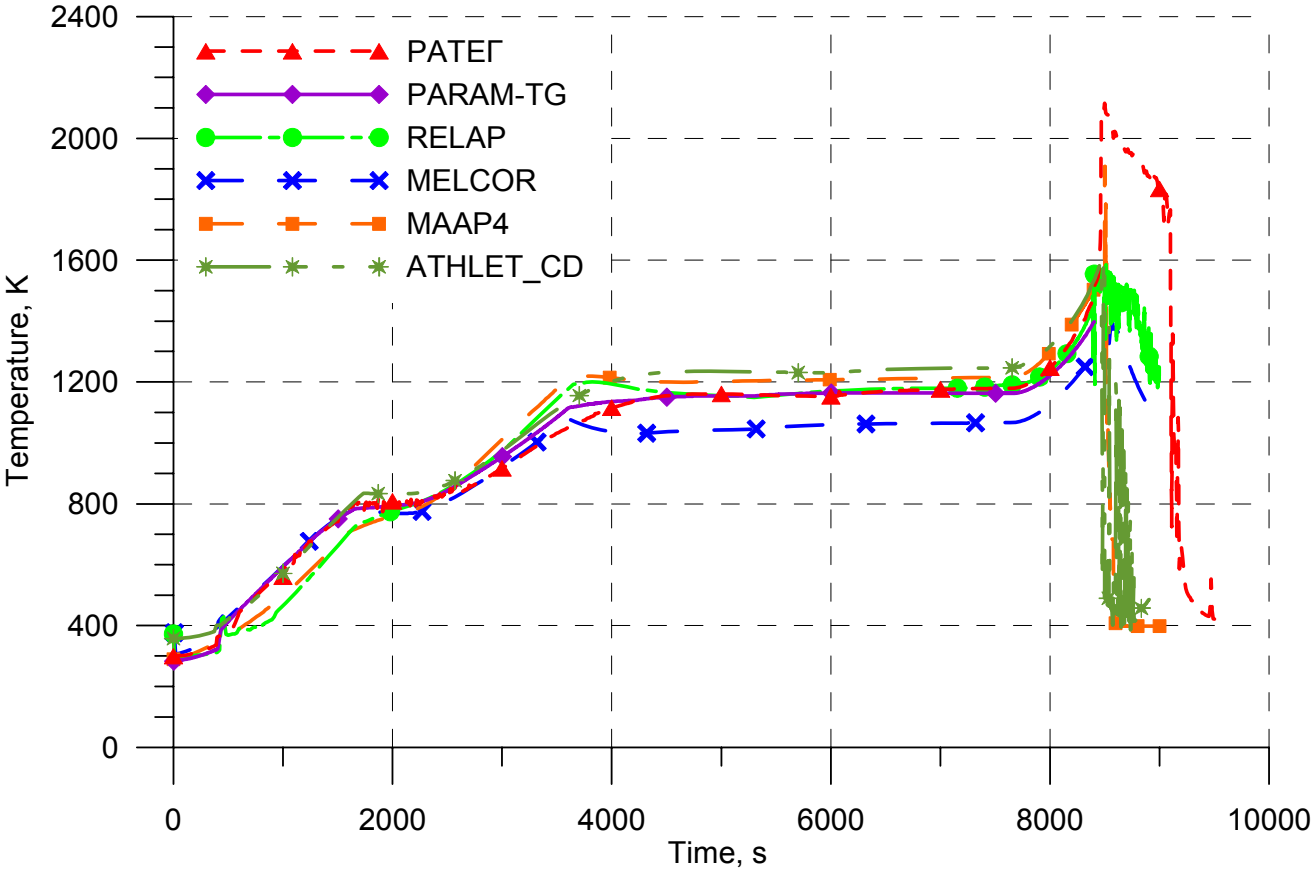

Figure 2.22 Coolant temperature at the elevation of 1000 mm

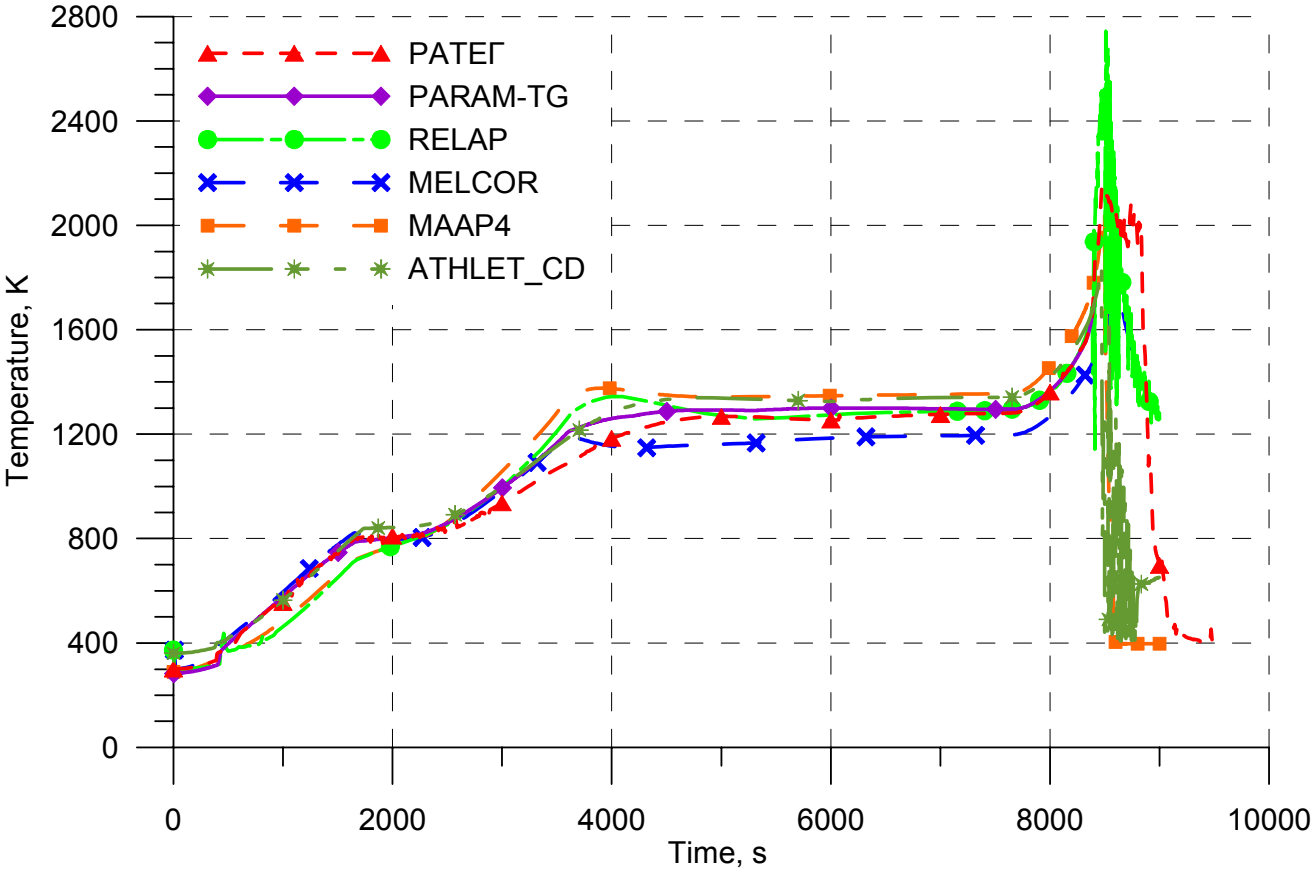

Figure 2.23 Coolant temperature at the elevation of 1250 mm

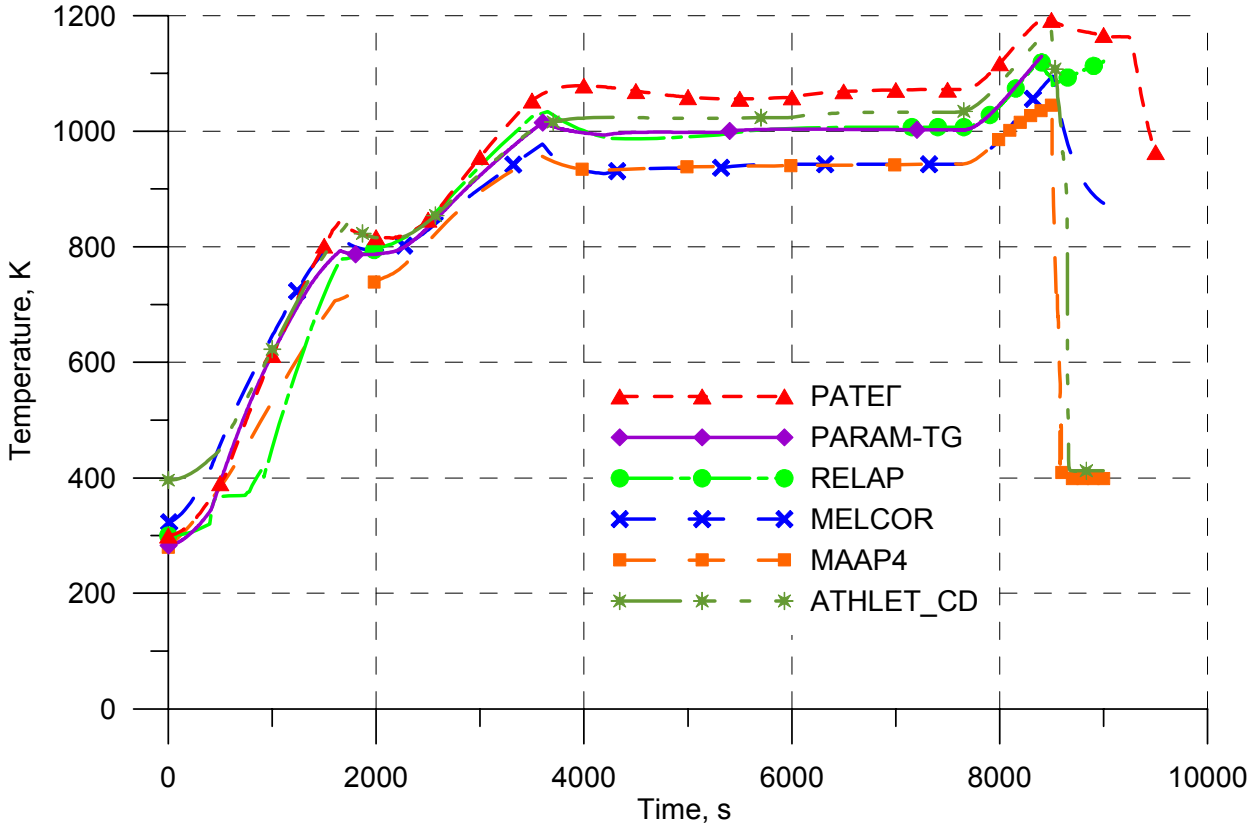

Figure 2.24 Cladding temperature of fuel rods of the 2nd row at the elevation of 200 mm

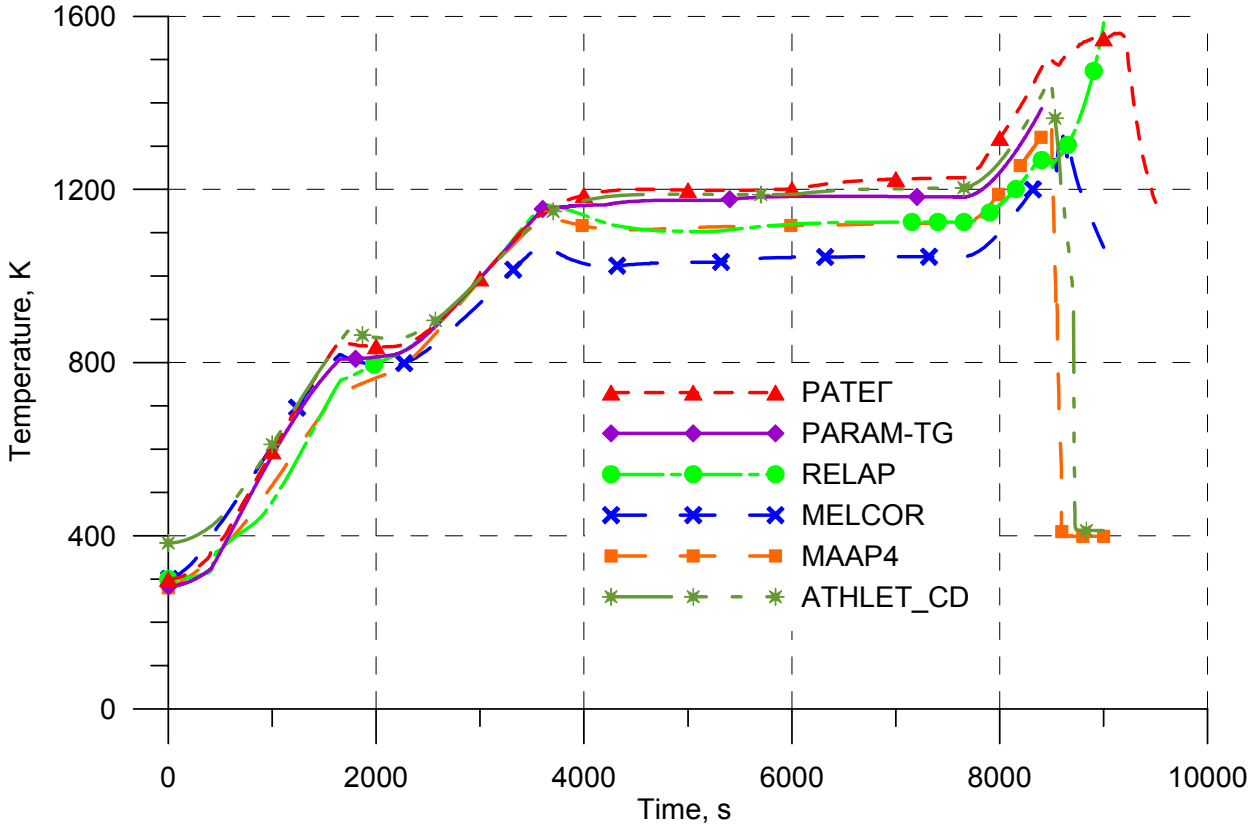

Figure 2.25 Cladding temperature of fuel rods of the 2nd row at the elevation of 600 mm

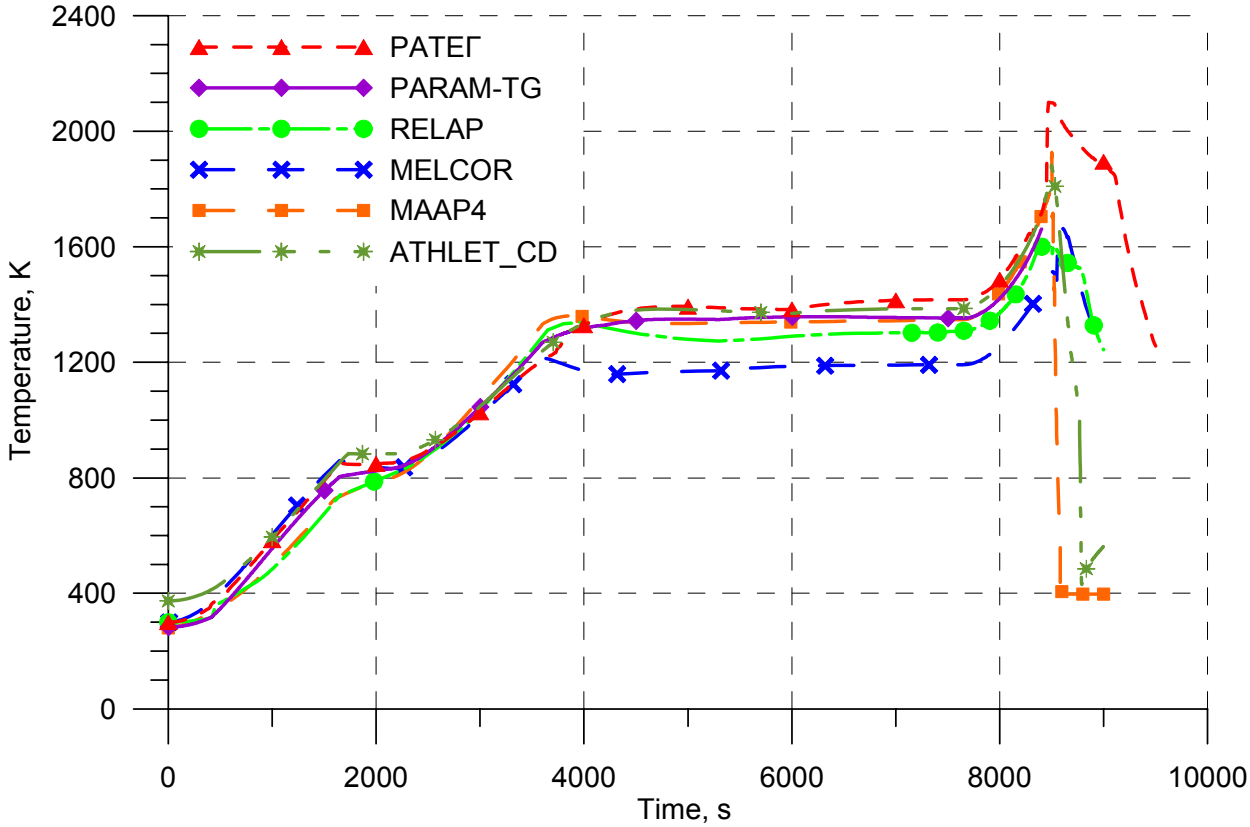

Figure 2.26 Cladding temperature of fuel rods of the 2nd row at the elevation of 1000 mm

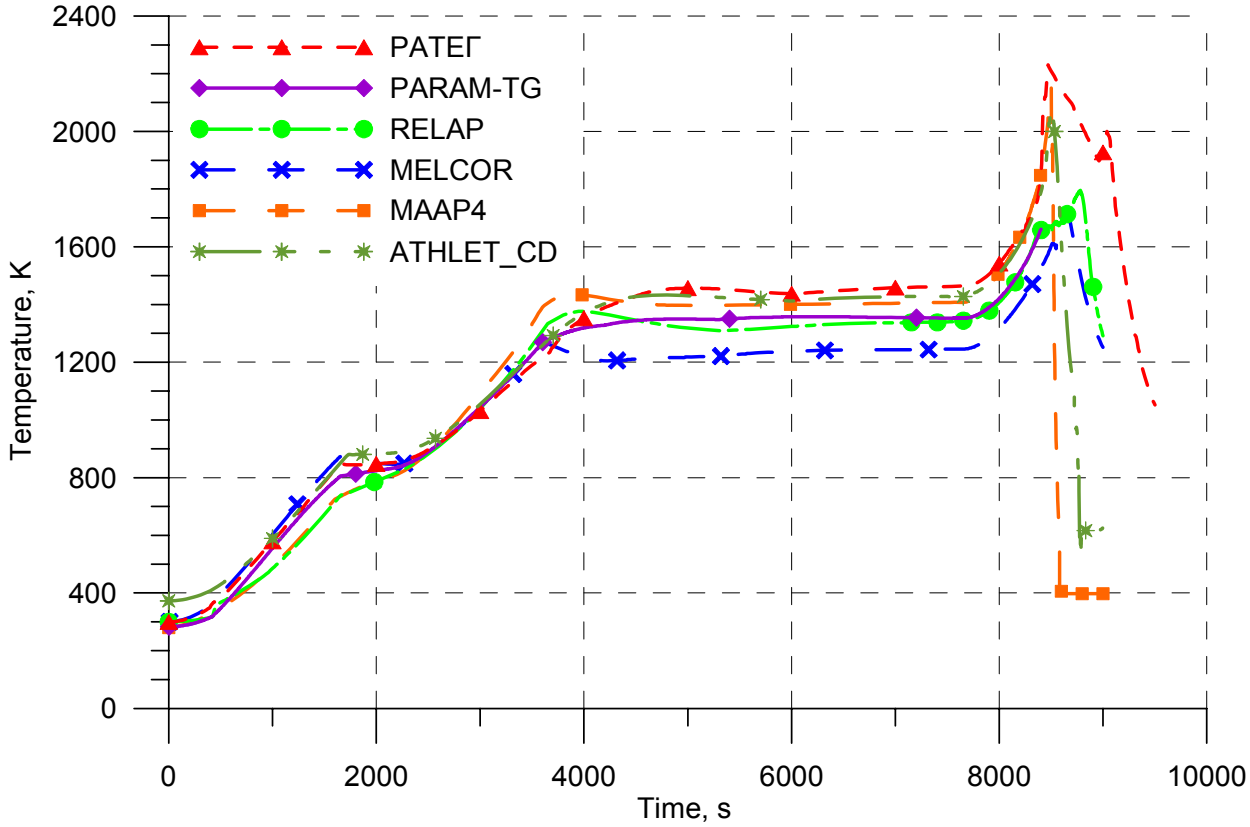

Figure 2.27 Cladding temperature of fuel rods of the 2nd row at the elevation of 1100 mm

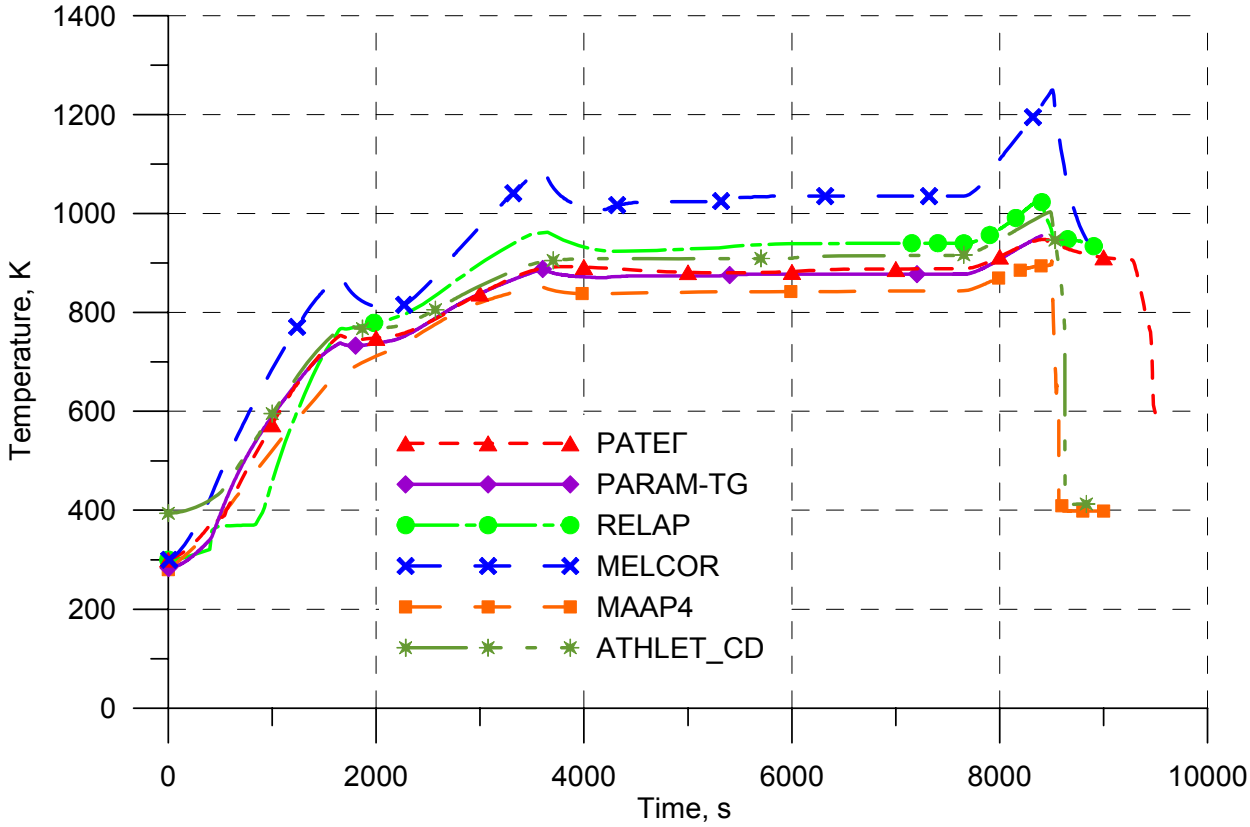

Figure 2.28 Cladding temperature of fuel rods of the 3rd row at the elevation of 0 mm

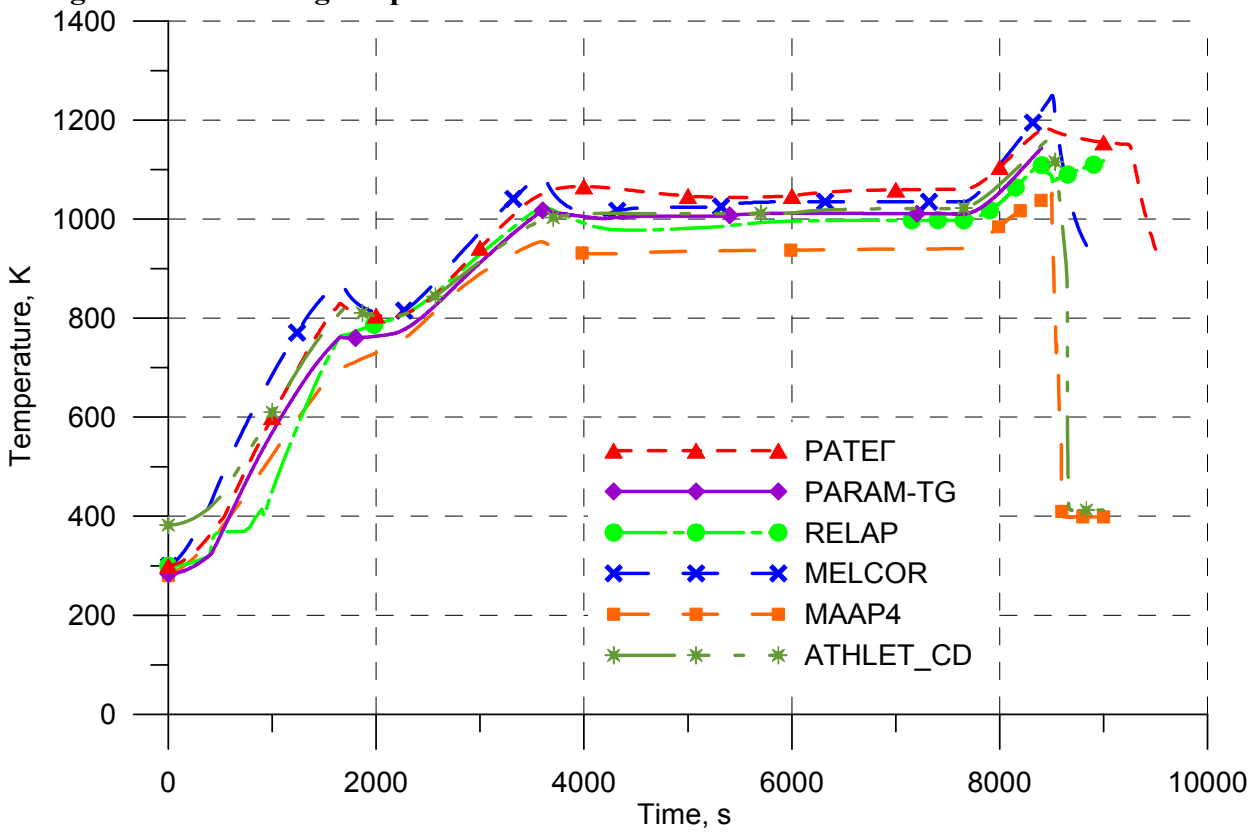

Figure 2.29 Cladding temperature of fuel rods of the 3rd row at the elevation of 200 mm

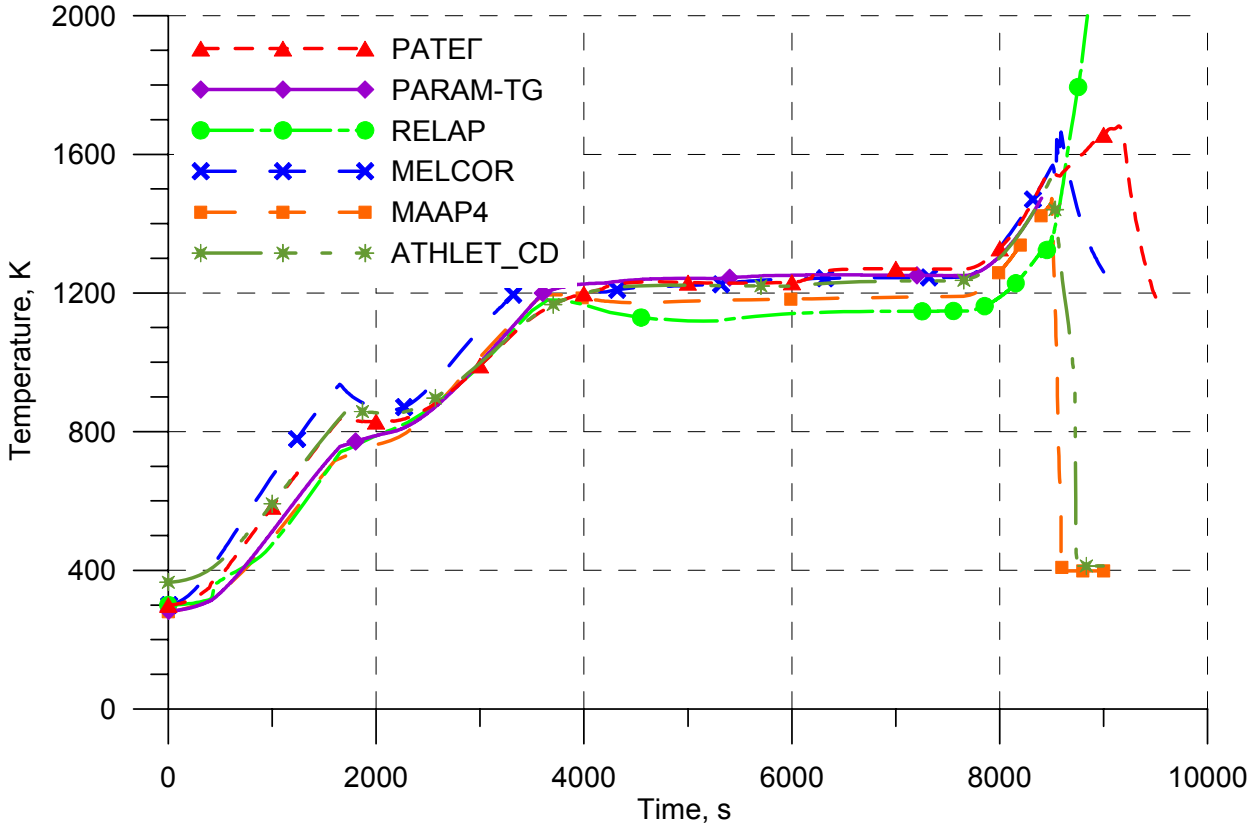

Figure 2.30 Cladding temperature of fuel rods of the 3rd row at the elevation of 700 mm

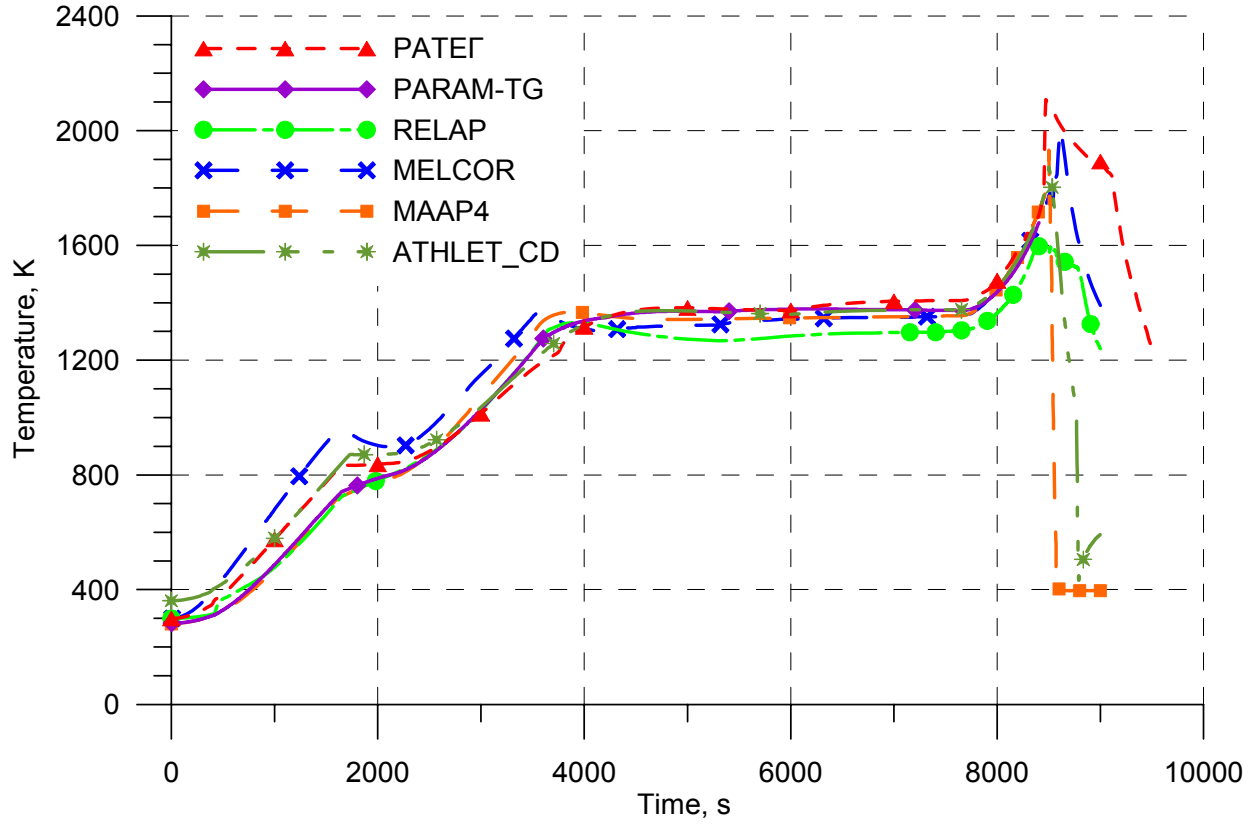

Figure 2.31 Cladding temperature of fuel rods of the 3rd row at the elevation of 1000 mm

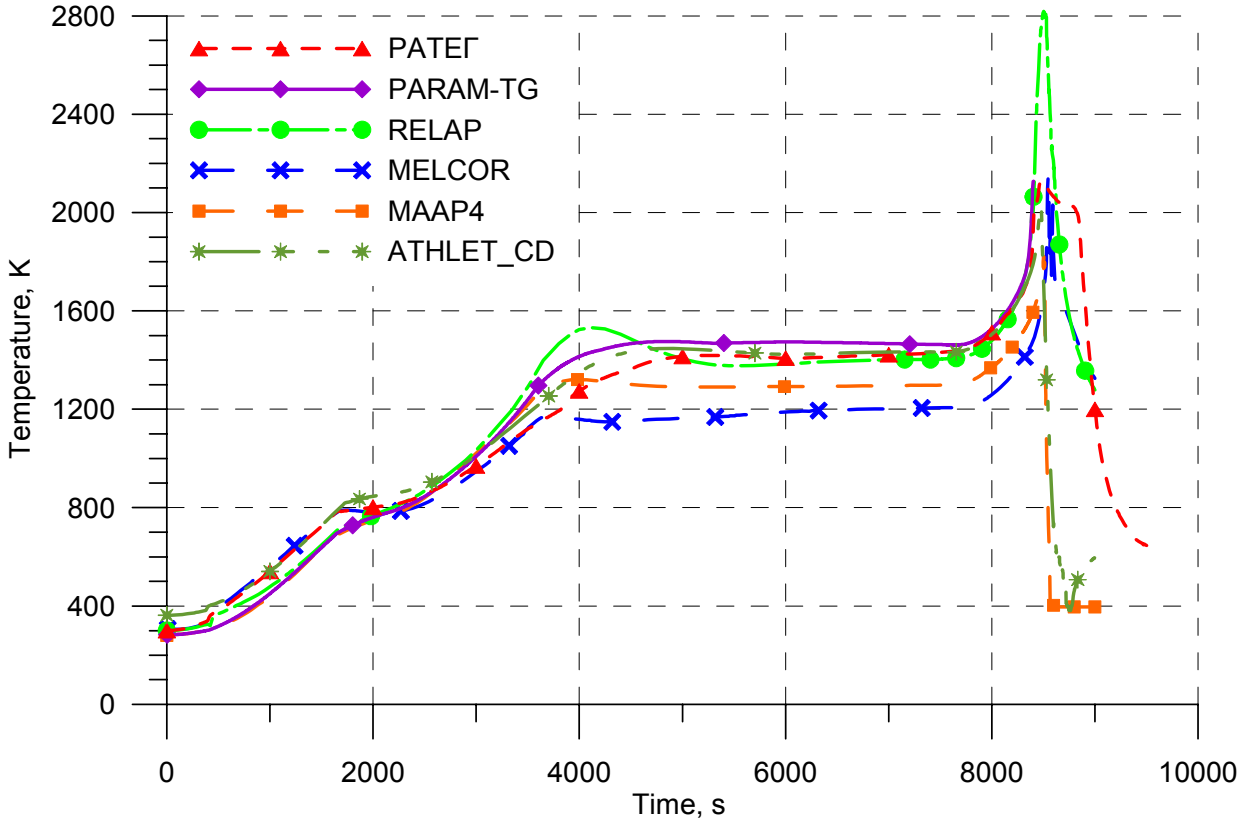

Figure 2.32 Cladding temperature of fuel rods of the 3rd row at the elevation of 1250 mm

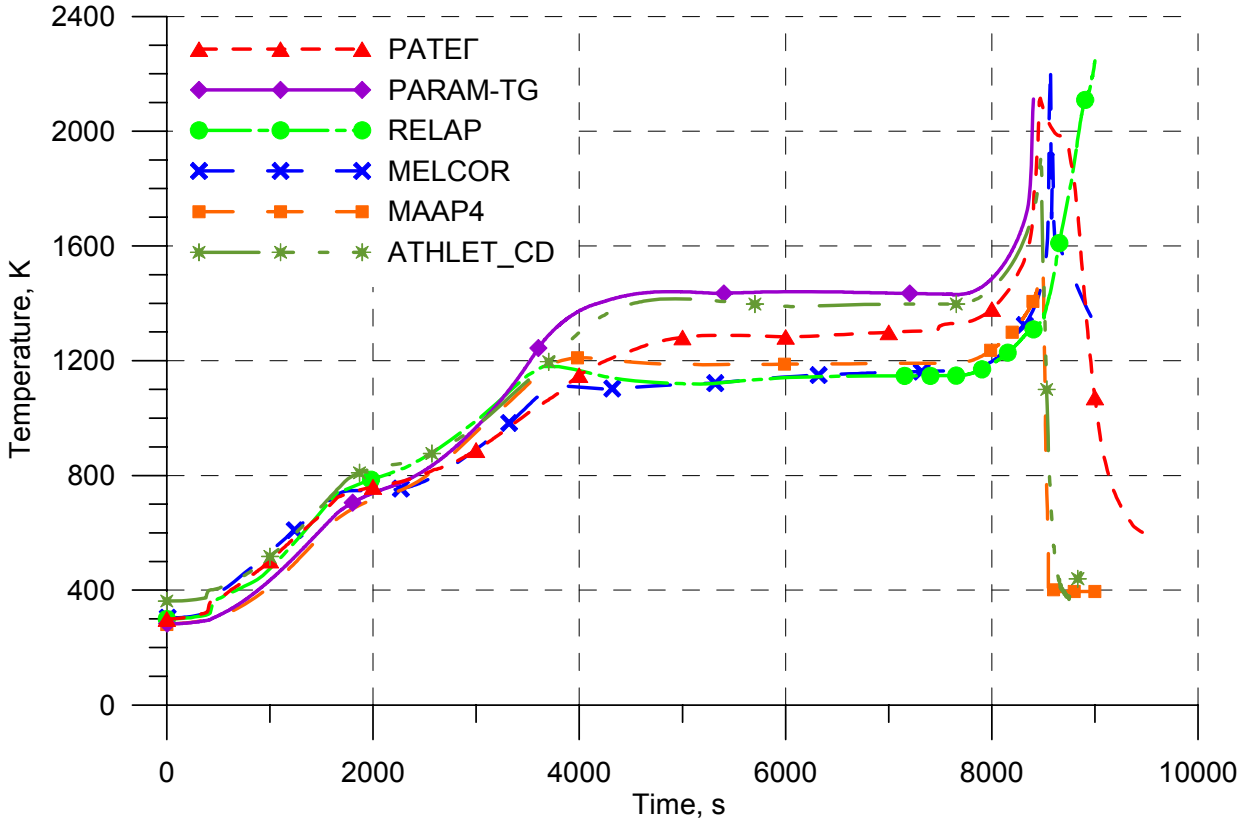

Figure 2.33 Cladding temperature of fuel rods of the 3rd row at the elevation of 1300 mm

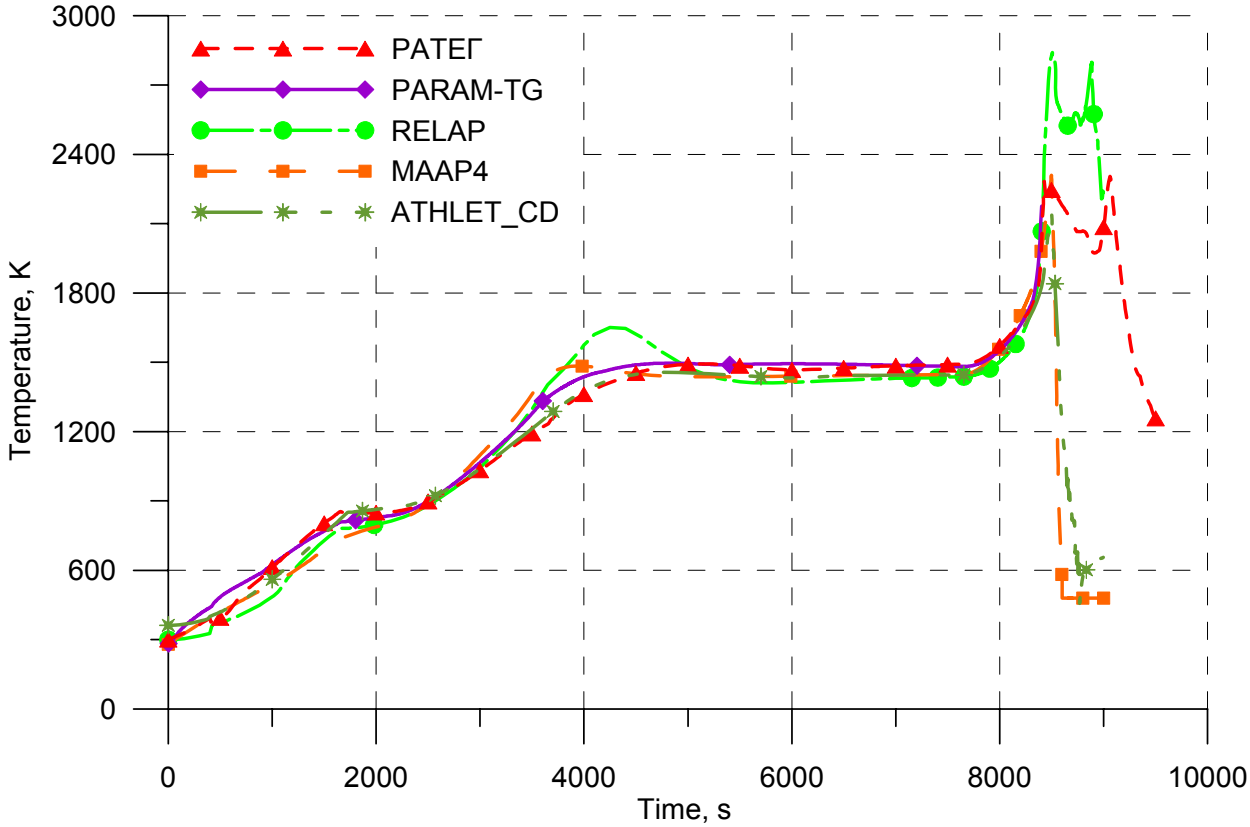

Figure 2.34 Maximum temperature of claddings

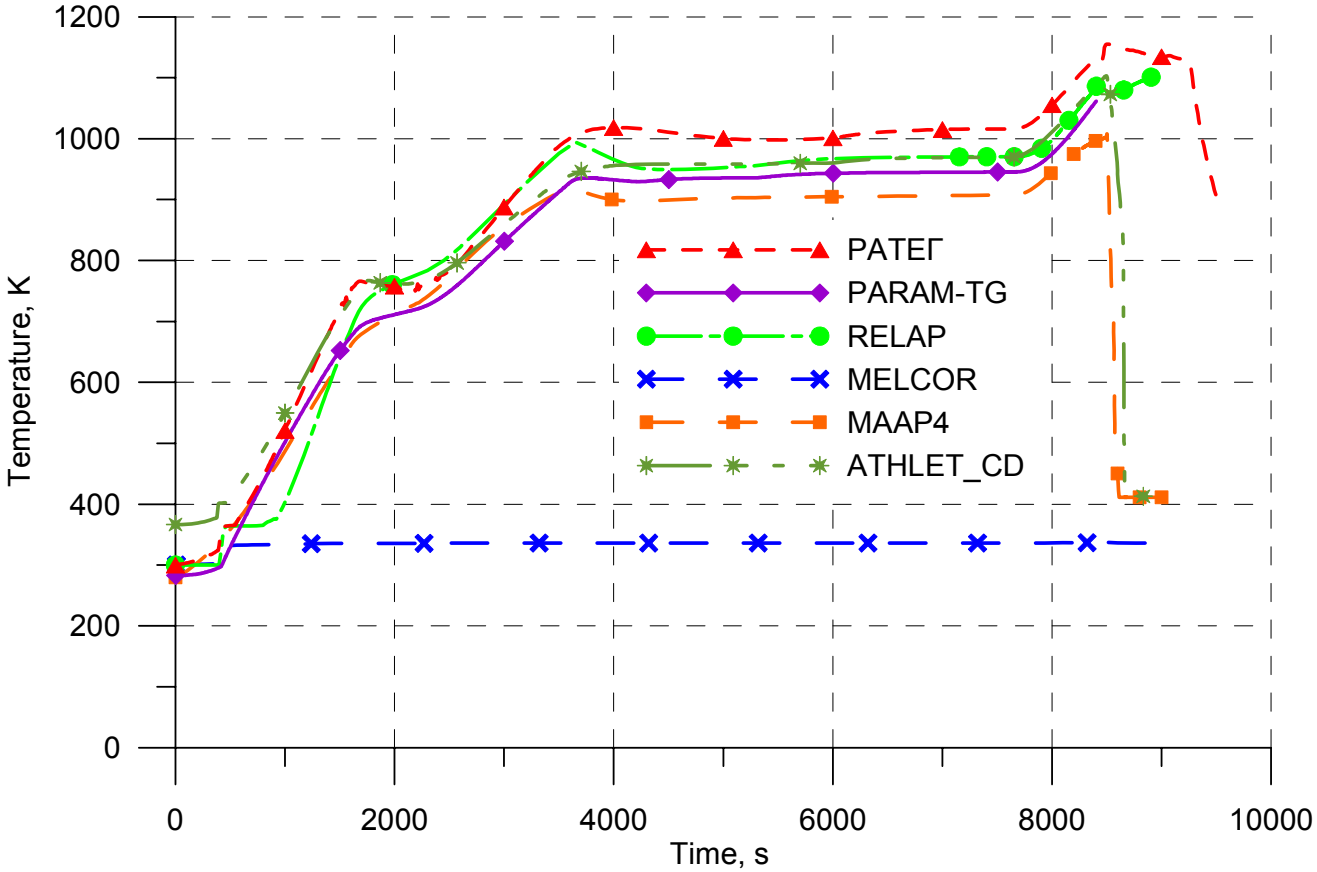

Figure 2.35 Shroud temperature at the elevation of 200 mm

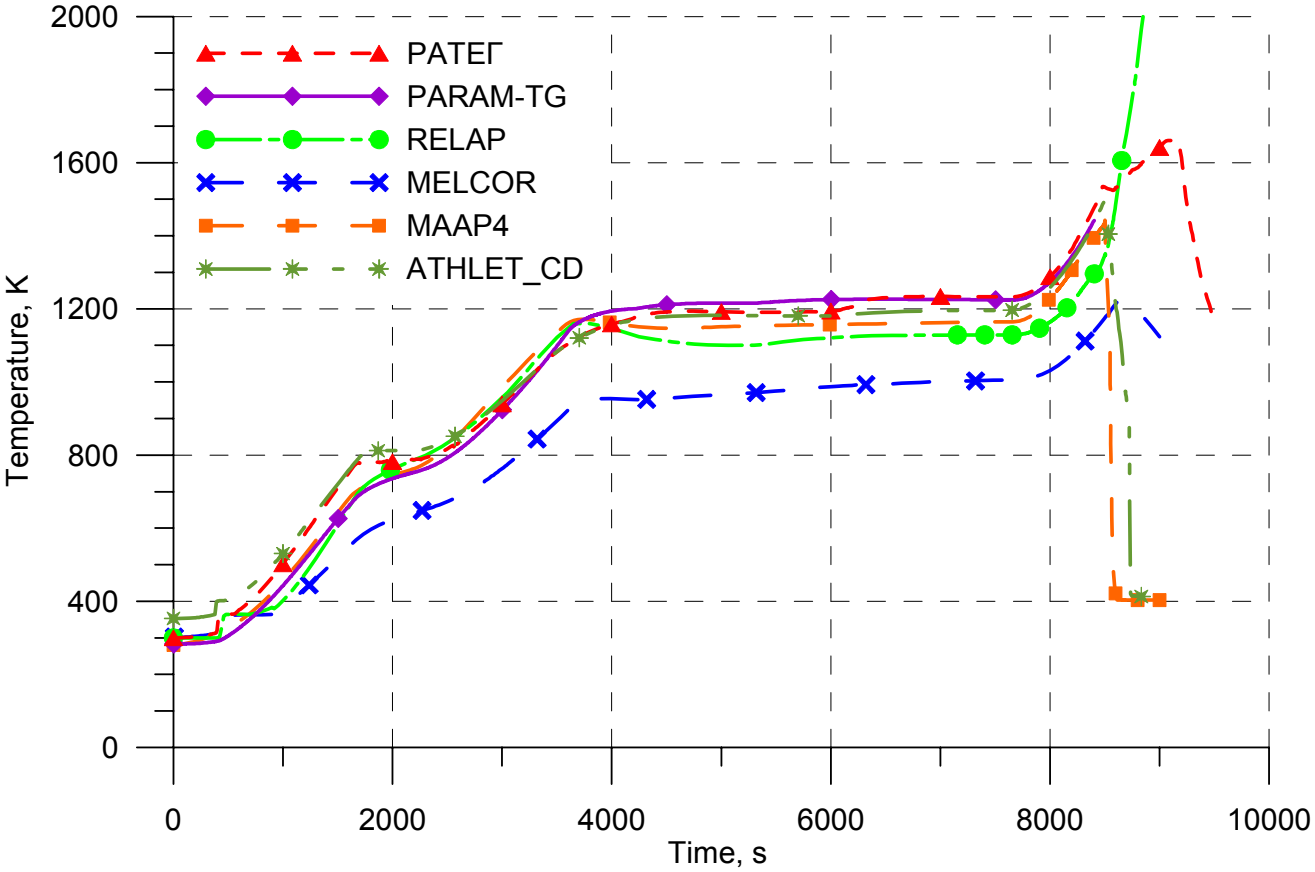

Figure 2.36 Shroud temperature at the elevation of 700 mm

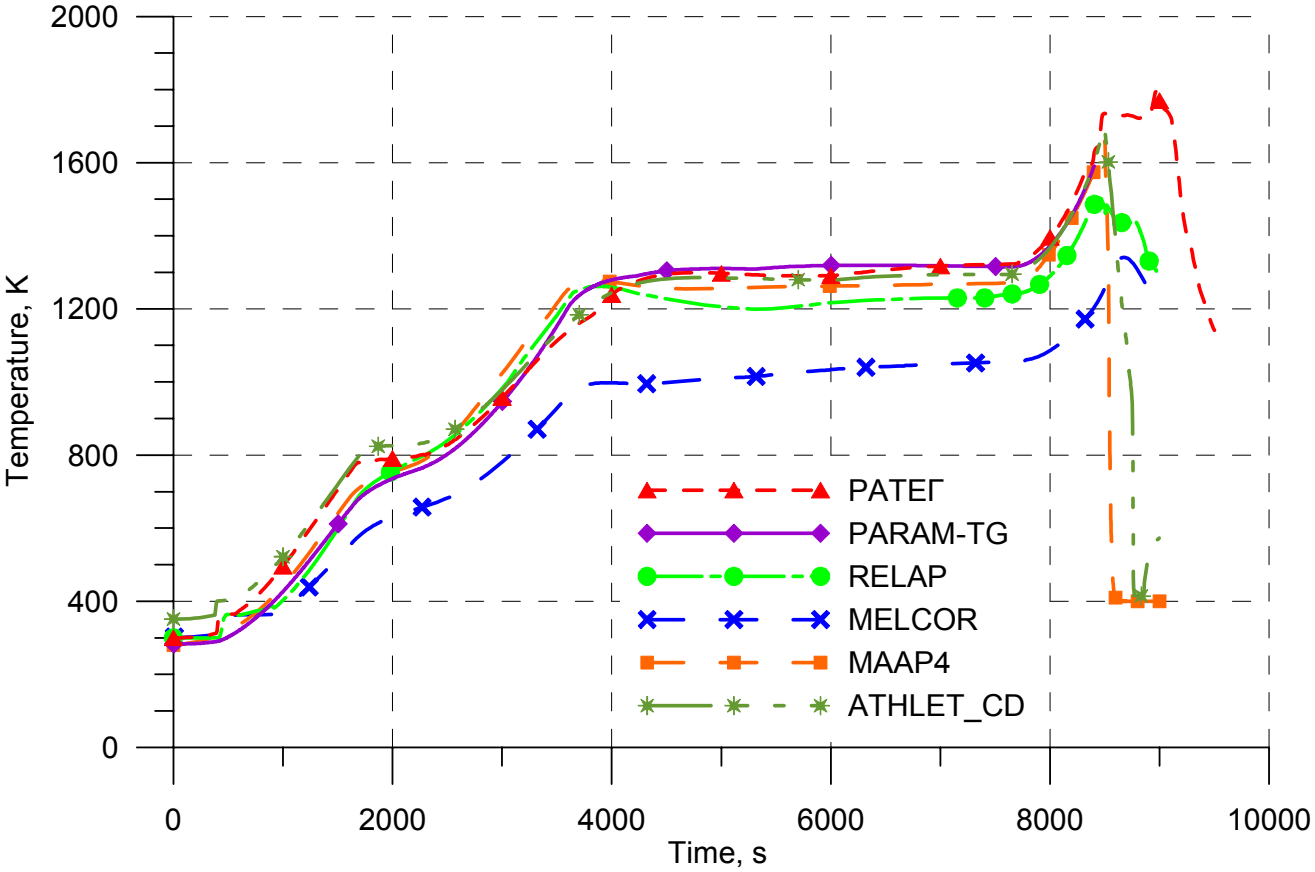

Figure 2.37 Shroud temperature at the elevation of 900 mm

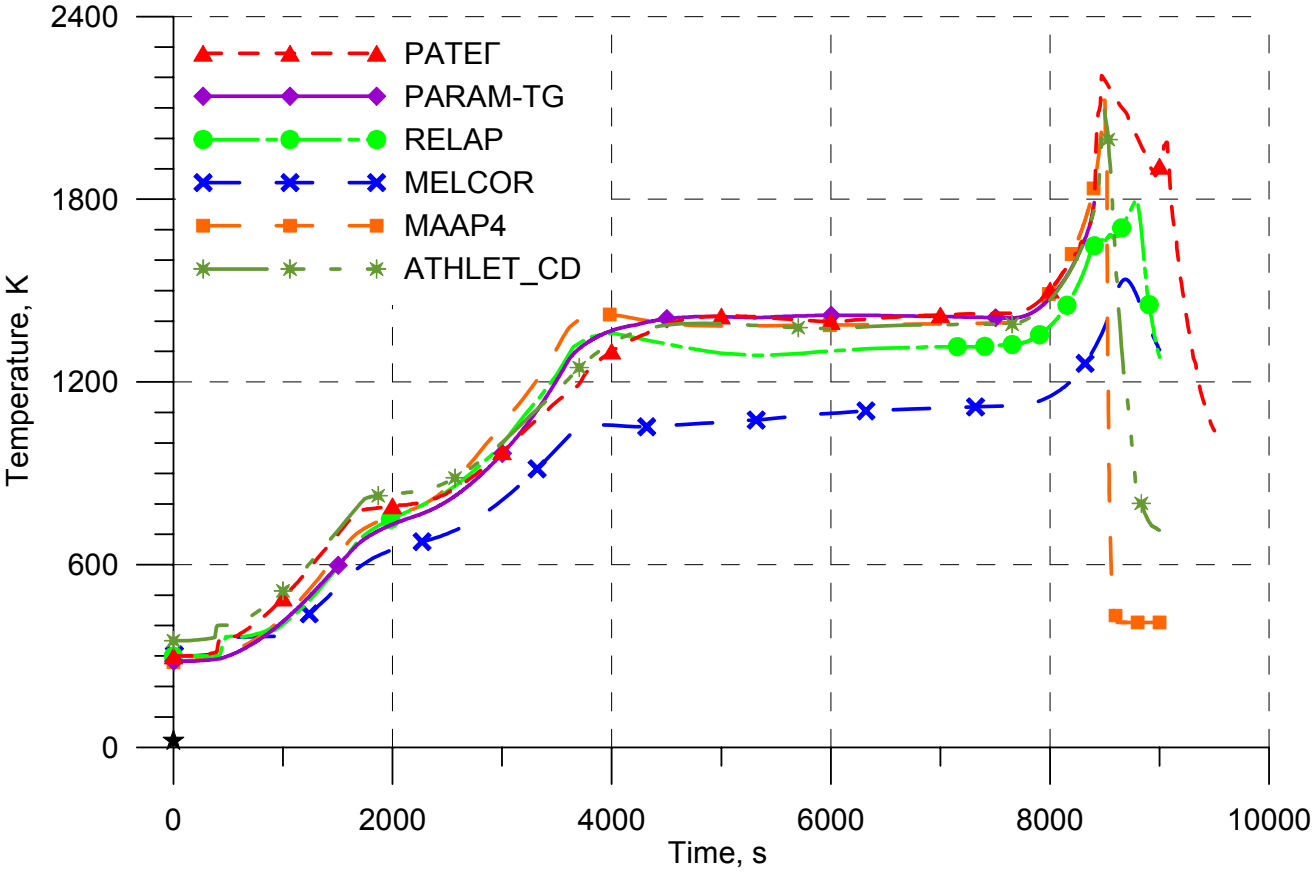

Figure 2.38 Shroud temperature at the elevation of 1100 mm

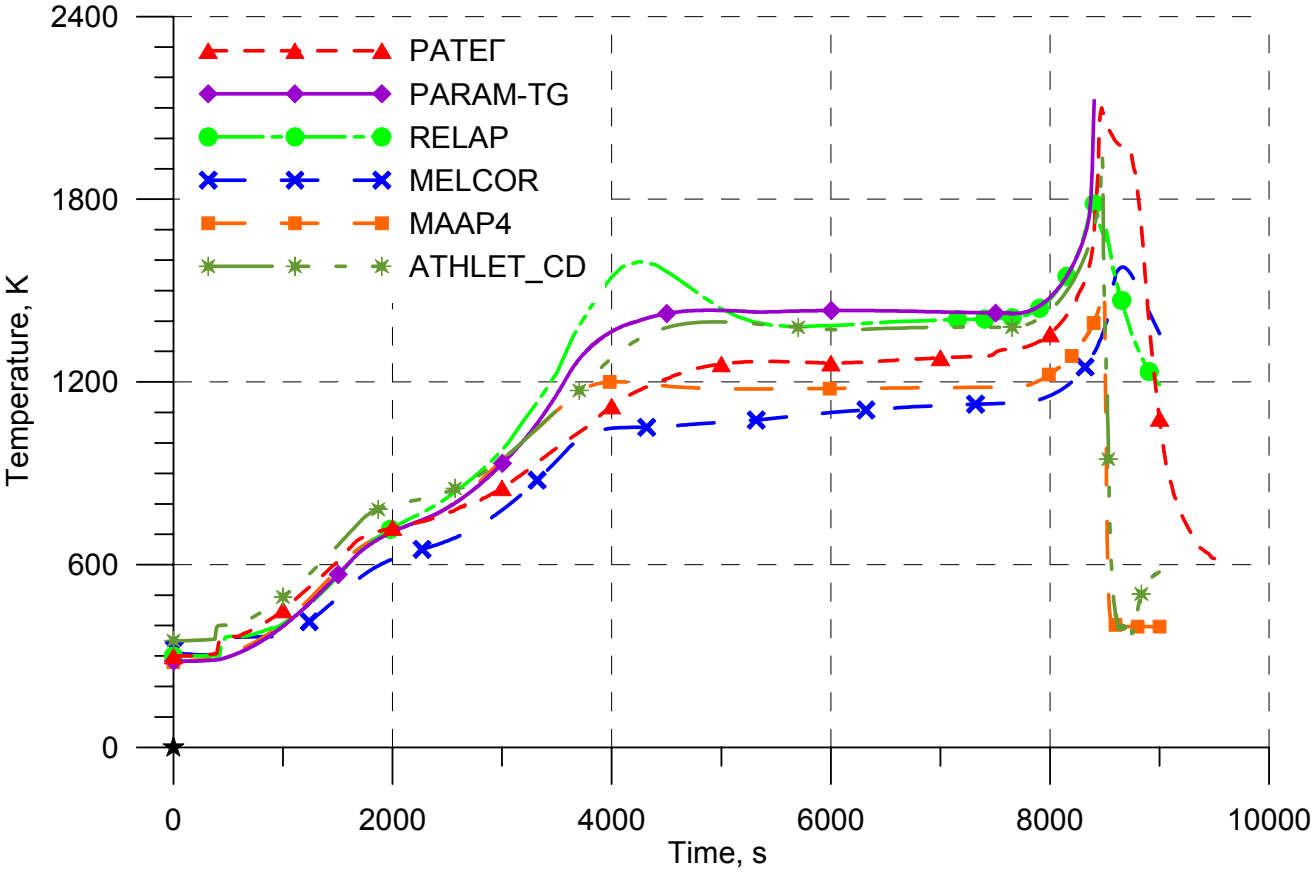

Figure 2.39 Shroud temperature at the elevation of 1300 mm

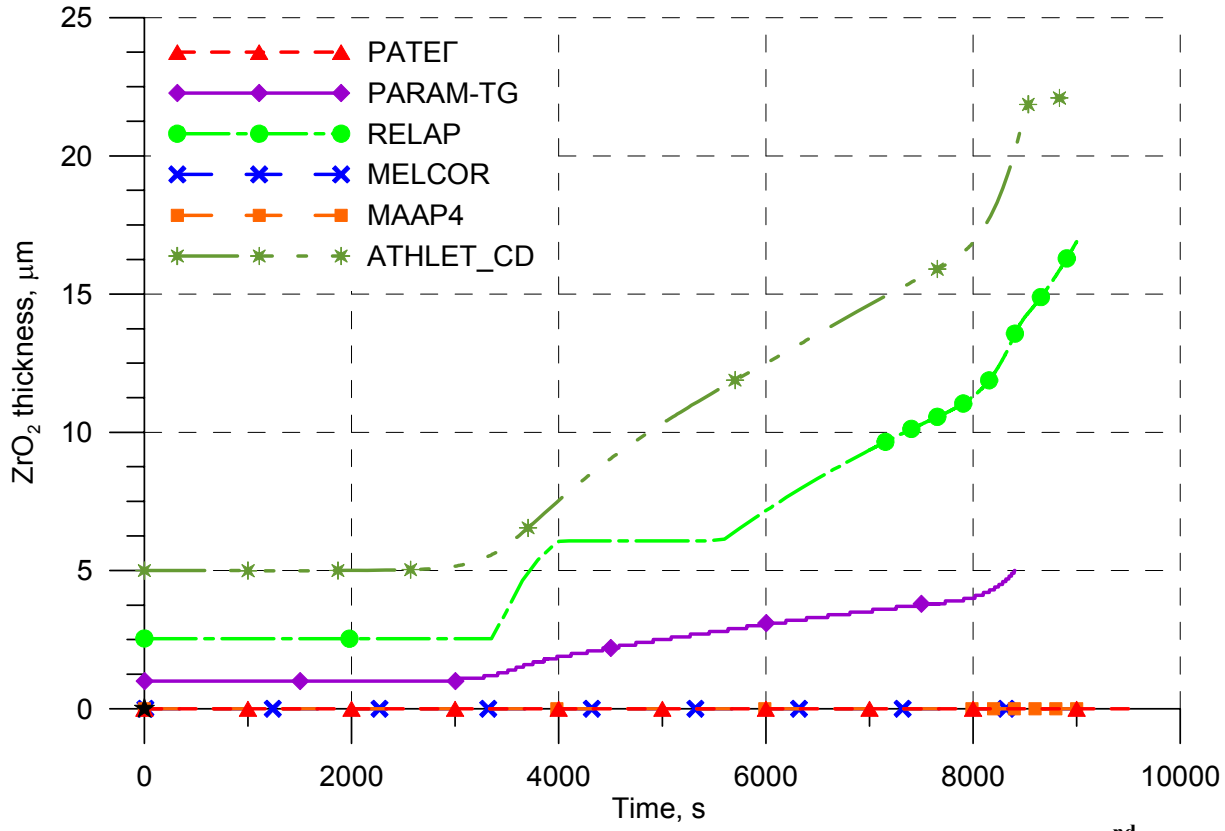

Figure 2.40 Thickness of the oxide scale of the claddings of the fuel rods of the 2nd row at the elevation of 200 mm

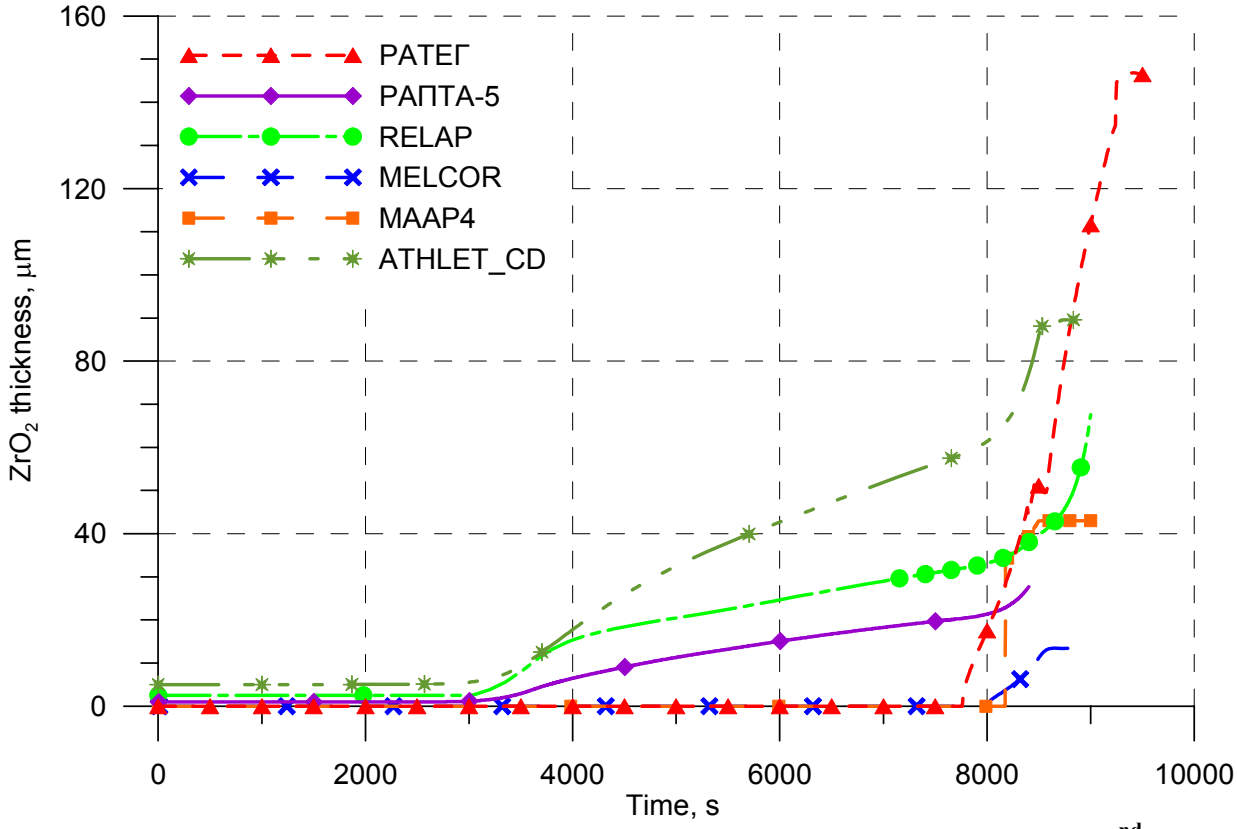

Figure 2.41 Thickness of the oxide scale of the claddings of the fuel rods of the 2nd row at the elevation of 600 mm

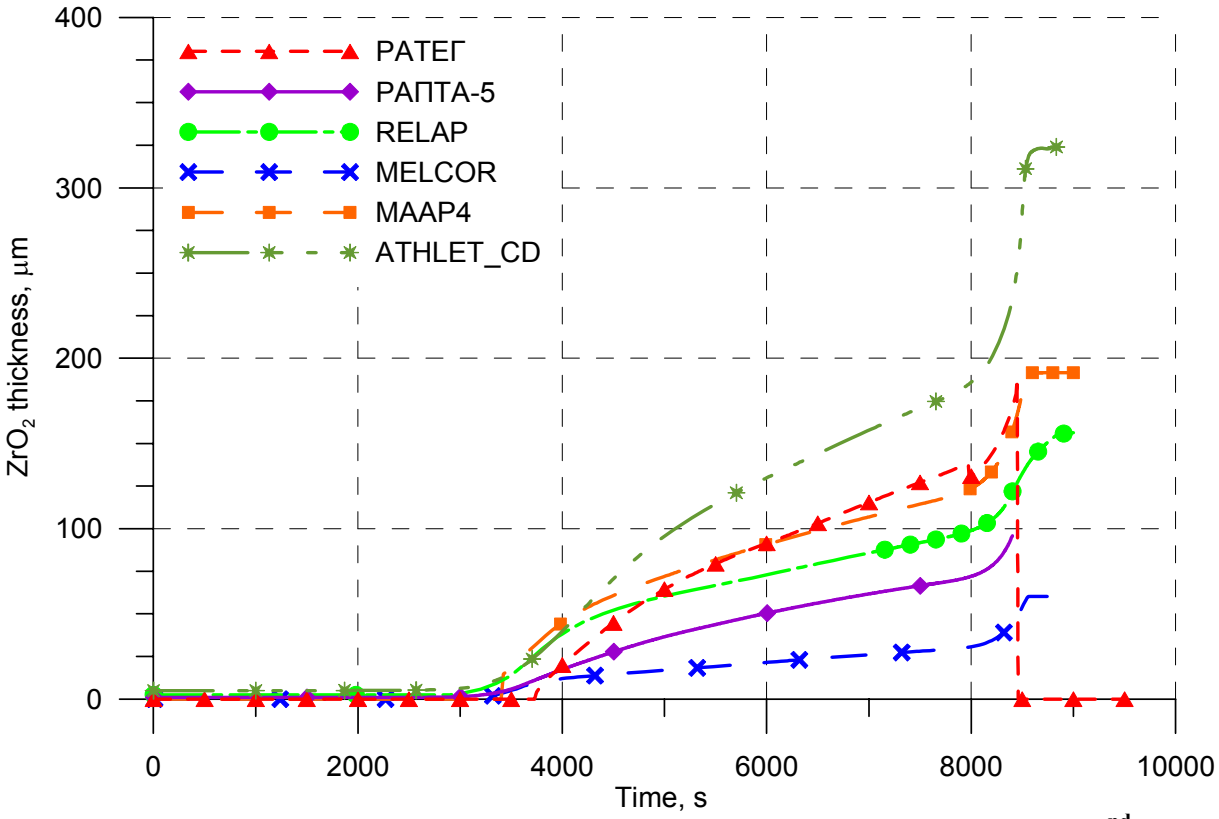

Figure 2.42 Thickness of the oxide scale of the claddings of the fuel rods of the 2nd row at the elevation of 1000 mm

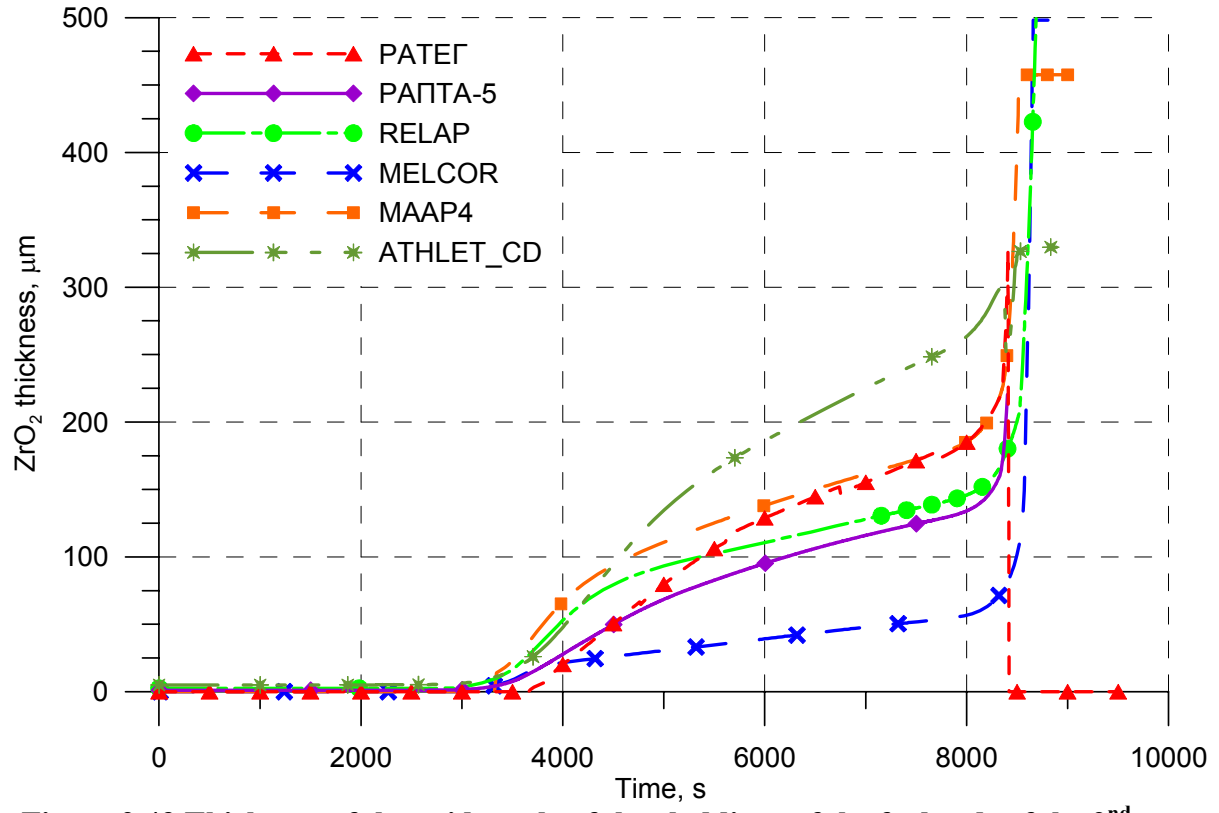

Figure 2.43 Thickness of the oxide scale of the claddings of the fuel rods of the 2nd row at the elevation of 1200 mm

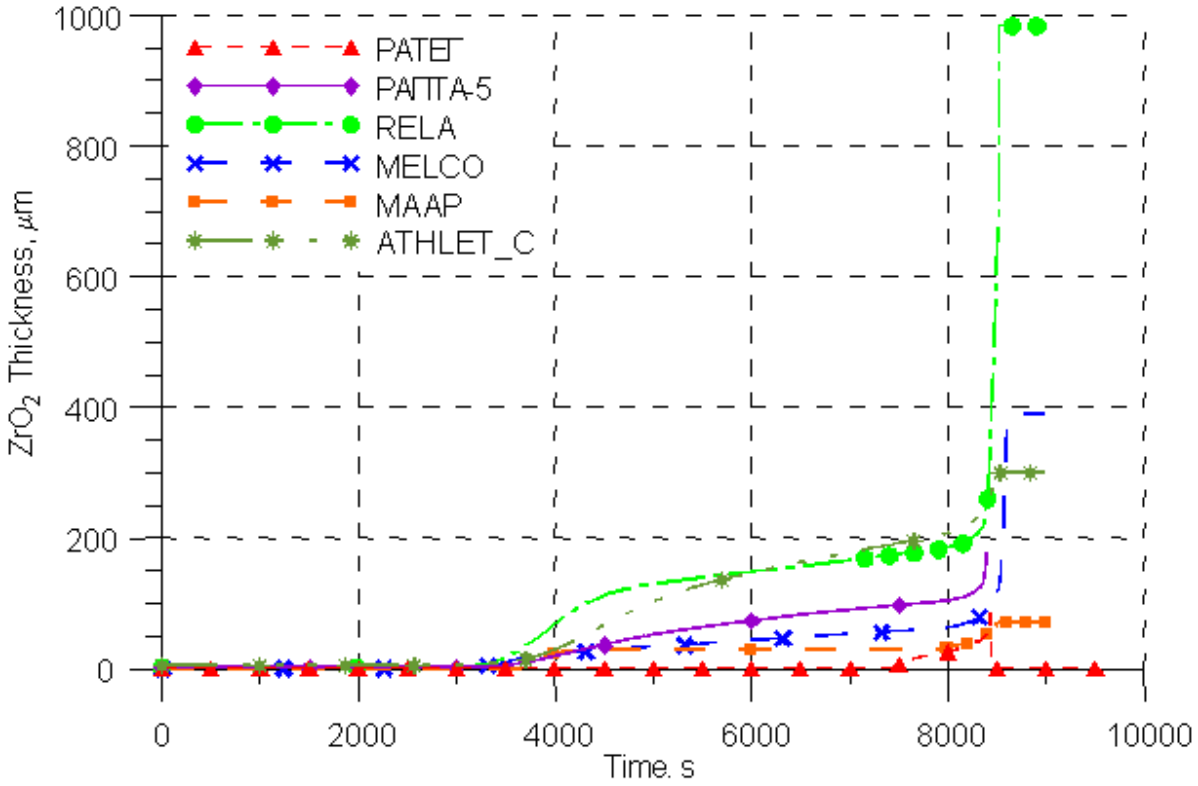

Figure 2.44 Thickness of the oxide scale of the claddings of the fuel rods of the 2nd row at the elevation of 1300 mm

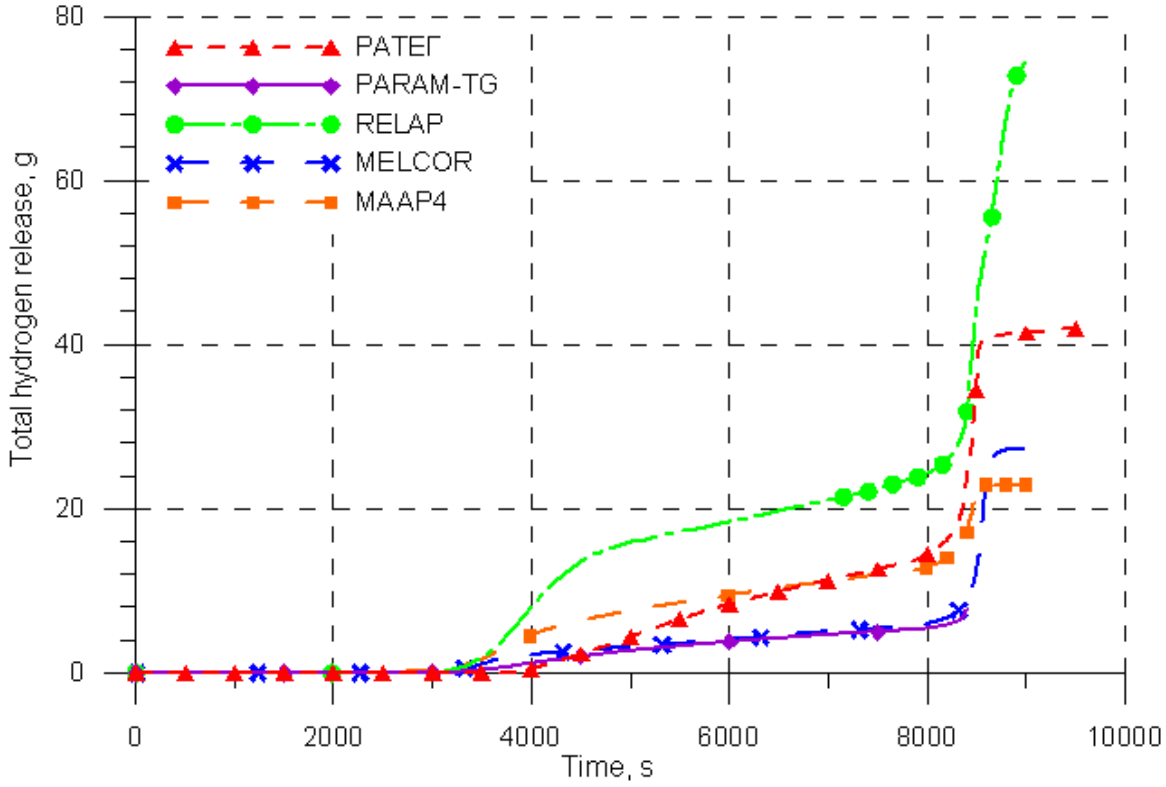

Figure 2.45 Hydrogen release

2.4.2 Cladding pre-oxidation calculation in the PARAMETER-SF1 experiment using the RAPTA-5 code

Analysis of the experimental data on isothermal oxidation of specimens made of alloy Э110 shows that the oxide film has a spalling structure at oxidization temperature below 1100°C. Therefore it is reasonable to minimize the time of reaching the isotherm 1200°C.

The following conditions of pre-oxidization are considered (Fig. 2.46):

1) 600 → 1100 °C during 1000 seconds;

2) 1100 → 1200 °C during 400 seconds;
3) isothermal exposure at 1200 °C.

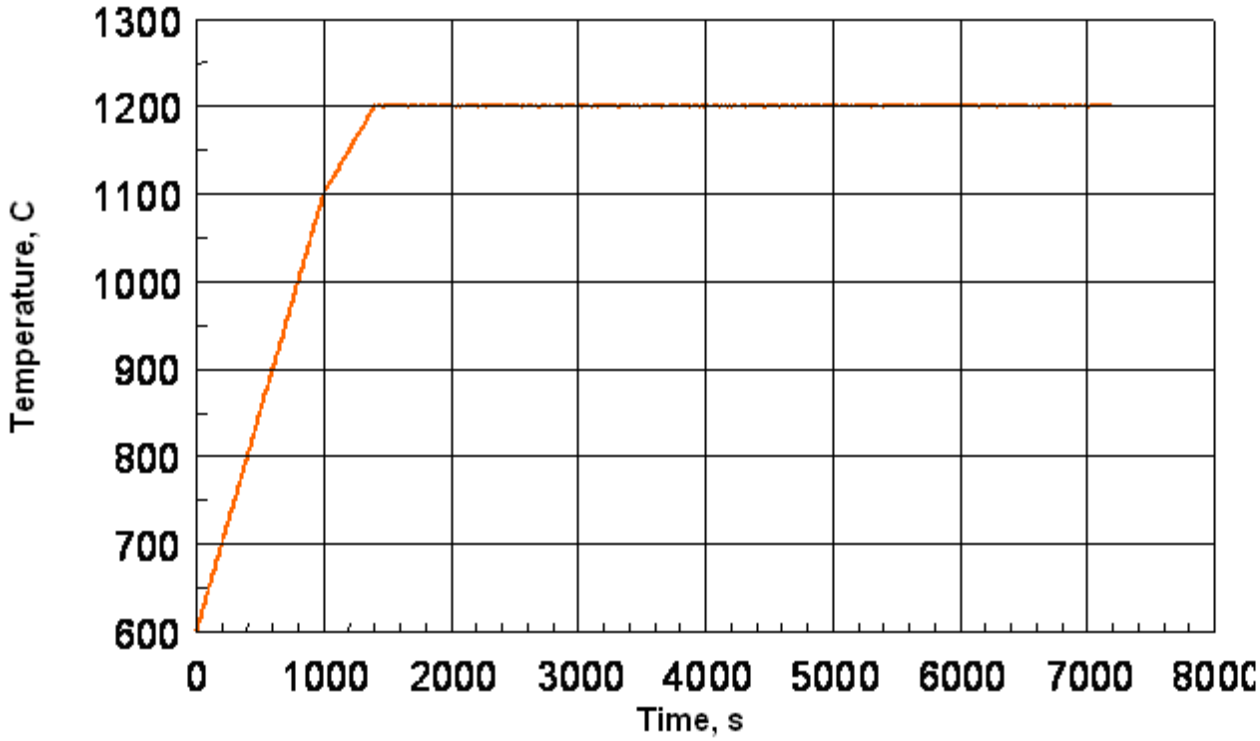

Figure 2.46 Temperature conditions of pre-oxidation

Figure 2.47 provides a comparison of the calculated oxidation kinetics (using weight gain as a measure of interaction of cladding material with steam), obtained with the code RAPTA-5 under the accepted temperature conditions, with the results of isothermal (time of reaching the isotherm of 1200 °C did not exceed 60 seconds) experiments on oxidation of Э110 alloy VVER cladding specimens on the facility with continuous recording of the speciment weight gain (the beginning of tests is combined with the moment of 1200 seconds of the running time). The obtained results shows that during the first 600 seconds the oxidation kinetics at temperature of 1200°C is well described by the realistic dependence for the weight gain implemented in the code RAPTA -5 [10]:

$W^2 = K \tau$,

$K = 1.59 \cdot 10^6 \exp (- 23040 / T)$ at $T < 1773K$, (1)

$K = 9.825 \cdot 10^5 \exp (- 20800 / T)$ at $T \geq 1773K$, where

W - specific weight gain, mg/cm^2 ,

τ - time, s,

K - reaction constant, $(mg/cm^2)^2 s^{-1}$,

T - temperature, K.

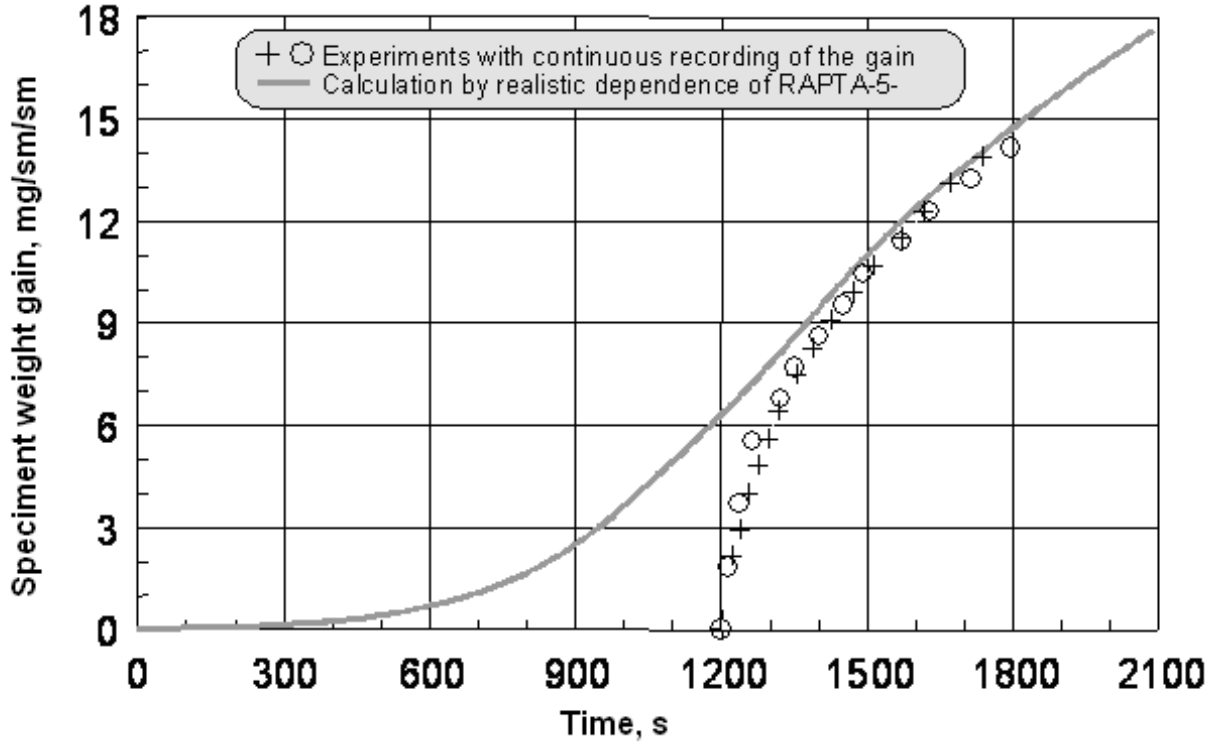

Figure 2.47 Oxidation kinetics during the initial stage of oxidation

Fig.2.48 presents the results of calculation data on oxide scale thickness under the given conditions of pre-oxidization using the code RAPTA-5.

Realistic dependence of the oxide layer thickness obtained on the basis of analysis of the experimental data for the temperature range 1173 – 1573 K has the form:

$$\Delta = 1.62 * 10^{-4} * \exp(- 13080 / T) \tau^{1/2}, \qquad (2)$$

where Δ – oxide thickness, μm.

"Conservative estimation" of the oxide layer thickness is obtained by the above-mentioned realistic dependence for the weight gain (1) under the assumption that the consumed oxygen transformed into the stoichiometric dioxide.

Fig.2.49 presents the equivalent cladding reacted layer (ECR) during the pre-oxidization phase at temperature 1200°C calculated with the use of the above-mentioned realistic dependence for the weight gain.

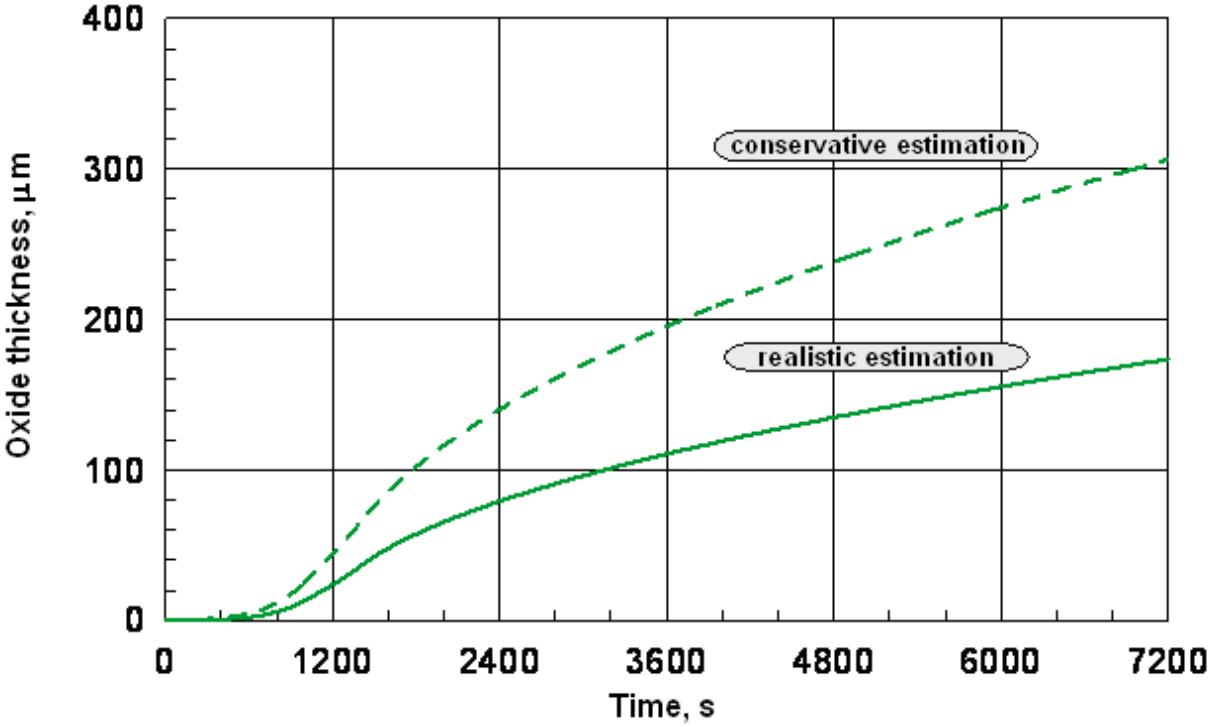

Figure 2.48 Cladding oxide layer thickness during the pre-oxidization phase

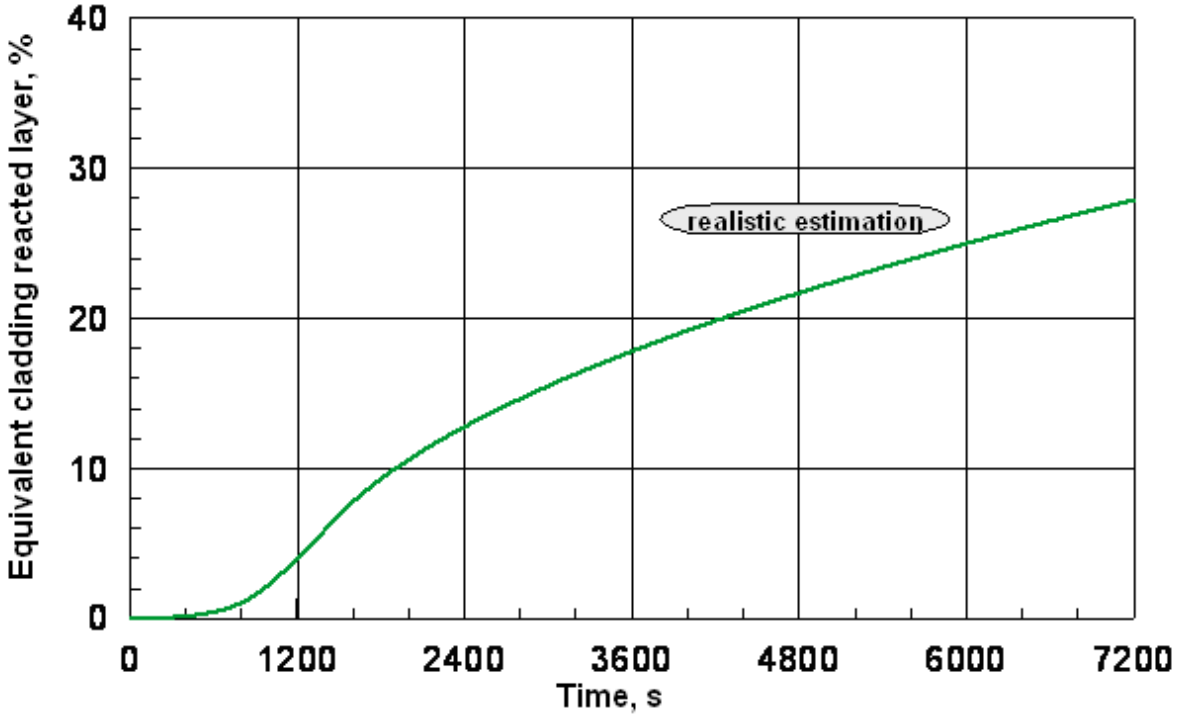

Figure 2.49 Estimation of the equivalent cladding reacted layer during the pre-oxidization stage

2.3.2 Description of the top flooding stage using the RELAP5/MOD3.3 code

The results of the numerical pre-test analysis of the SF1experiment were presented above only for the stage of the assembly heating. The results of the numerical pre-test analysis for the top flooding phase are given below.

The specific features of top flooding system of the experimental facility should be account for in nodalization scheme to correct modelling of the rewetting process. The top water is injected through the collector of top flooding system in the upper part of the test section and 20 capillary tubes, ∅3x0,16 located vertically from the collector through the isolation flange of the test section into the space between fuel rods of the upper part of the model FA. The length of capillary tubes below the

isolation flange is ~3-5 mm. Water of the top flooding system streams down from the capillary tubes inside the guiding cylinder, ∅ 69x2, enters the heated part of the model assembly into the space between the outer row of 12 simulators and the inner row of 6 simulators. In nodalization scheme the water injection system was modelled by the node with the cross-section being equal to 20 capillary tubes one and with hydraulic diameter equal to the capillary tube inner diameter with designed water flow rate. Water is supplied to the hydraulic element of the nodalization contacting the wall and the outer row of simulators. Results of calculations for the two versions of power supply and temperature of steam for two channels are presented in Figs. 2.50÷2.53.

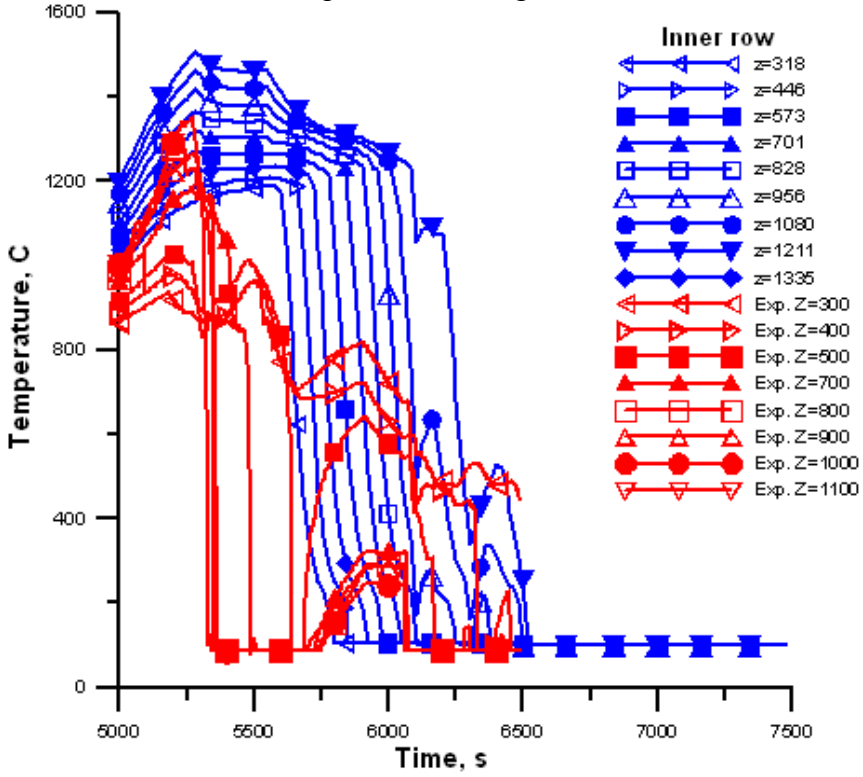

Figure 2.50 Temperature for the inner channel (row) during the flooding phase (version 1)

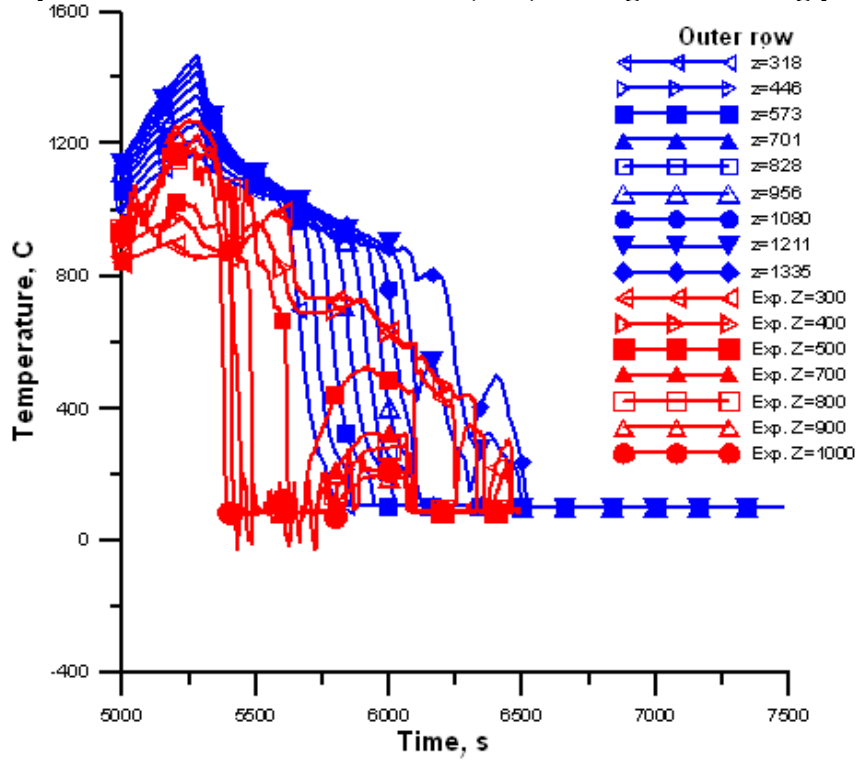

Figure 2.51 Temperature for the outer channel (row) during the flooding phase (version 1)

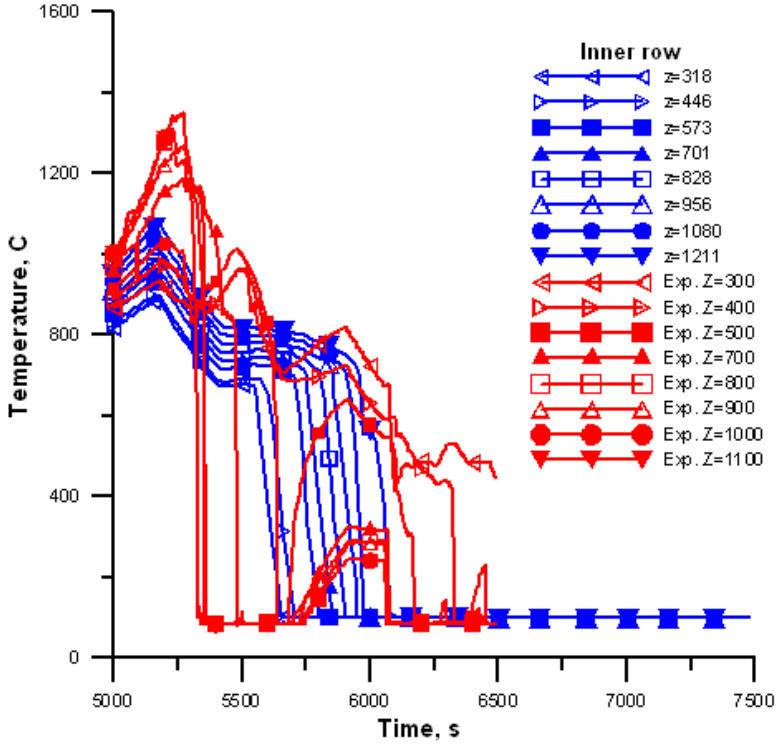

Figure 2.52 Temperature for the inner channel (row) during the flooding phase (version 2)

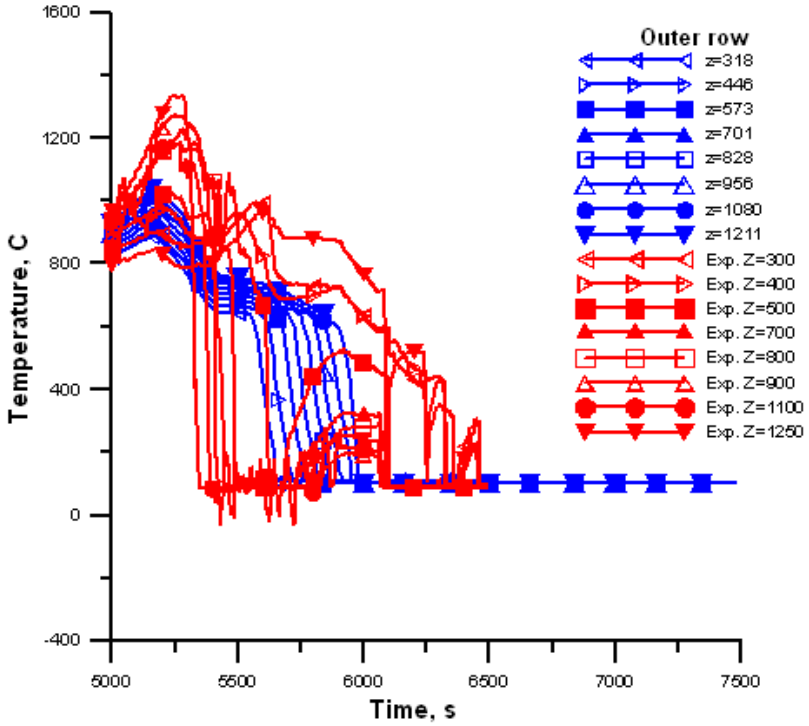

Figure 2.53 Temperature for the outer channel (row) during the flooding phase (version 2)

The following conclusions can be made by these calculations.

In the experiments the lower part of the inner row of simulators and the middle of the outer row rewet first of all, but the rewetting front moves from top to bottom. The upper part of the inner and outer rows of simulators and the lower part of the outer row are rewetted considerably later than other parts.

In the calculations the cooling front always moves from bottom to top, with this, for the inner row the temperatures remain higher for a longer time, but then the process of rewetting is accelerated. The process of the temperature reincreasing that could be recorded in version 1 because there were time intervals with short-term power increase, was not recorded practically. Temperature level in version 2 is somewhat lower in comparison with version 1.

3 Post-test analysis of the PARAMETER-SF1 experiment

On the basis of the experiment scenario and considering the obtained experimental data on FA temperature behaviour, hydrogen release, results of material studies, designed features of the test section, the following basic processes governing the assembly behaviour and its state after the tests should be consider:

- the fuel rod simulators heating-up du to electric power supply within the flow of argon and steam-argon mixture;
- steam condensation on the facility body;
- convective and radiative heat transfer between the coolant, fuel rod simulators and shroud, heat transfer by heat conduction from the shroud into thermal insulation;
- steam leakages into process channels (bypassing);
- thermal insulation wetting;
- oxidation of fuel rods and shroud;
- zirconium melting;
- fuel dissolving with melt;
- dissolving of oxide films;
- restriction of cooling water entering during top flooding stage due to counter steam flow (CCF phenomenon);
- melt relocation;
- melt oxidation;
- melt solidification and blockage formation.

It should be noted that some of the mentioned processes (condensation, bypassing) are specific for the SF1experiment, they occur du to design peculiarities of the test section.

In the lower and upper part of the tests section there are no shroud and thermal insulation, the steam directly contacts the inner surface of the test section body. With rather cold body a condensation of the hot steam entering the assembly is possible. The steam condensed in the assembly upper part can penetrate the thermal insulation through holes in the zirconium plate, made for insertion of thermocouples into the thermal insulation. It should be also noted that the test section provides with water cooling system for the test section body. Apparently switching on the body cooling system at 10250 s resulted in more intensive steam condensing in the lower and upper parts on the bundle.

It should be also noted that during visual examination of the assembly after the experiment it was revealed that the bottom head, isolating the thermal insulation from the steam-gas mixture, was broken. Therefore the steam-gas mixture entering the assembly could partially penetrate the process gaps between the thermal insulation and the shroud as well as between the thermal insulation shroud and the test section body. Evidently, this loss of integrity is also caused by switching on the cooling system.

Steam condensation and bypassing results in decreasing in steam flow through the assembly. The decreased steam flow through the assembly does not lead to the conditions of “oxygen starvation” (such a conclusion is made from the analysis of the SOV-3 hydrogen content measuring system readings, indicating the continuous rise in hydrogen concentration), however it should affect the assembly temperature behaviour by means of heat transfer processes between the steam and assembly components (fuel rods, shroud). Thermocouples readings confirm this conclusion: the assembly hottest zone displaces gradually down from the level of ~1250 mm to the level of ~1100 mm.

Steam condensation and bypassing complicate the task of assessing of self-consistency of the SF1 experimental results: alongside with the uncertainty of experimental data (coolant flow rate through the assembly under the conditions of failure of fuel rods and the surrounding structures; damage of shroud and thermal insulation leading to reduction in cooling the melt nucleus, numerous failure of thermocouples at high temperatures) some uncertainty is added in the steam flow rate through the intact assembly.

The initial conditions of the experiment PARAMETER-SF1 include the values of temperatures in the assembly, shroud, insulation, body at the beginning of the experiment (t=0), corresponding to room conditions, the axial and the angular (if we consider absence of axial symmetry) dependences (profiles) of these temperatures. The same time moment (t=0) is assumed at

the moment of the beginning of modelling using various computer codes. In modelling with all codes, except for the code PARAM-TG, the axial symmetry was supposed.

The boundary conditions of the experiment SF1 include a wider list of not only temperature, but also thermohydraulic parameters including temperatures and conditions of heat transfer at the boundaries of the test section as well as the flow rate and temperature of steam and argon entering the test section, pressure at the test section outlet. With this, all the parameters are assigned for the whole temperature range from t=0 to $t=t_{end}$, corresponding to the experiment scenario. The list of the boundary conditions includes also the temperature and flow rate of water supplied to the assembly under flooding.

3.2 Post-test calculations using codes RATEG/SVECHA, ICARE, RELAP, MAAP4, PARAM-RG

Considering the uncertainties in the steam flow rate through the assembly for the adequate numerical analysis of the experiment the additional modelling of the steam condensation processes and its bypassing is necessary. Uncertainties in the times of forming the bypasses, size of unsealing zones and other factors allow to give only the approximate description of the bypassing phenomenon. Figs. 3.1 – 3.2 present the calculated data on the flow rate of steam and argon through the assembly, obtained with the use of RATEG/SVECHA code as a result of self-consistent numerical analysis. Users of other codes assigned the flow rate as the approximation (see Figs. 3.1 – 3.2). For comparison the plots show the indications of the test facility flow metering devices reflecting the flow rate of steam and argon at the assembly inlet.

Fig. 3.3 presents the value of the supplied electric power, and Fig. 3.4 presents the value of Joule heating power in the heated section (along the tantalum heater). It is seen from Fig. 3.4 that almost for all codes (except for the MAAP4code) the values of Joule heating power in the heated section are practically similar.

Figs. 3.5 –3.7 present the calculated data on coolant temperature at three elevations and the corresponding thermocouples readings.

Figs. 3.8 – 3.13 present the calculated data on cladding temperatures of fuel rods of the 2nd row and the corresponding thermocouples readings, Figs. 3.14 – 3.19 - for fuel rods of the 3rd row. Figs. 3.20 – 3.22 present the calculated data on claddings oxide scale thickness.

On the whole, all the computer codes give satisfactory description of fuel rod cladding temperature behaviour during first 10000 seconds of the running time. The calculated data are in good agreement with each other, as well as with thermocouples readings. Beginning from 10000 second the results of the calculation of cladding temperature behaviour at the levels of 1100-1300 mm become different. It should be noted that this is the hottest part of the assembly, the cladding temperature at these levels is very sensitive to steam flow rate due to considerable contribution into the total heat balance from the processes of cladding cooling with steam. At the pre-oxidization stage this difference reaches 600 degrees (at the elevation of 1300 mm). It can be supposed that causes of the difference are the simplified modelling of condensing and bypassing. The difference becomes still greater at the end of transient phase (just before flooding). A number of codes (RATEG/SVECHA, ICARE) show that during this time period the melting of metal zirconium occurs in the assembly – the calculated temperatures exceed 2000◦C.

Fig. 3.23 presents the hydrogen release. We can see a qualitative agreement of the calculated and experimental data. The main difference is at the end of the transient stage and during the flooding stage. Just during this period the zirconium melting occurs, as well as release of the formed melt on fuel rod surfaces and its rapid oxidation. The codes simulating these processes show a high hydrogen release. However from a comparison of the calculated and experimental data it is seen that all the codes used for post-test numerical analisys underestimated mass of hydrogen released in the course of the experiment.

The more detailed numerical analysis of the experiment base stages by SOCRAT (RATEG/SVECHA) code is presented below.

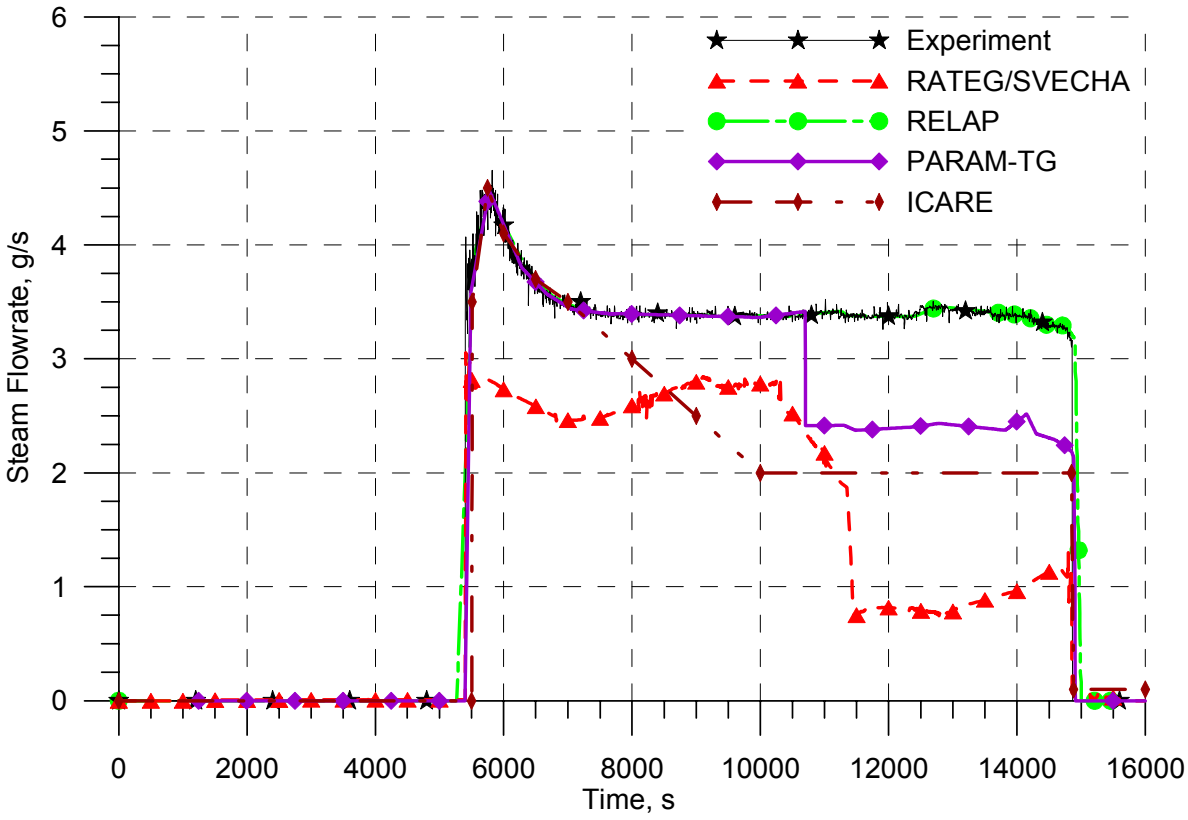

Figure 3.1 Steam flow rate (at the assembly inlet) and its calculated approximations (through the assembly)

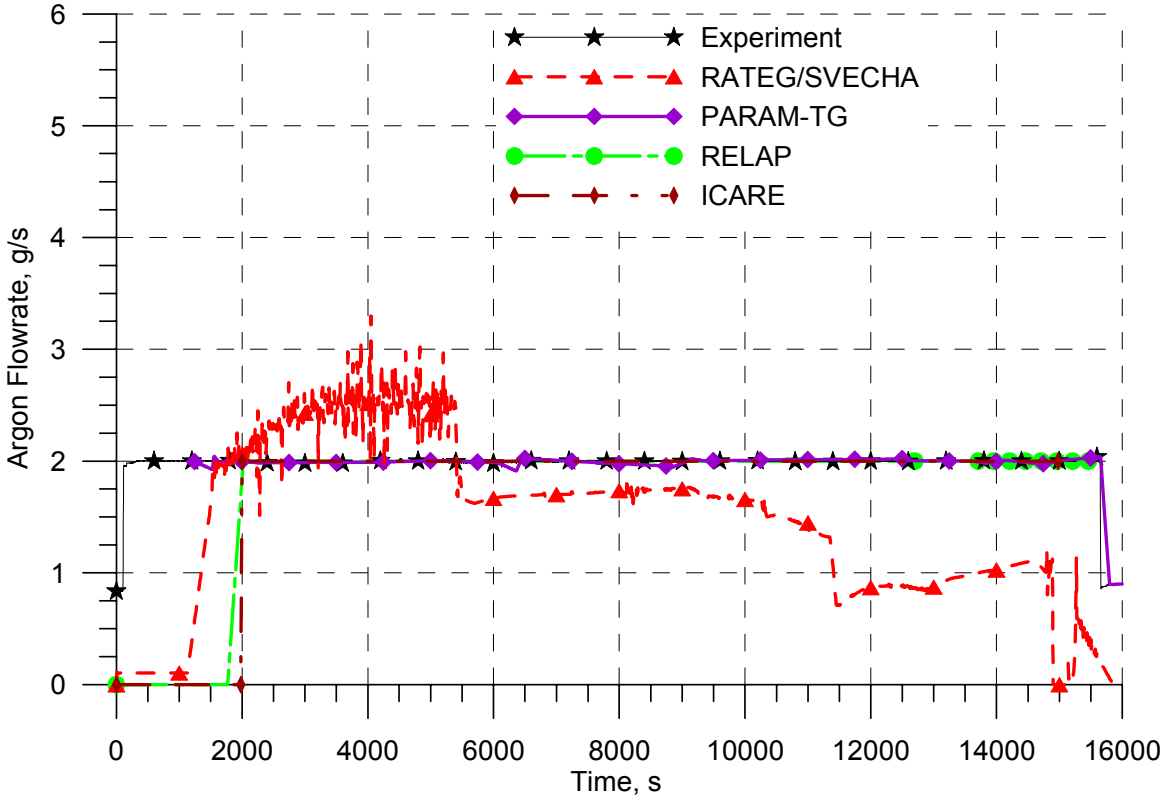

Figure 3.2 Argon flow rate (at the assembly inlet) and its calculated approximations (through the assembly)

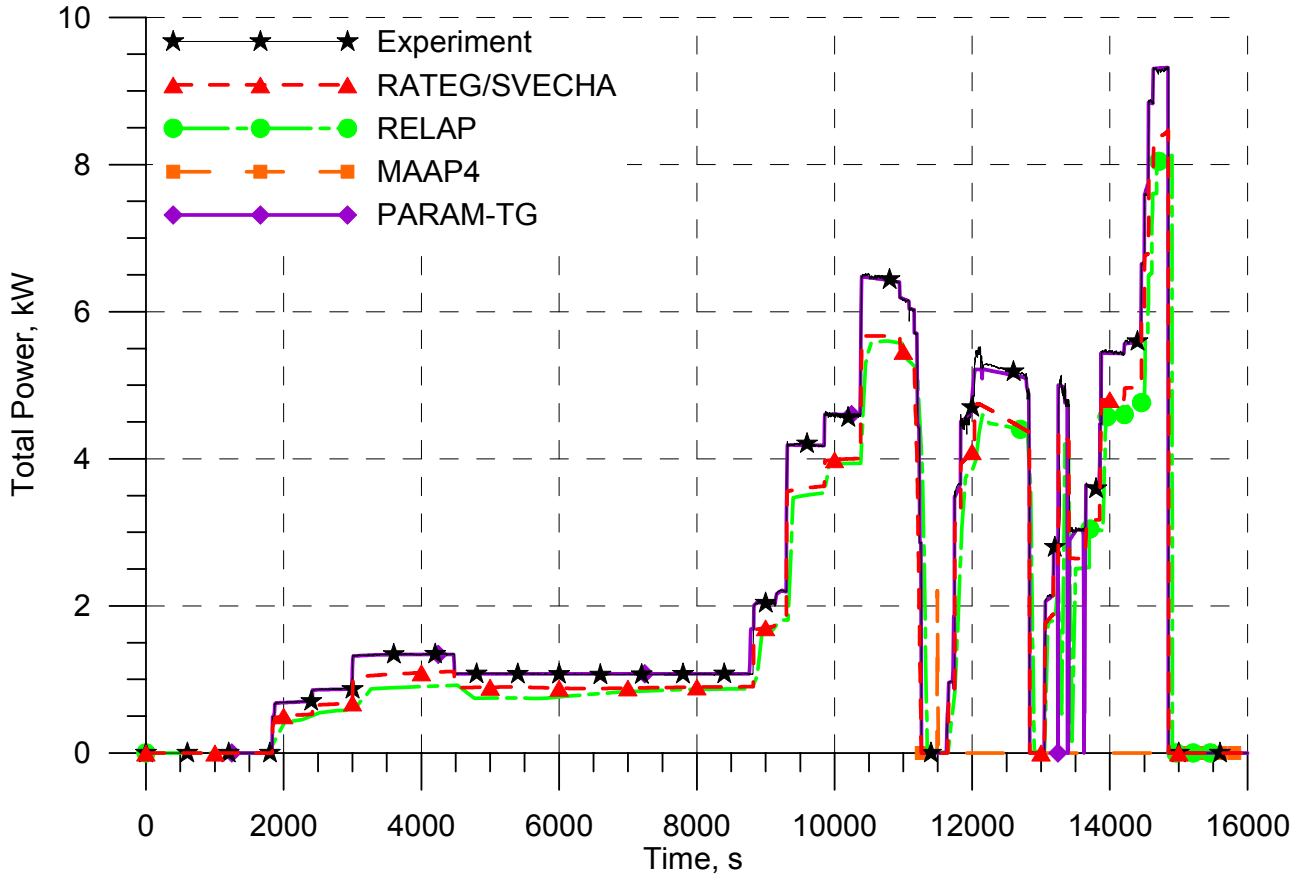

Figure 3.3 Electric power supply

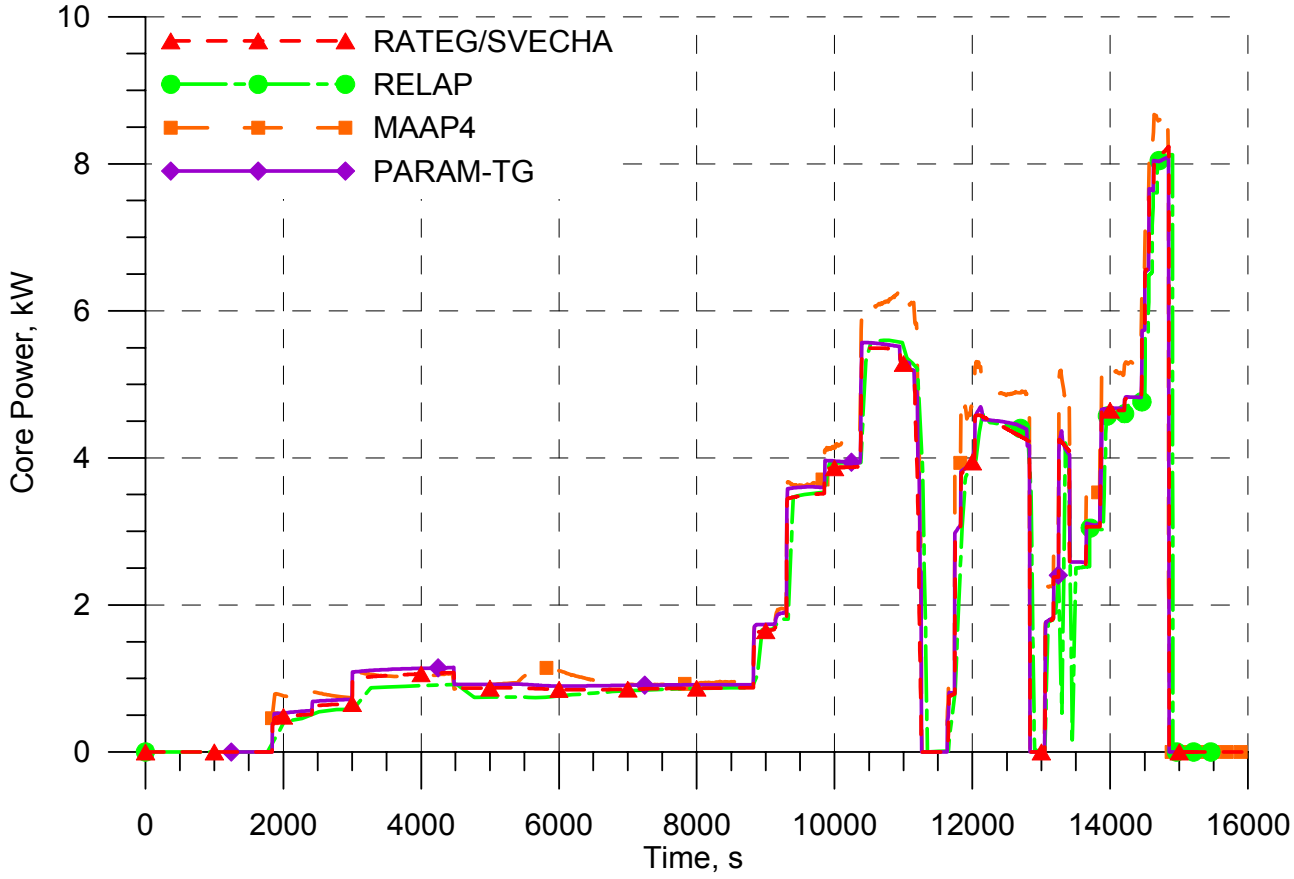

Figure 3.4 Joule heating power

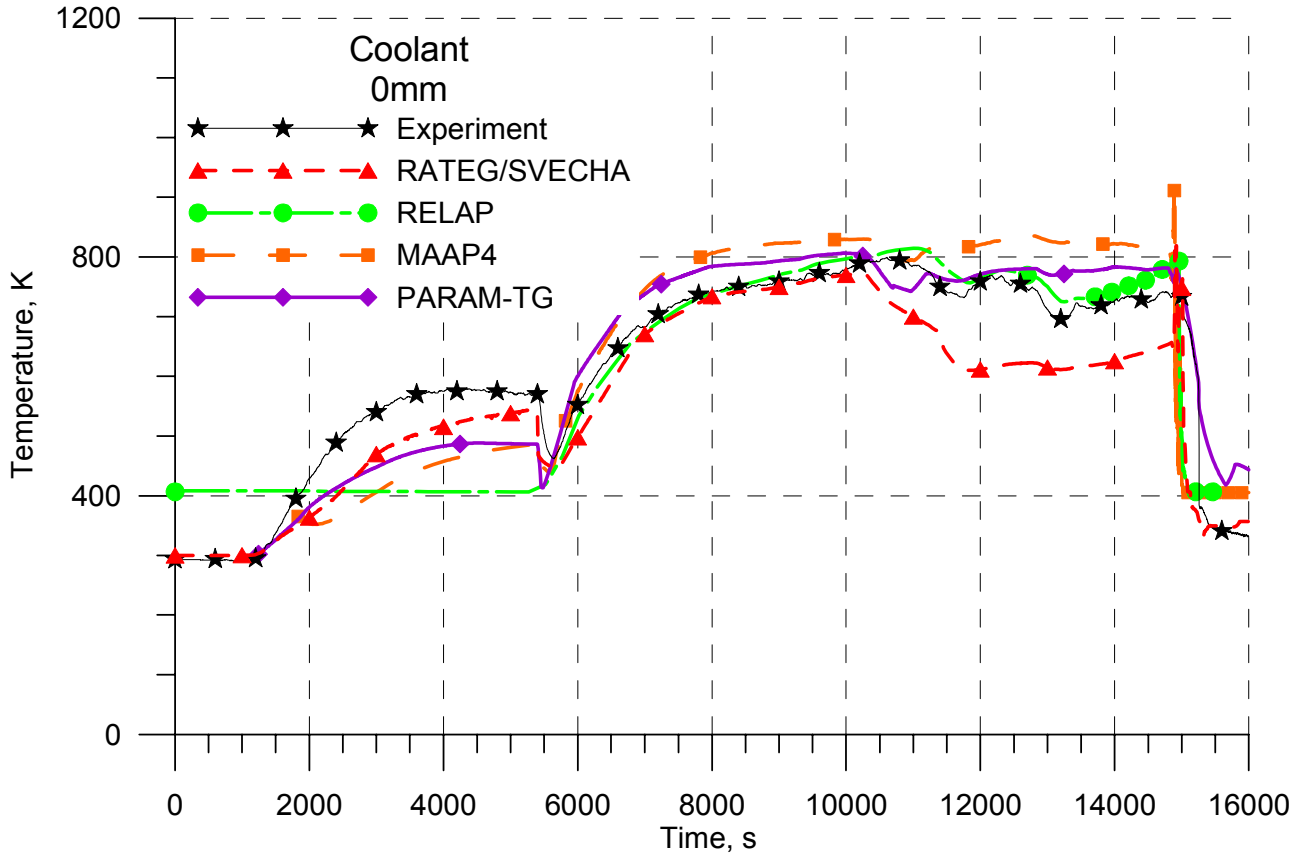

Figure 3.5 Temperature of steam-gas mixture at the lower elevation of heated part (0 mm elevation)

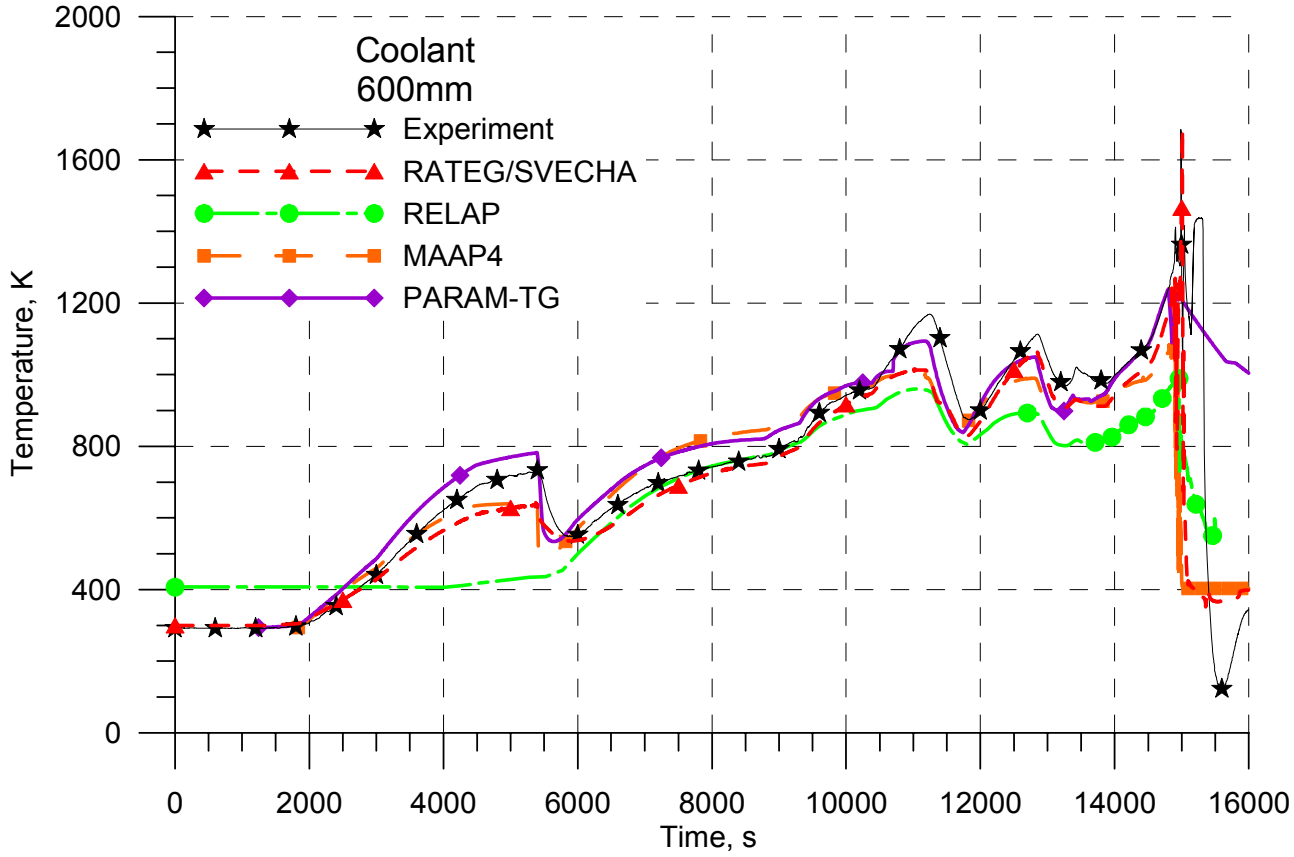

Figure 3.6 Temperature of steam-gas mixture at the ekevation of 600 mm

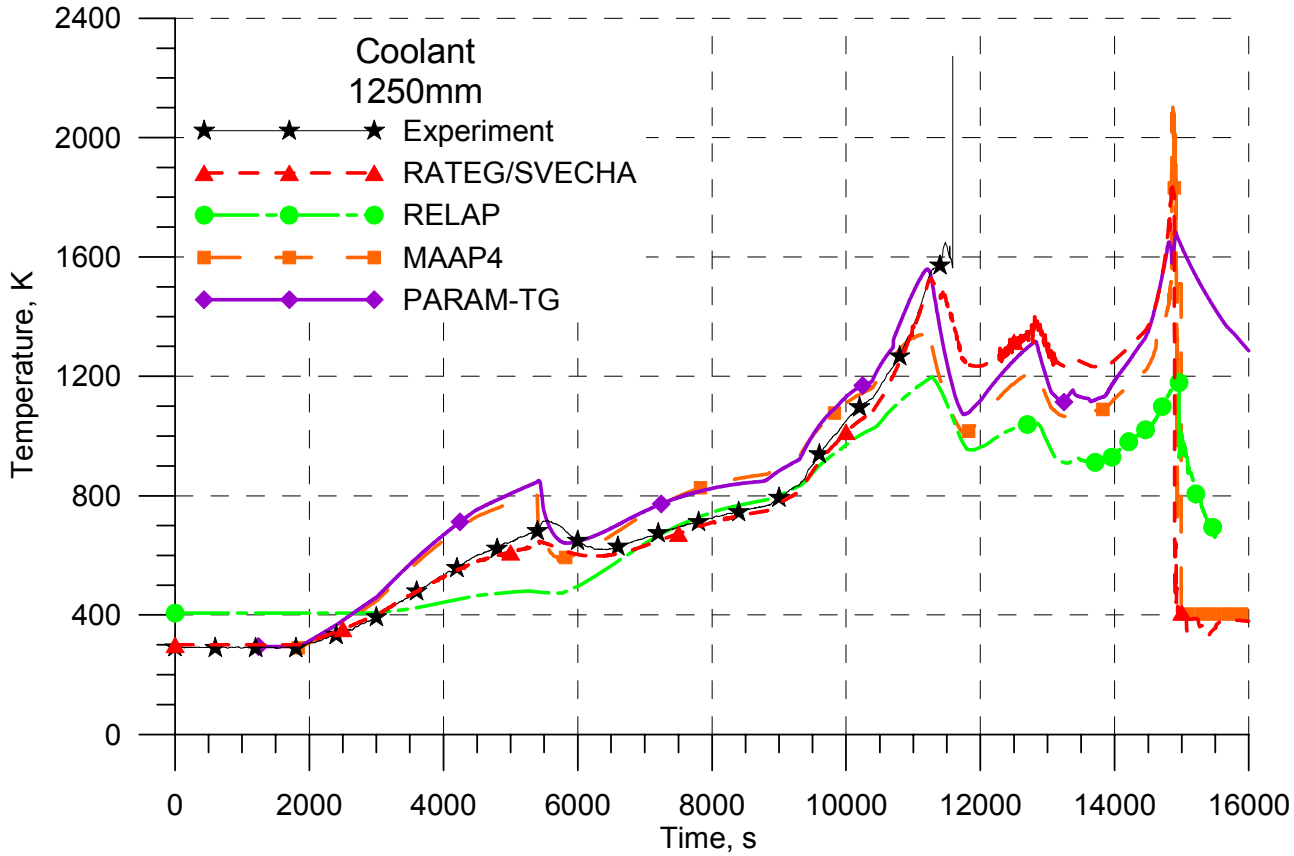

Figure 3.7 Temperature of steam-gas mixture at the elevation of 1250 mm

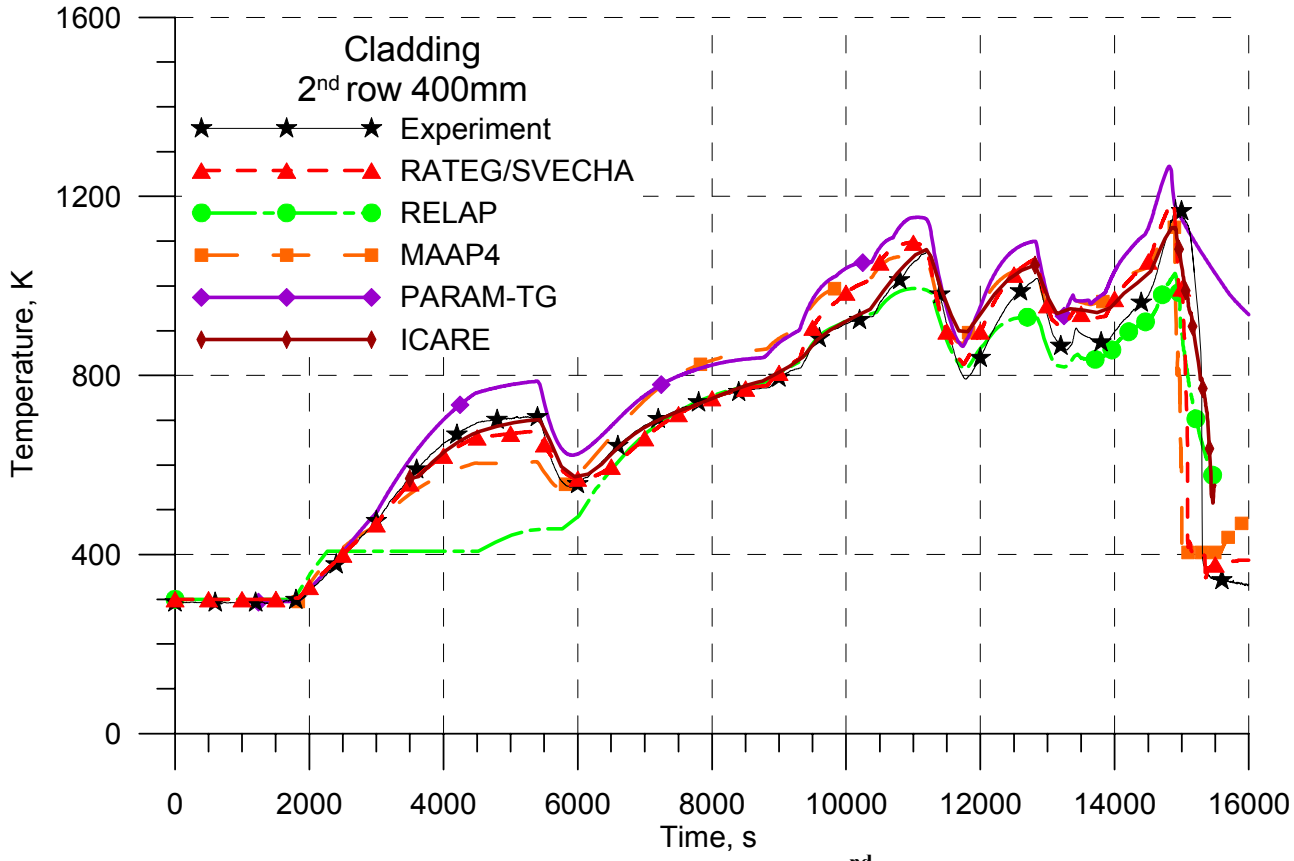

Figure 3.8 Temperature of claddings of the fuel rods of the 2nd row at the elevation of 0 mm

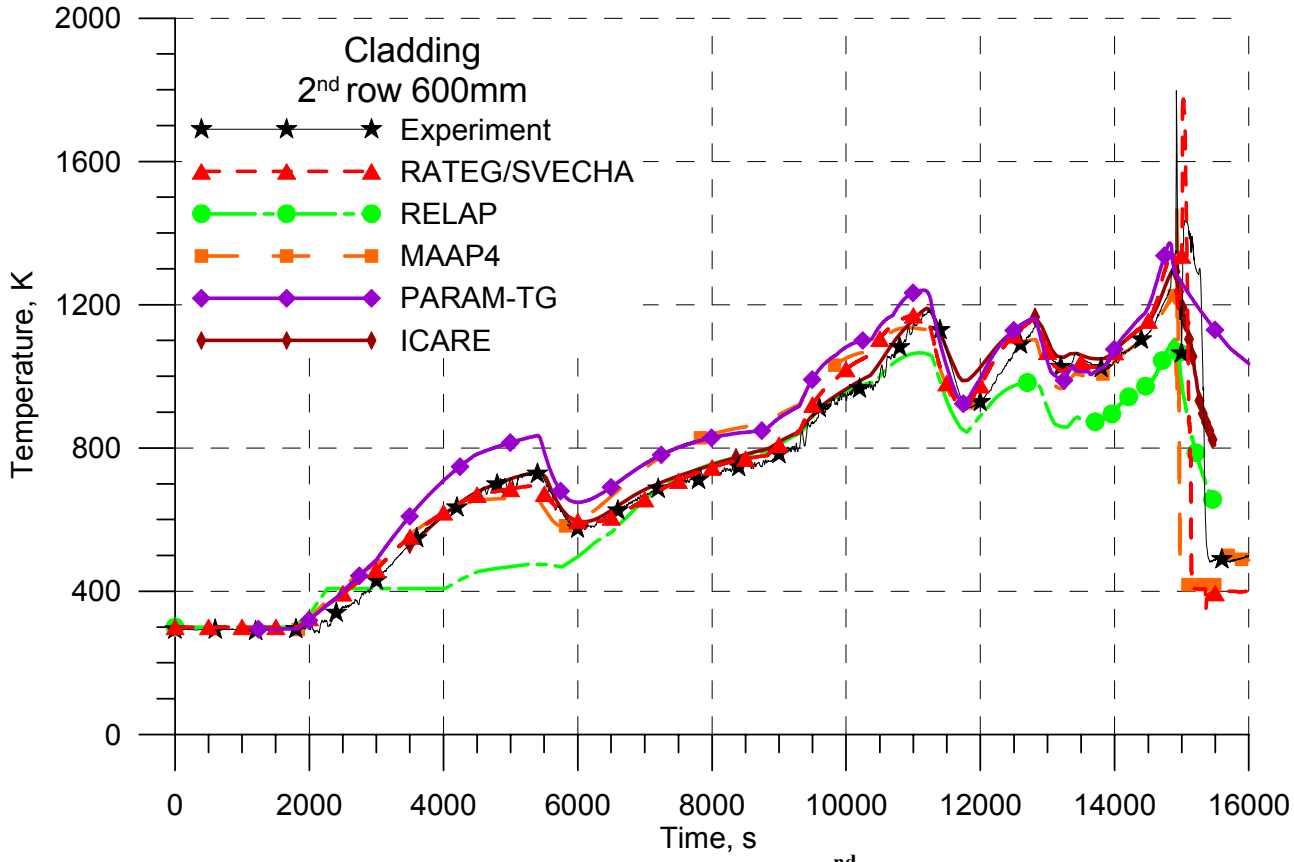

Figure 3.9 Temperature of claddings of the fuel rods of the 2nd row at the elevation of 600 mm

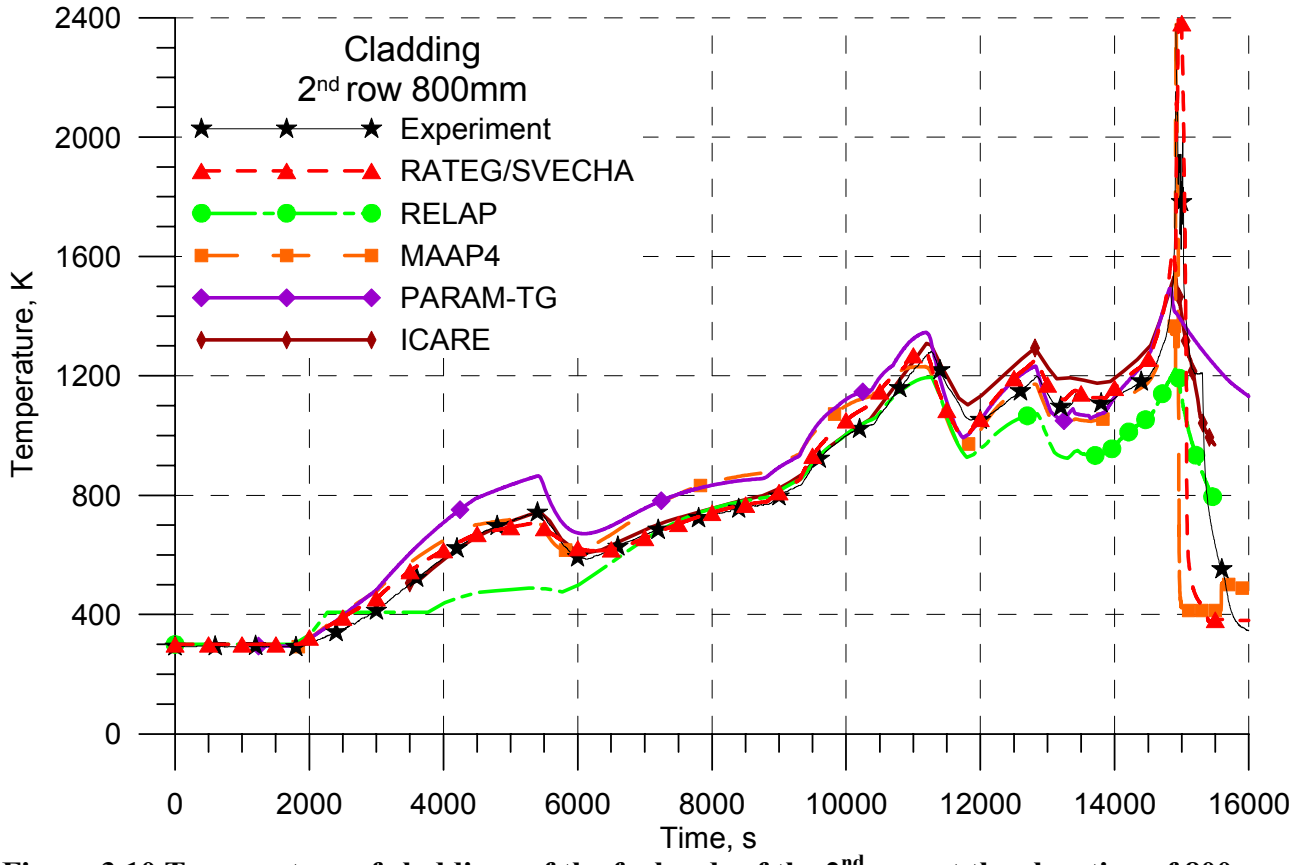

Figure 3.10 Temperature of claddings of the fuel rods of the 2nd row at the elevation of 800 mm

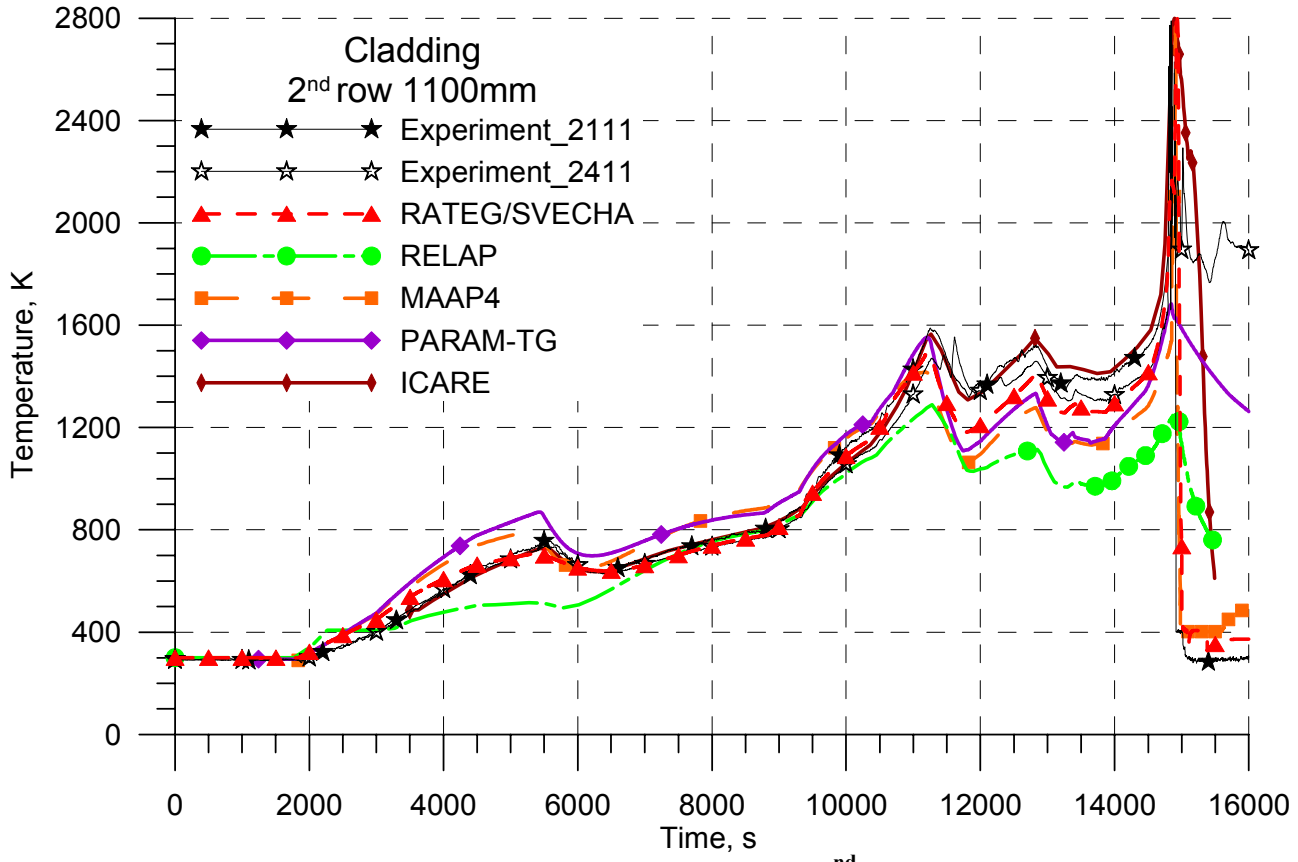

Figure 3.11 Temperature of claddings of the fuel rods of the 2nd row at the elevation of 1100 mm

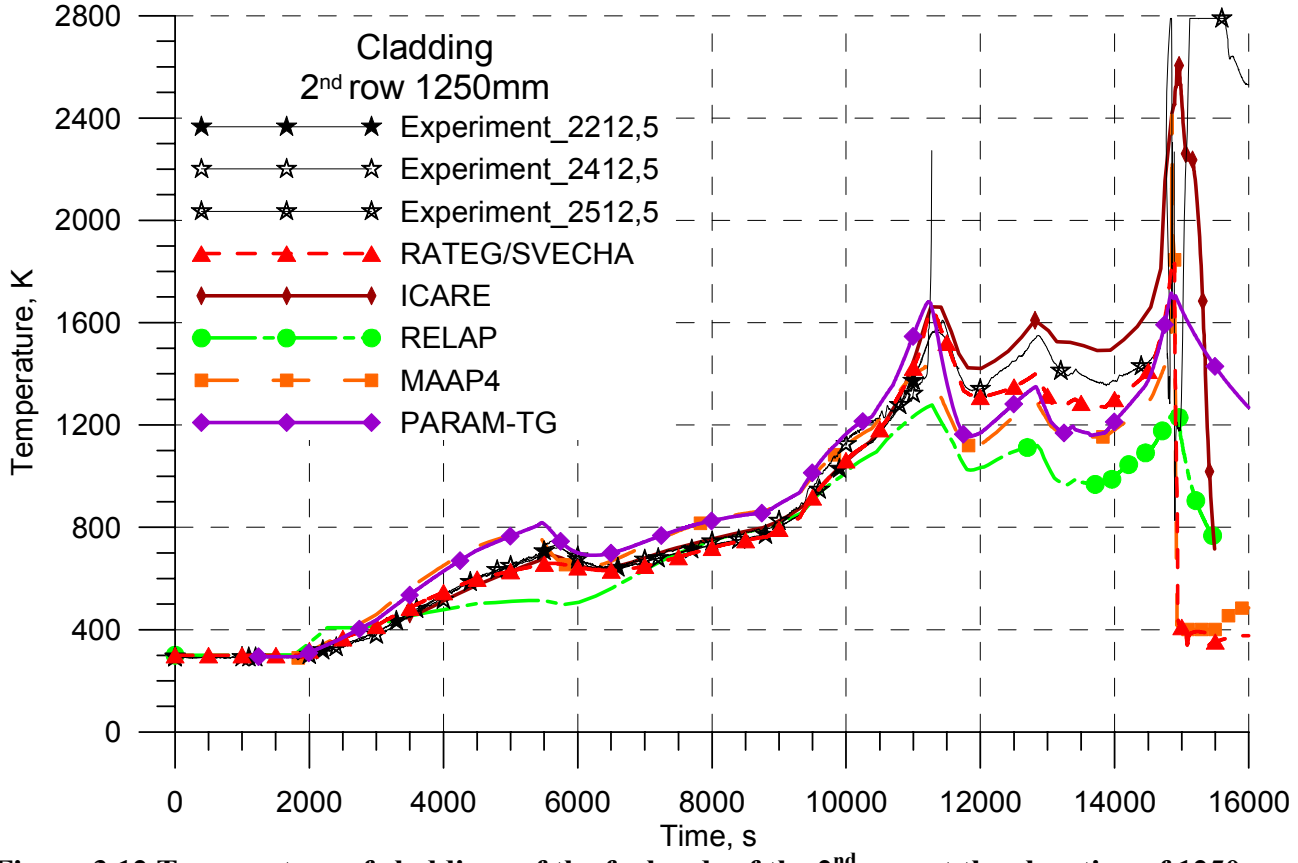

Figure 3.12 Temperature of claddings of the fuel rods of the 2nd row at the elevation of 1250 mm

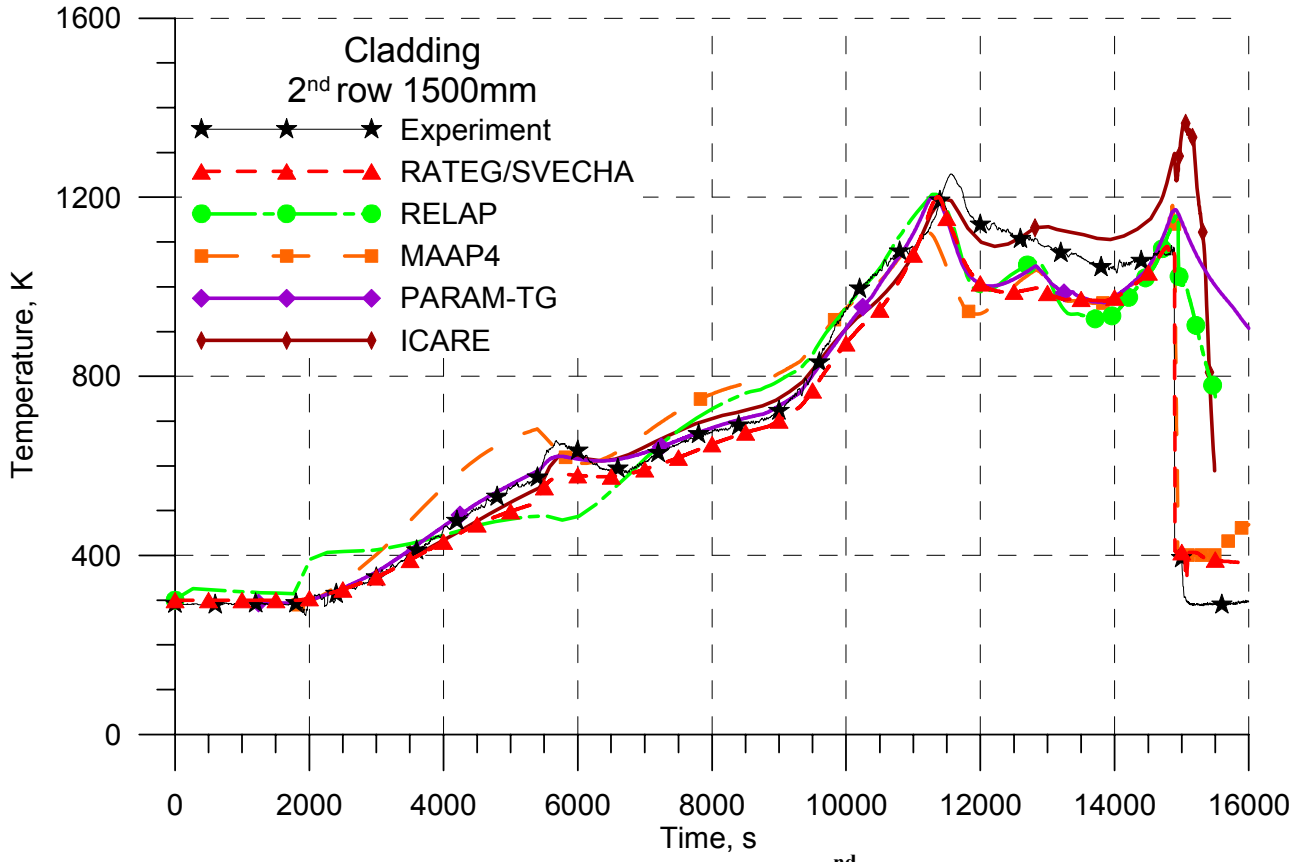

Figure 3.13 Temperature of claddings of the fuel rods of the 2nd row at the elevation of 1500 mm

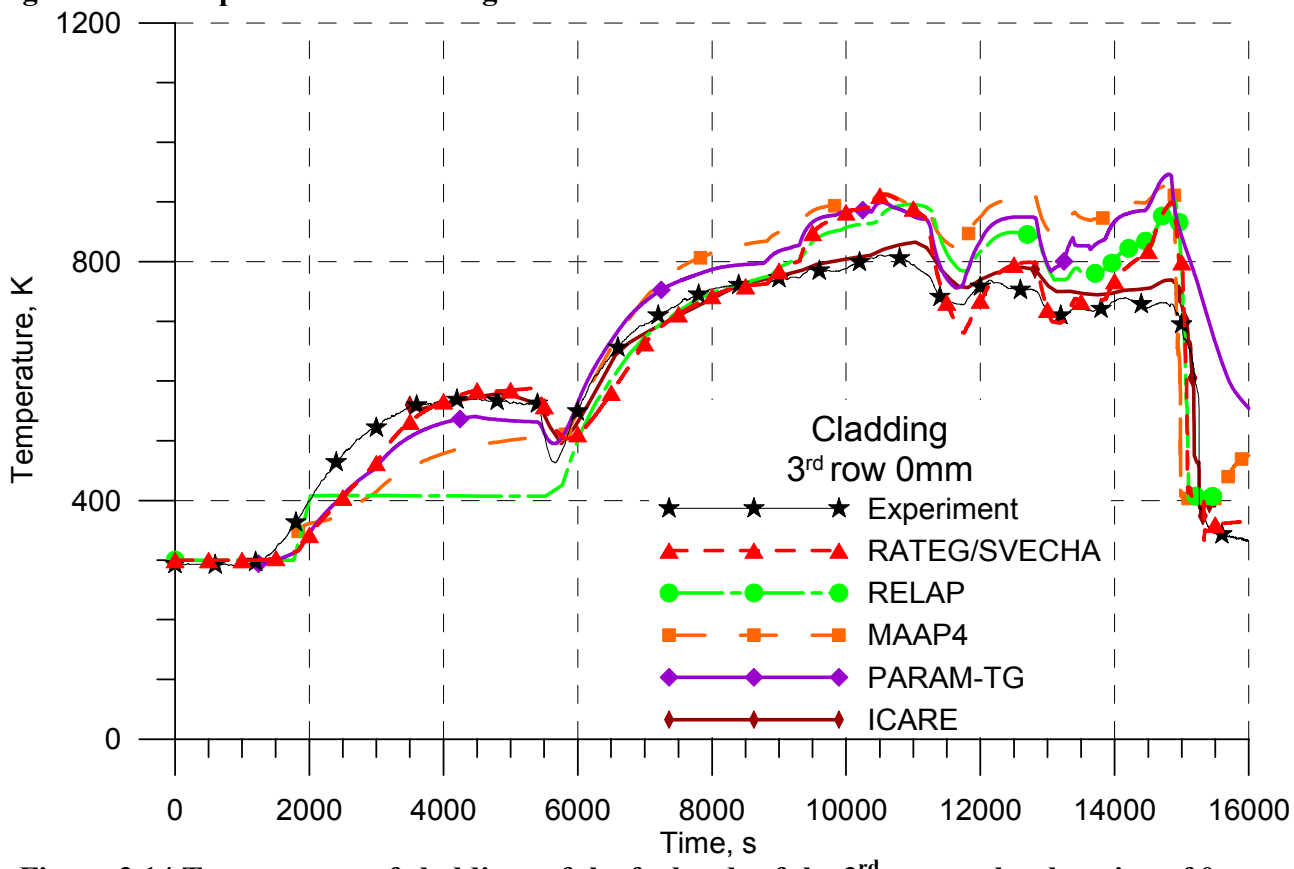

Figure 3.14 Temperature of claddings of the fuel rods of the 3rd row at the elevation of 0 mm

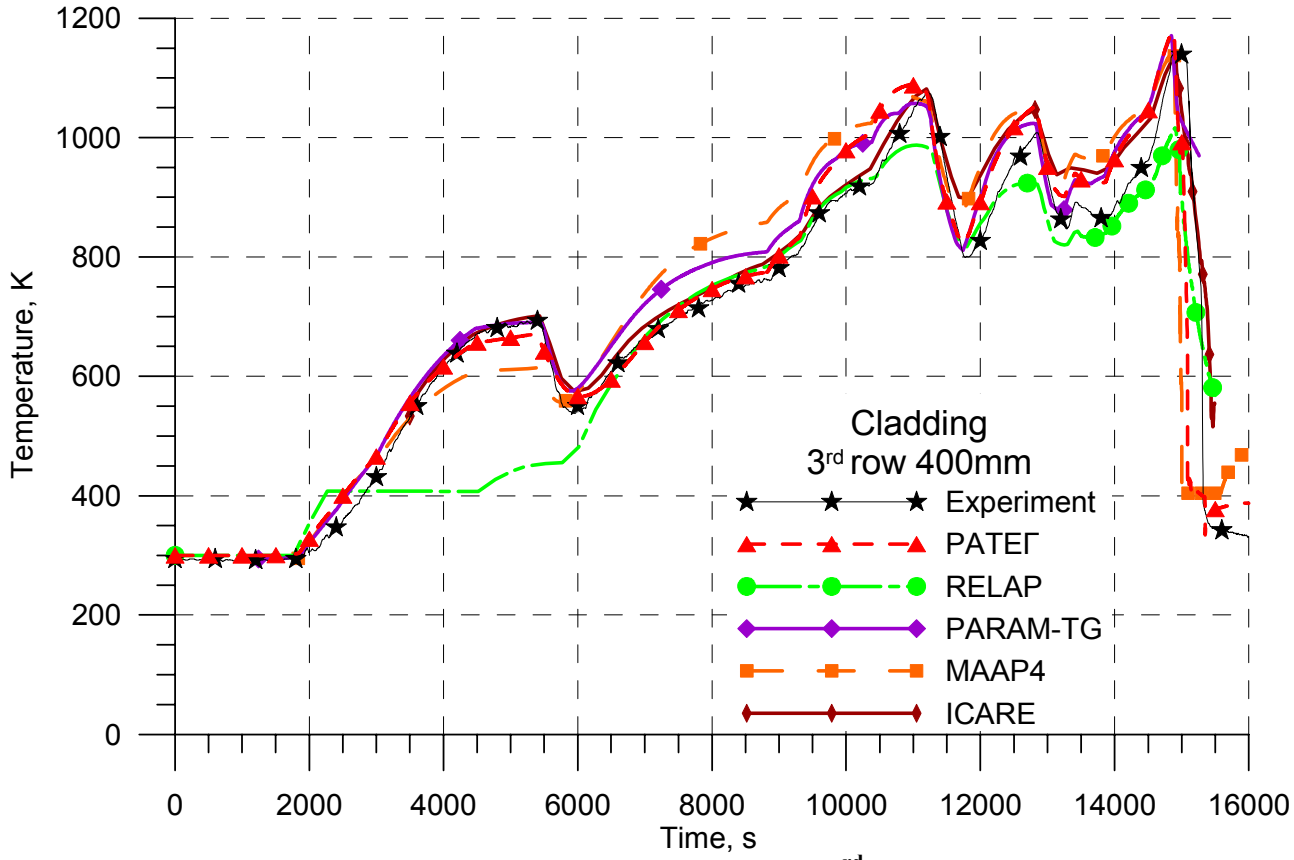

Figure 3.15 Temperature of claddings of the fuel rods of the 3rd row at the elevation of 400 mm

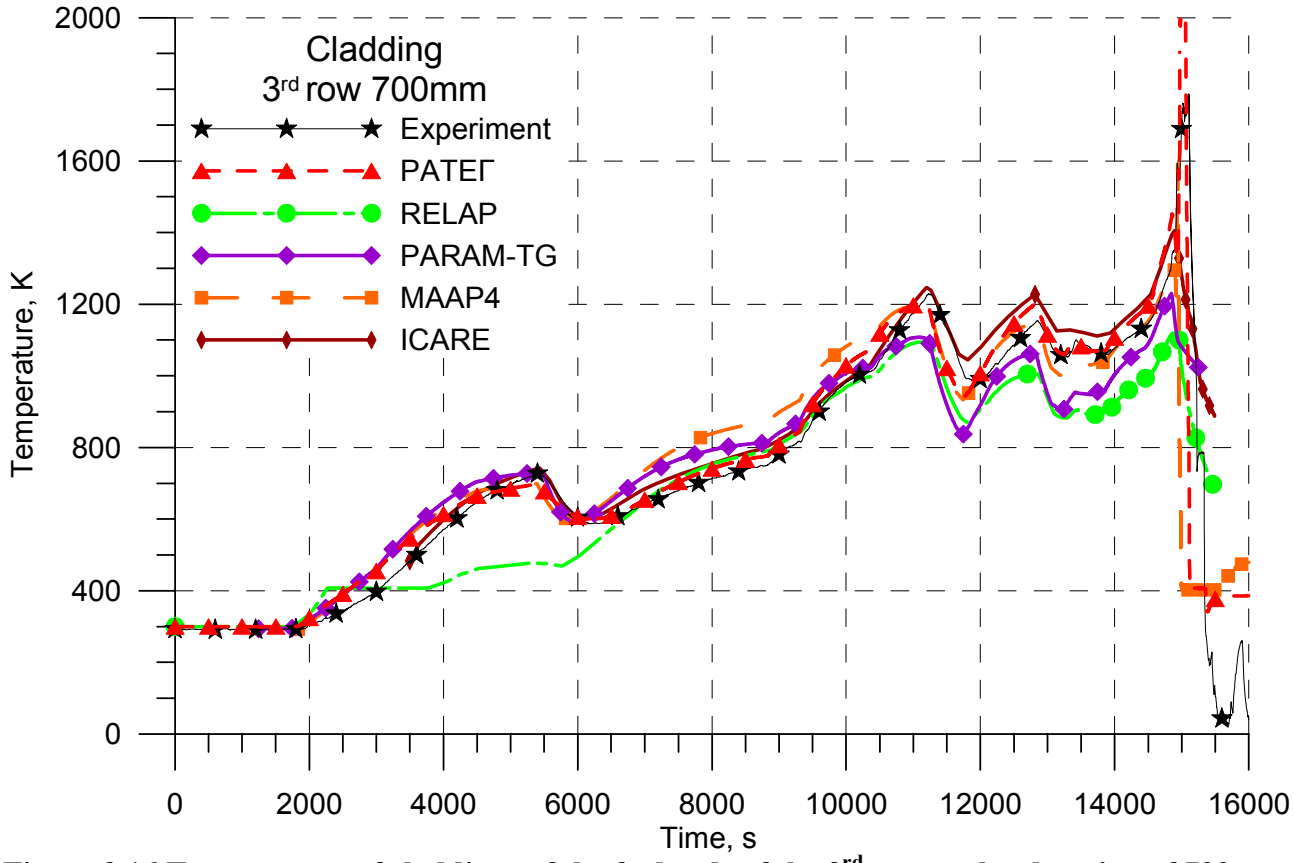

Figure 3.16 Temperature of claddings of the fuel rods of the 3rd row at the elevation of 700 mm

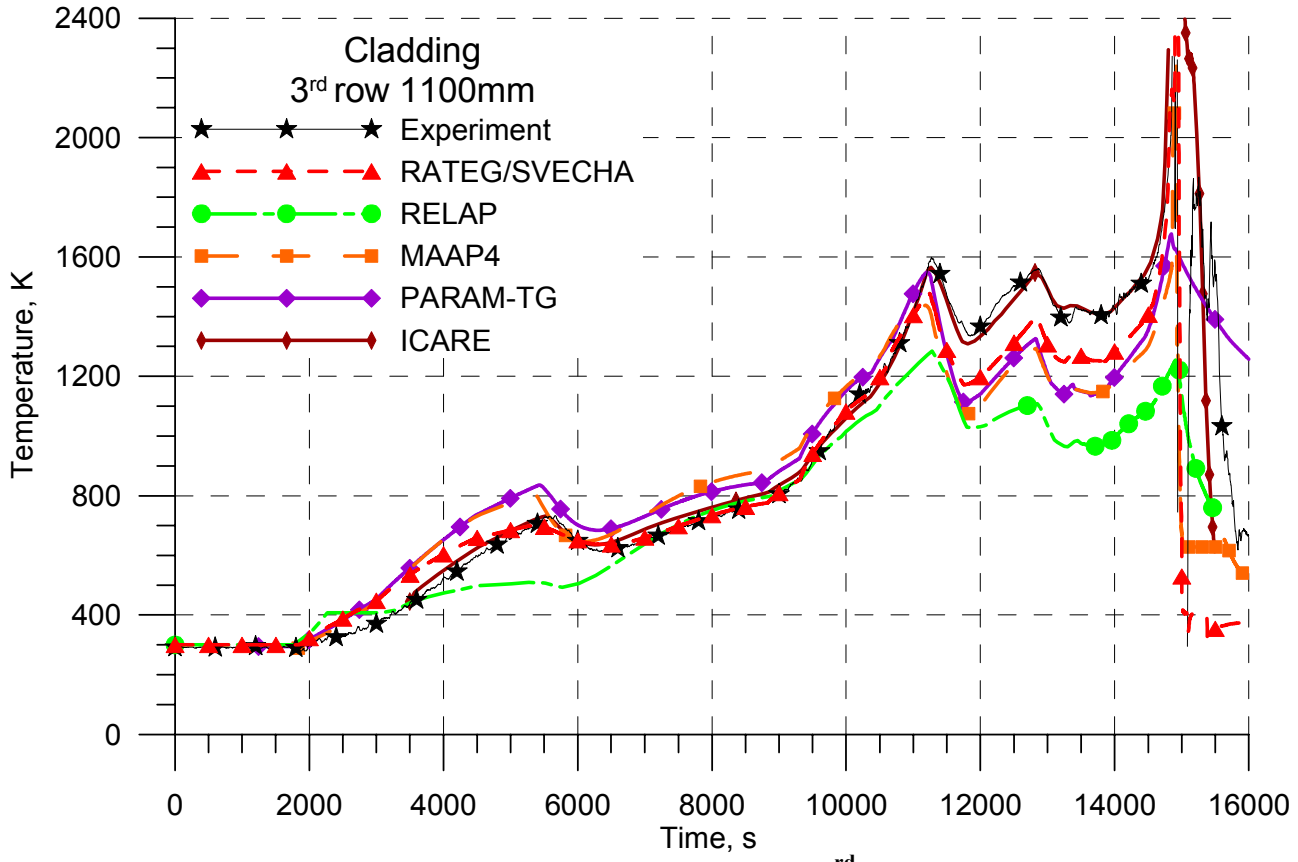

Figure 3.17 Temperature of claddings of the fuel rods of the 3rd row at the elevation of 1100 mm

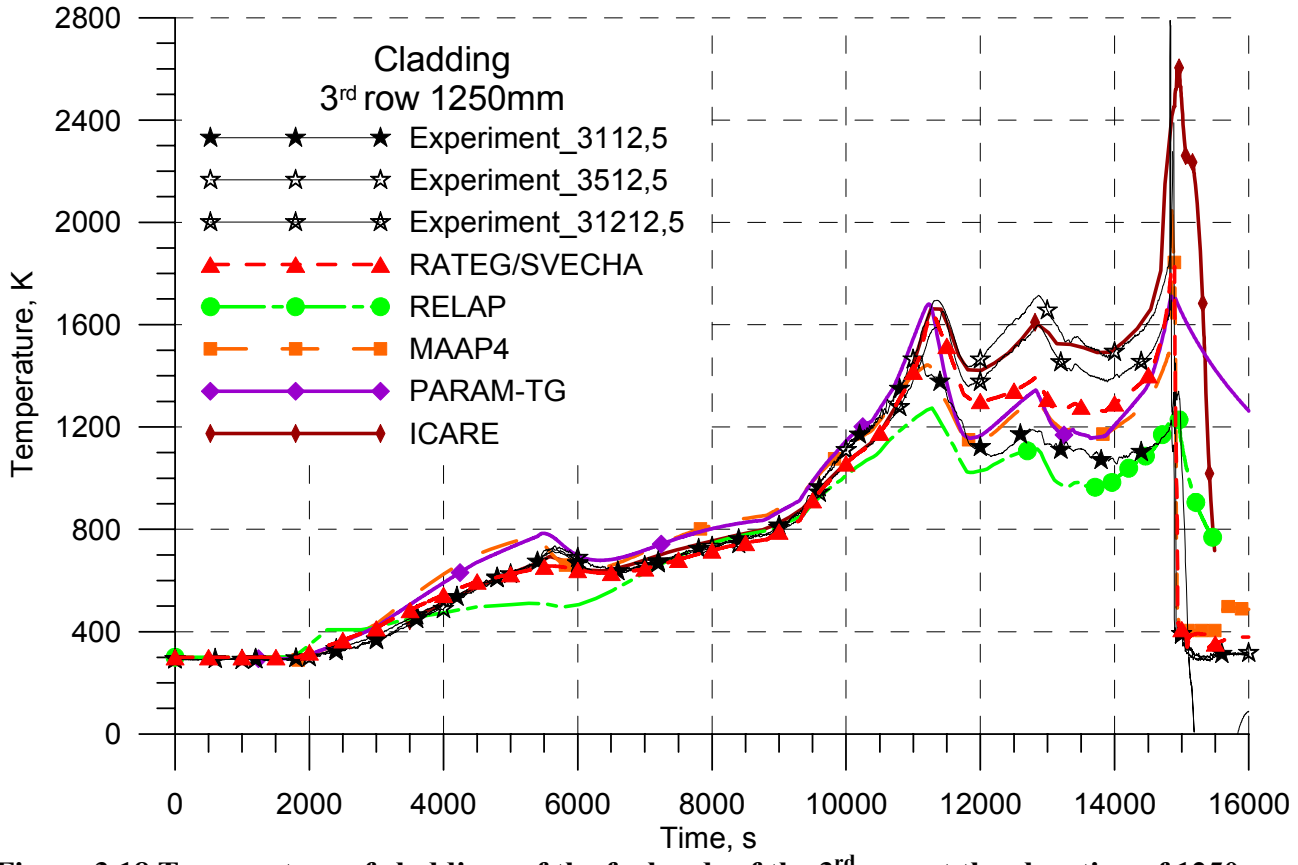

Figure 3.18 Temperature of claddings of the fuel rods of the 3rd row at the elevation of 1250 mm

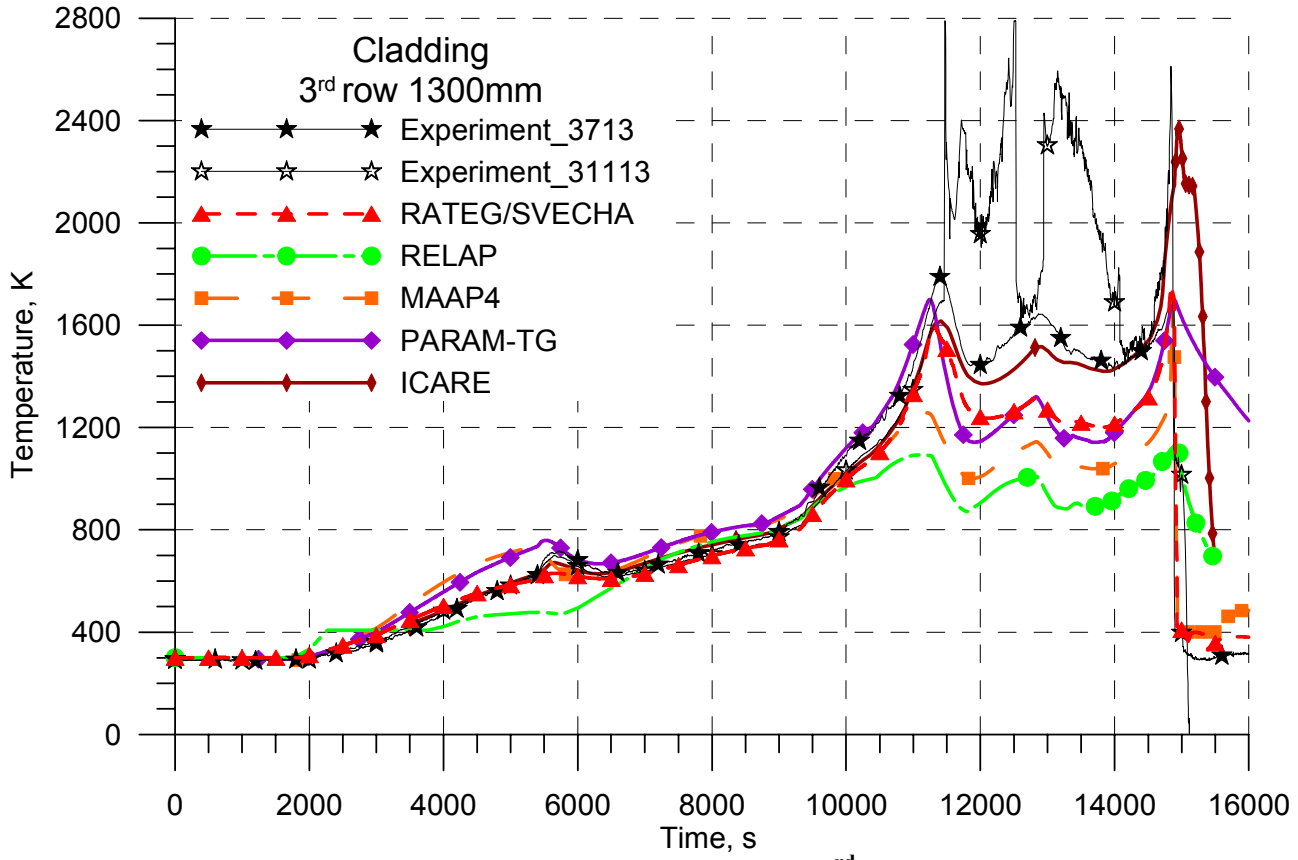

Figure 3.19 Temperature of claddings of the fuel rods of the 3rd row at the elevation of 1300 mm

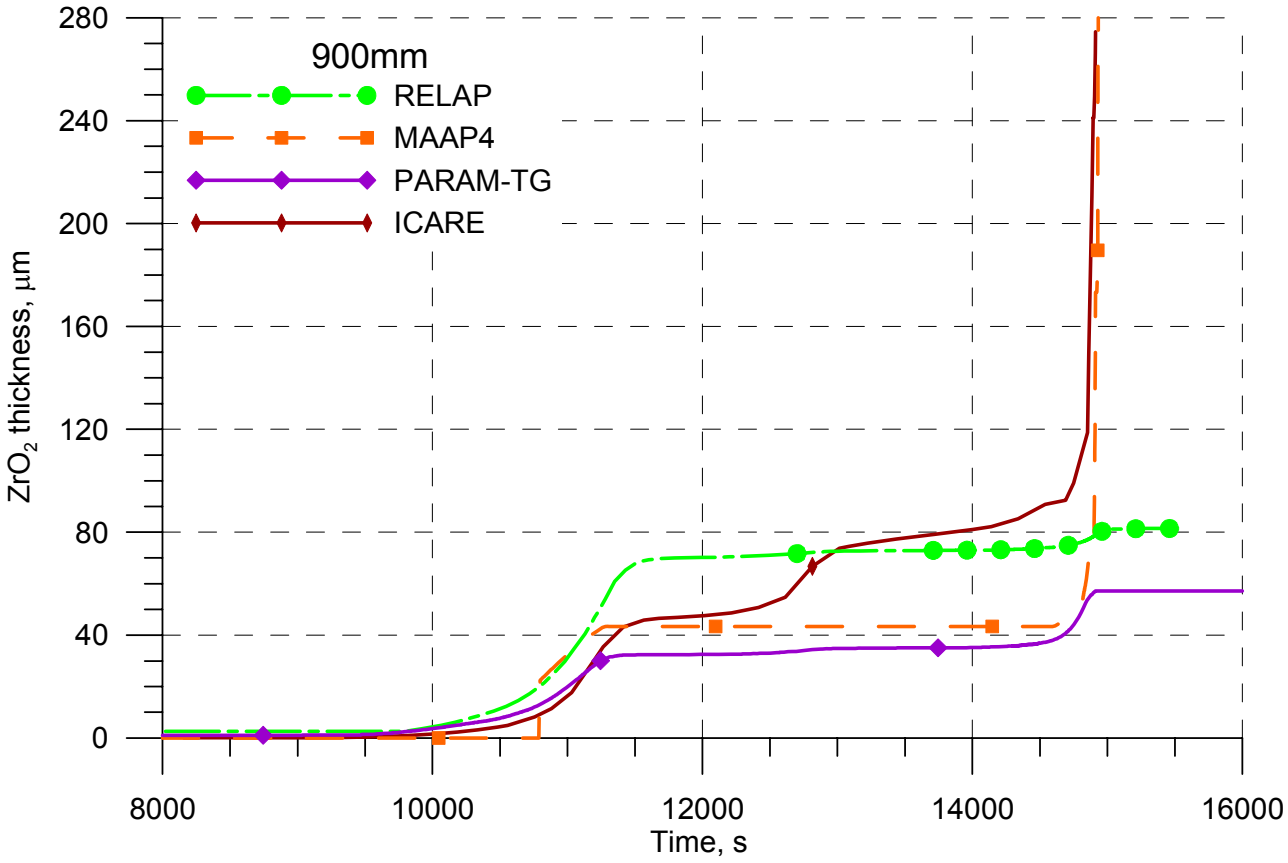

Figure 3.20 Oxide scale thickness at the elevation of 900 mm

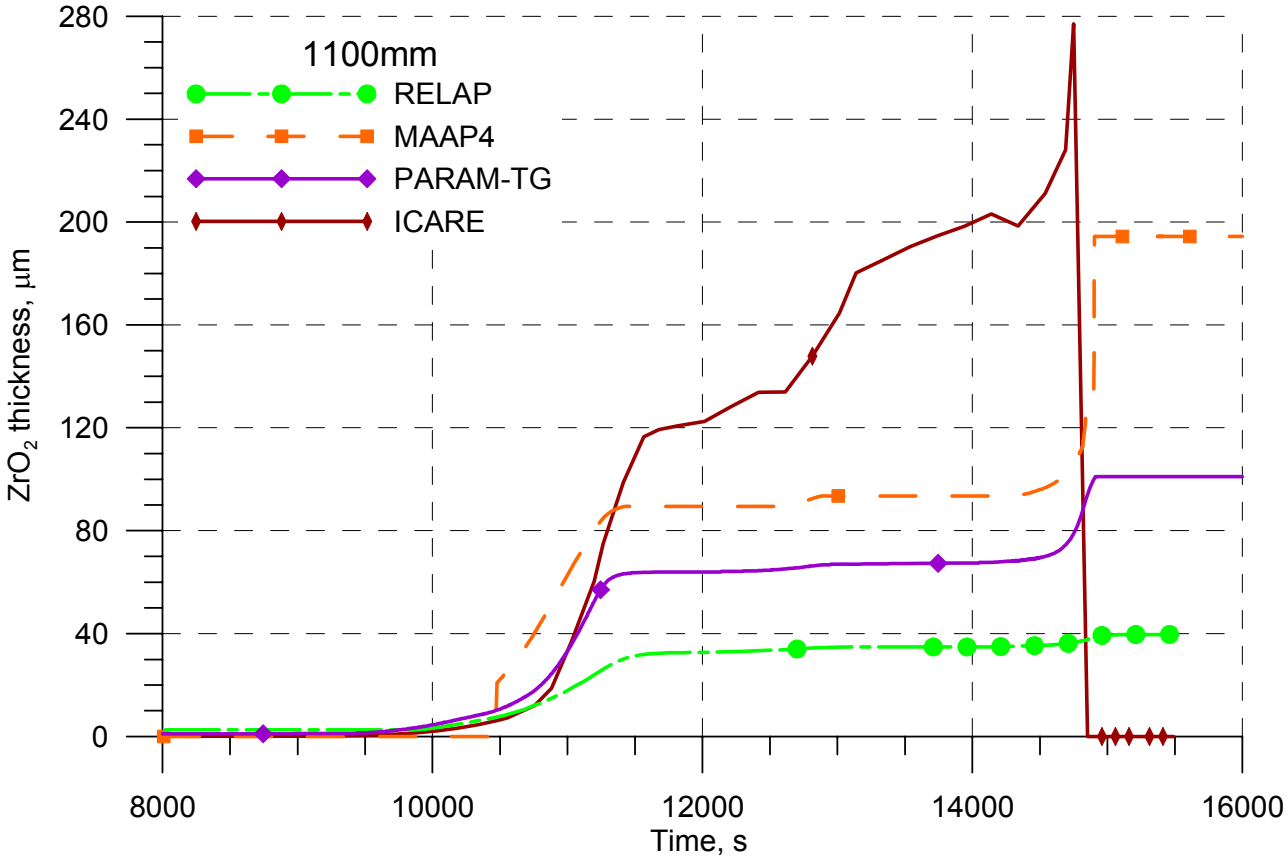

Figure 3.21 Oxide scale thickness at the elevation of 1100 mm

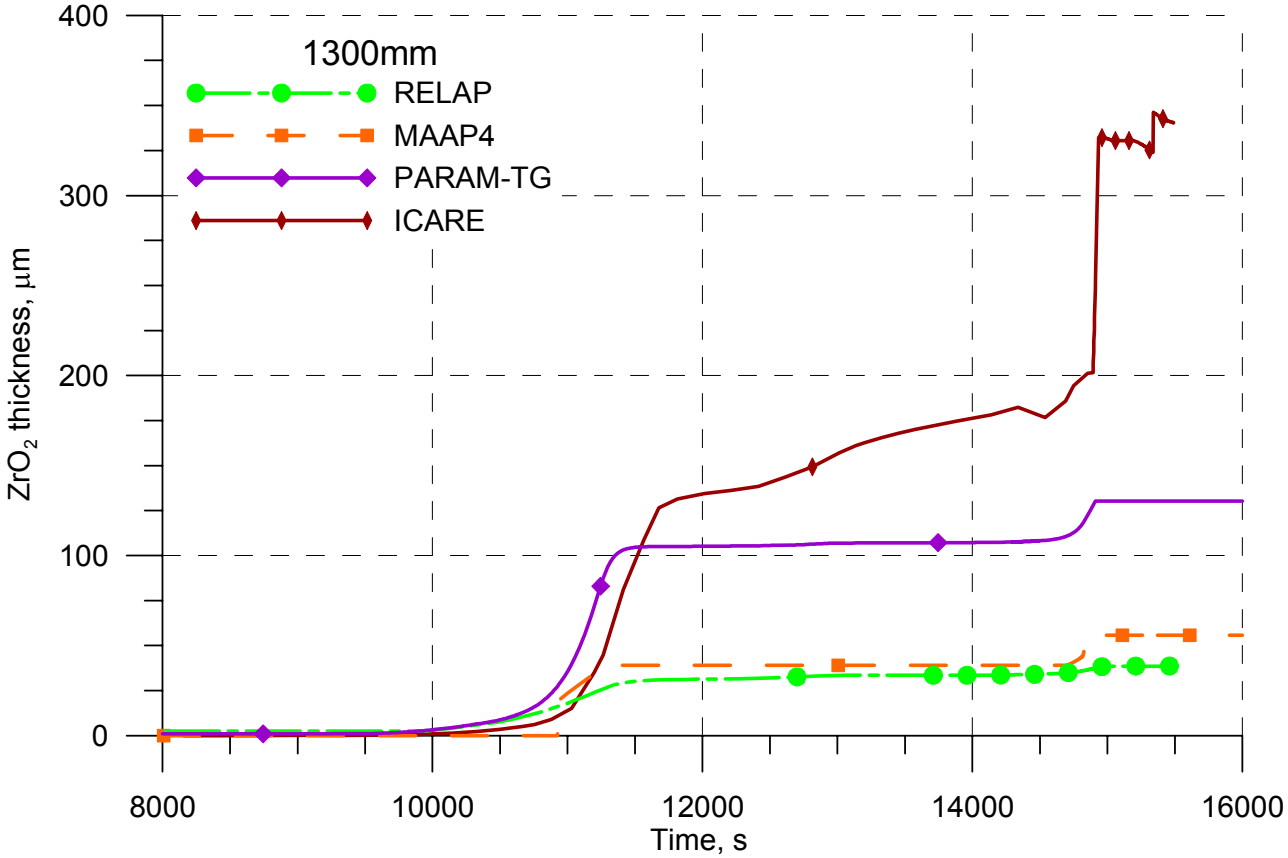

Figure 3.22 Oxide scale thickness at the elevation of 1300 mm

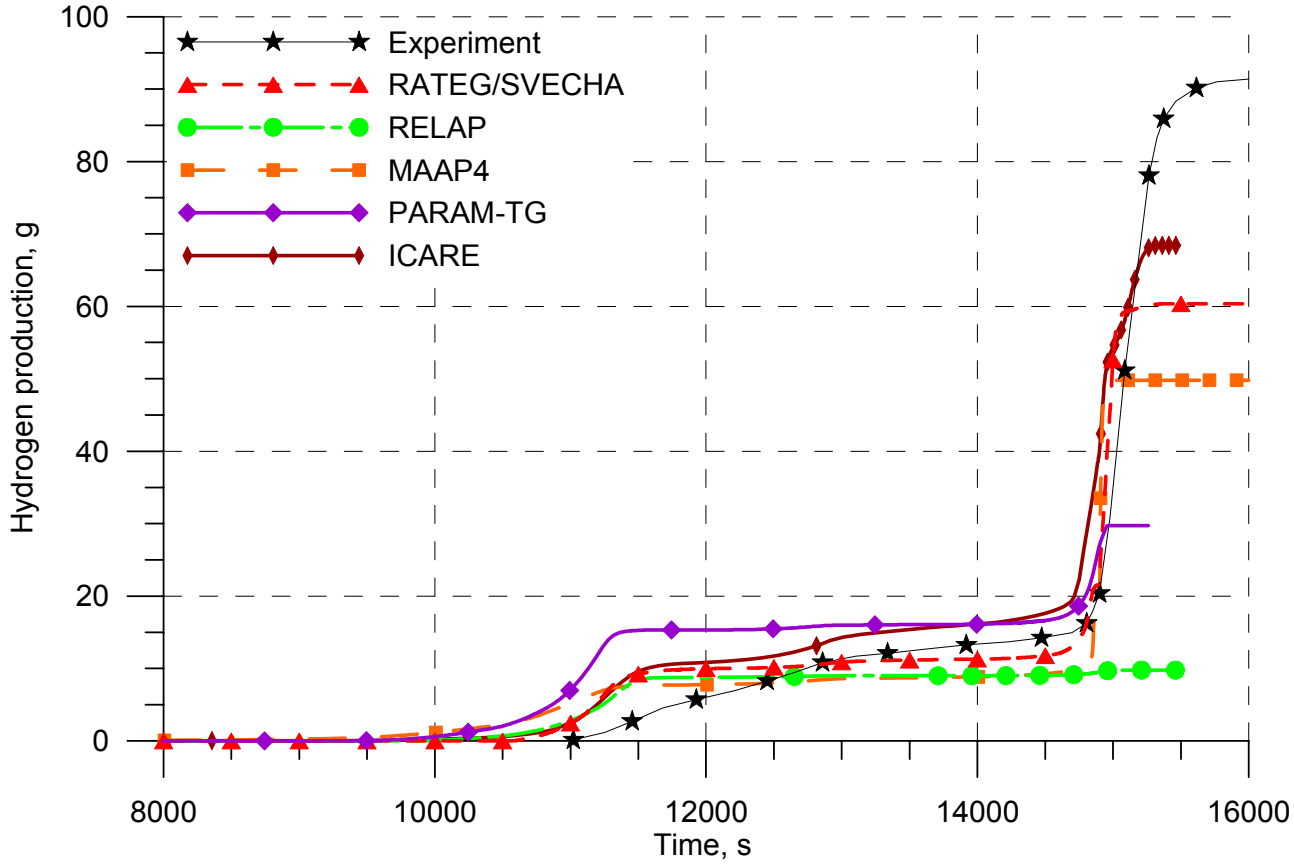

Figure 3.23 Hydrogen production

3.3 Numerical analysis of the PARAMETER-SF1 experiment by SOCRAT/B1 code

Steam condensation and bypassing complicate the task of assessing of self-consistency of the SF1 experimental results: alongside with the uncertainty of experimental data (coolant flow rate through the assembly under the conditions of failure of fuel rods and the surrounding structures; damage of shroud and thermal insulation leading to reduction in cooling the melt nucleus, numerous failure of thermocouples at high temperatures) some uncertainty is added in the steam flow rate through the intact assembly. Therefore the experiment protocol had been studied carefully, for the analysis of the bundle response to the personnel's actions the additional experimental data had been used, for confirming the formulated hypotheses, explaining the assembly behaviour, the multi-variant numerical calculations have been performed for all stages of the experiment. The nodalization developed for the pre-test calculations of the experiment SF1 was made more complicated for description of the condensing and bypassing. The nodalization for the post-test analysis of the SF1experiment is presented in Fig. 3.24.

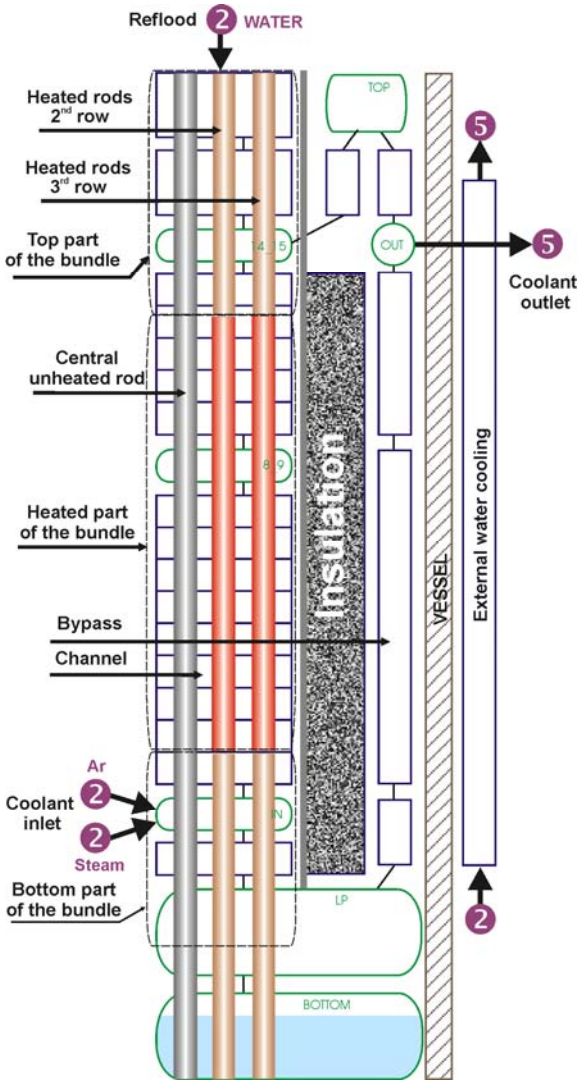

Figure 3.24 Nodalization of the test section for the post-test calculations of the SF1experiment for the SOCRAT code

One should pay attention to the fact that the test section components (shroud, thermal insulation, thermal insulation shroud, the test section body, the water cooling jacket), located at the elevation of the FA heated section, are not modelled in detail but represented as two circular heat elements with a channel between them.

The phenomena specific for the experiment SF1 – condensing and bypassing – were modelled by the condensation in the presence of non-condensable gas model and by introducing the bypasses.

|The numerical analysis shows that during experiment the steam flow through the assembly is settled of about 2.5 g/s (version 1 in Fig. 3.25). Fig. 3.26 presents the corresponding calculated data on temperature behaviour of claddings of the 2nd row at the elevation of 1000 mm, Figs. 3.27 -3.28 – for the 2nd and 3rd rows at the elevation of 1250 mm. For comparison the thermocouples readings are given. It is seen that starting from 11000 s (onset of pre-oxidization stage) the calculated values differ from the experimental values, and at the end of the transient stage (14890 s) the calculated temperature of claddings is so different from the experimental value that it does not allow to describe the melting and dissolution of oxide film observed in the course of the experiment (see Fig. 3.28), although the qualitative description of the temperature behaviour is correct: the hottest zone is displaced downwards the assembly. The main cause of such low calculated temperatures during the pre-oxidization phase and at the transient phase could be intensive cooling of the assembly components with steam. Probably the steam flows through the assembly with still less flow rate. During the detailed studying of the test protocol it can be noted that at the time moment 10250 s the body cooling system was switched on, at 10400 s the valve B22 was opened and a part of the condensate was discharged from the assembly lower part. It is possible that body cooling and water discharge led to the more intensive steam condensing. In any case let's assume that beginning from 10400 s the steam flow rate through the assembly became still less. To check this hypothesis the numerical analysis was made with the assumption of the additional steam leakage channels. Diameter of the additional bypass channel was chosen to fit the calculated and experimental temperatures. The best coincidence was obtained with the steam flow rate presented in Fig. 3.25 – version 2. In Figs. 3.26-3.28, demonstrating temperature behaviour of claddings of fuel rods at the 1000 and 1250 mm elevations, as well as in Fig. 3.29, demonstrating temperature distribution over the assembly height at the pre-oxidization phase and at the end of the transient phase, the corresponding calculation results are presented. In these Figures it is clearly seen that the assumption of steam bypassing allowed to obtain the observed evolution of the temperature profile by calculations. The appropriate modelling of the temperature throughout the experiment allows, in its turn, to give a rather accurate description also for the fuel rod claddings oxidation degree. Fig. 3.30 presents the results of calculation of oxide layer thicknesses for the three time moments: at the beginning of pre-oxidation phase (11800 s), at the end of the transient phase just before flooding onset (14890 s) and after the assembly cooling (16000 s). The code predicts that in 800 s after the beginning of the pre-oxidization phase in the hottest zone at the 1100-1300 mm elevations the protective oxide film grew on fuel rod cladding surfaces with thickness of 100-160 μm. At the elevations where temperature did not exceed the zirconium melting point the film became thicker with the time. The thickest film was at the 1200 mm elevation, it thickness being 250 μm before flooding at the time moment 14890 a, and 300 μm – after the assembly cooling. In the assembly middle part the fuel rod claddings were dissolved with the melt formed in the assembly. At the elevations between 1100 and 1200 mm the oxide films have been already damaged by the beginning of flooding (14890 s), the hot melt appeared on the fuel rods surface and started to flow downwards. Melt relocation to the lower elevations (to 700 mm elevations) was accompanied with moving downwards the considerable amount of energy stored in the hot melt. The melt heated the claddings up to the zirconium melting point, the dissolution of the cladding oxide scale inside and outside occurred. The melt flew cold to 600 mm elevation and below not causing considerable changes in the assembly geometry. Let's compare the calculated data on oxide layers thickness with the results of metallographic analysis designated with asterisks presented (Fig. 3.30). It is seen that there is a good agreement between them in the assembly upper and lower parts. In the assembly middle part there are no films both in the experiment, and according to the numerical analysis.

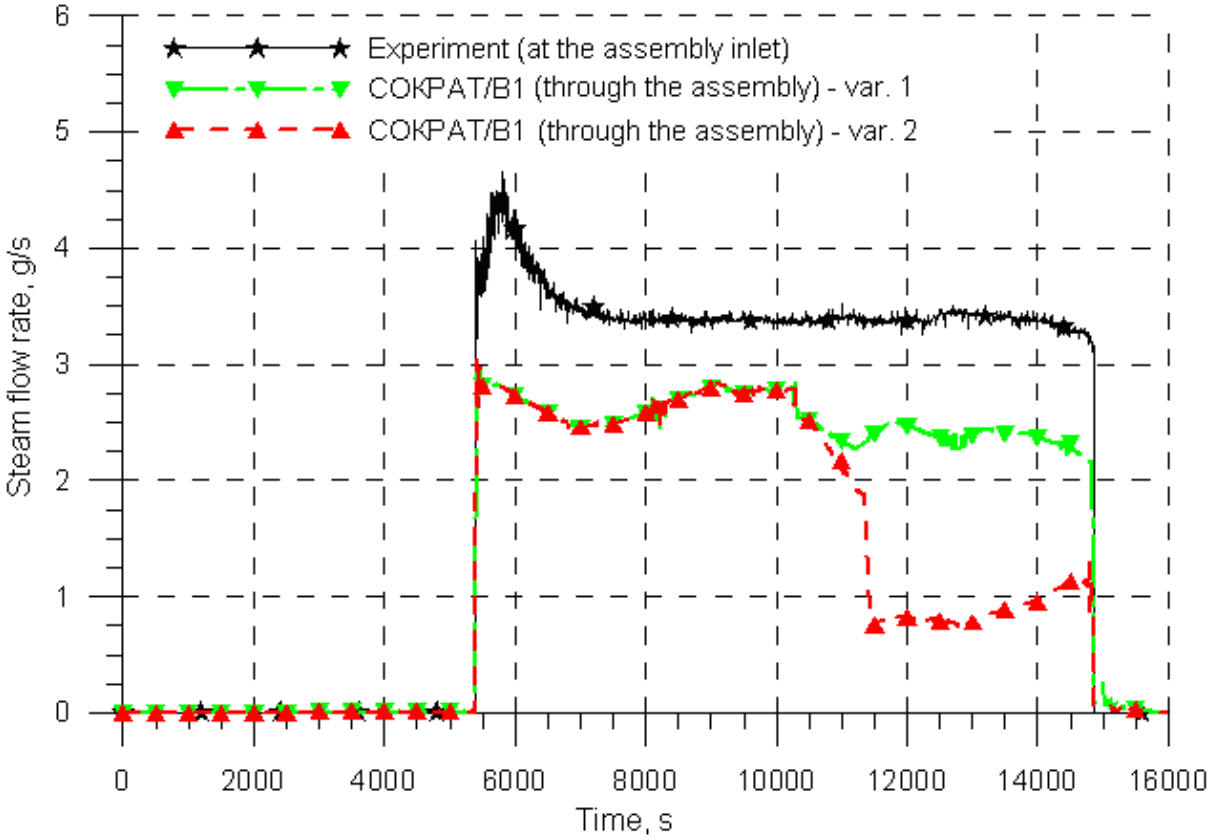

Figure 3.25 Steam flow rate through the assembly

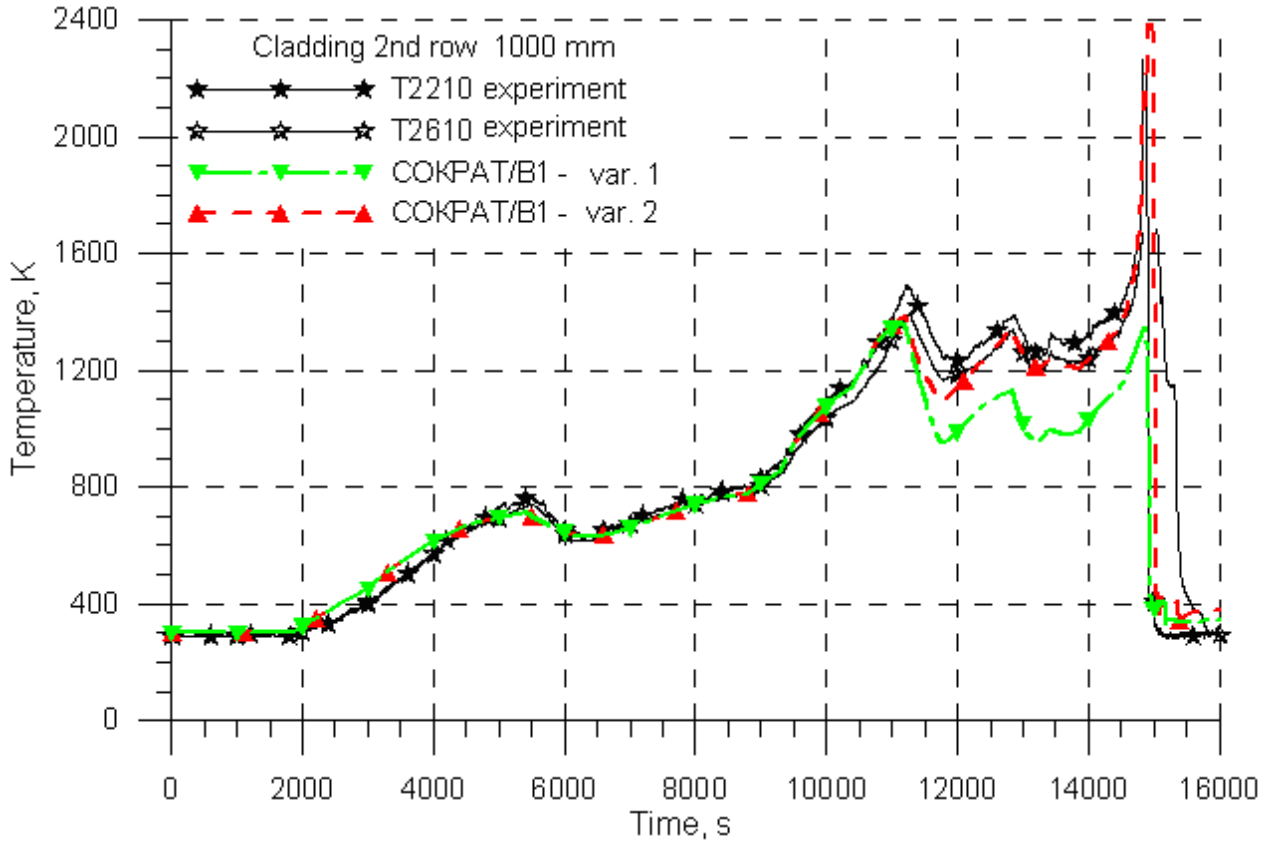

Figure 3.26 The 2nd row rods claddings temperature excursion at the 1000 mm elevation

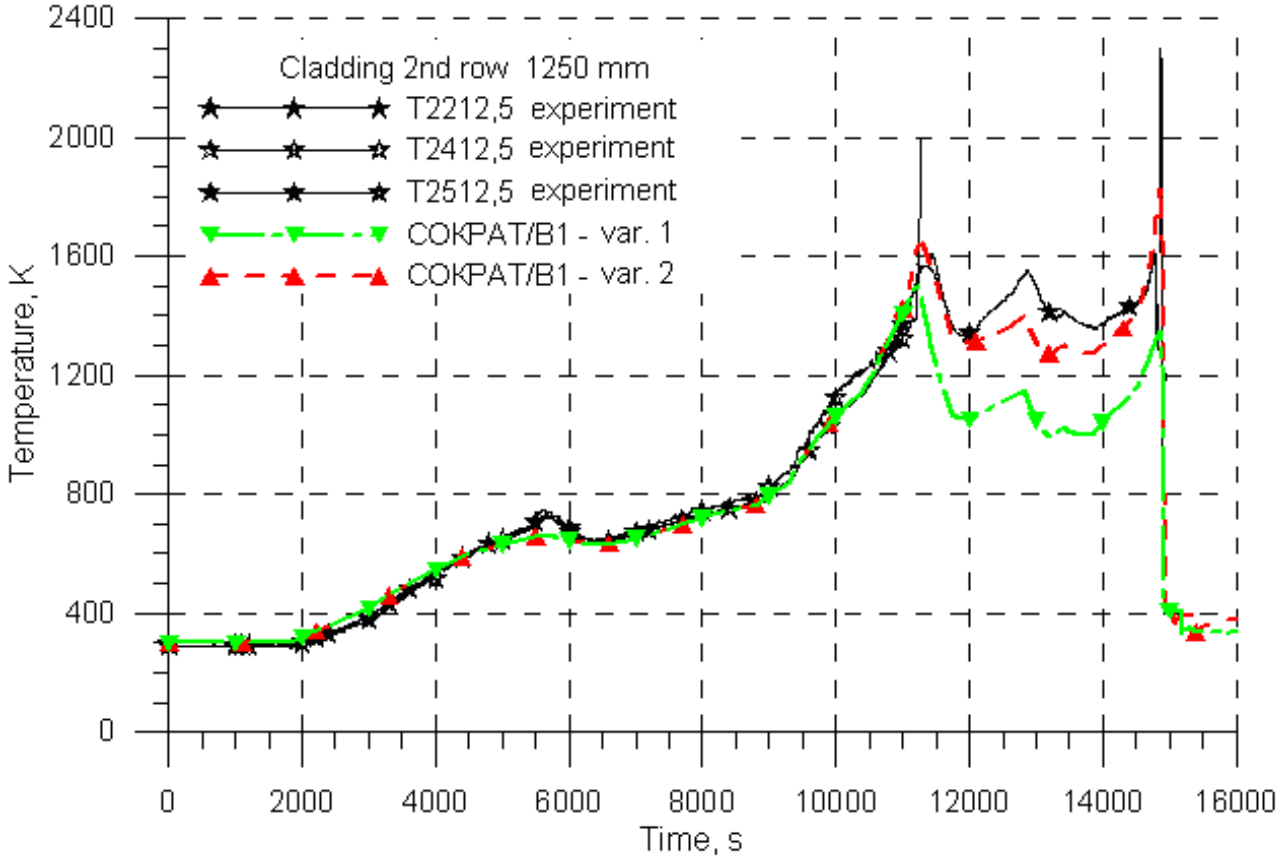

Figure 3.27 The 2nd row rods claddings temperature excursion at the 1250 mm elevation

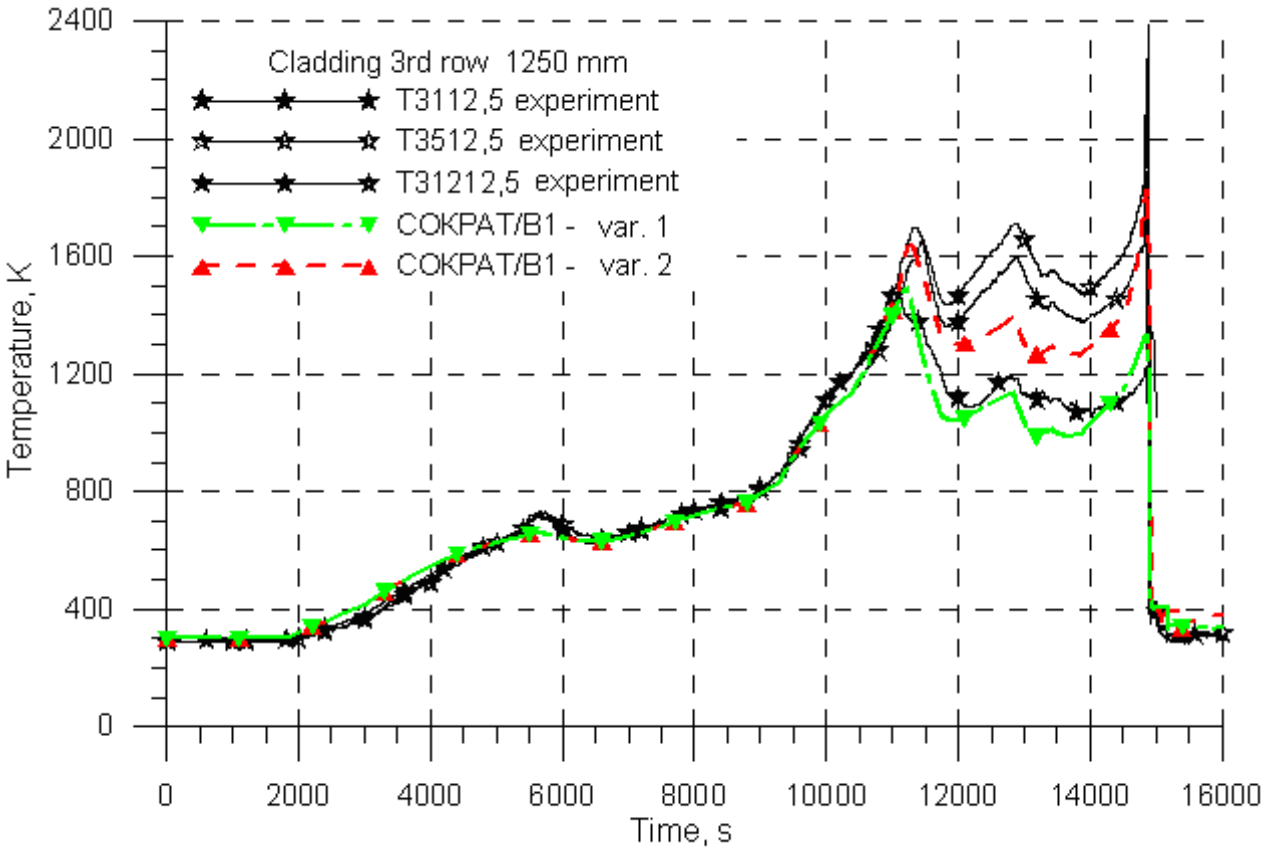

Figure 3.28 The 3nd row rods claddings temperature excursion at the 1250 mm elevation

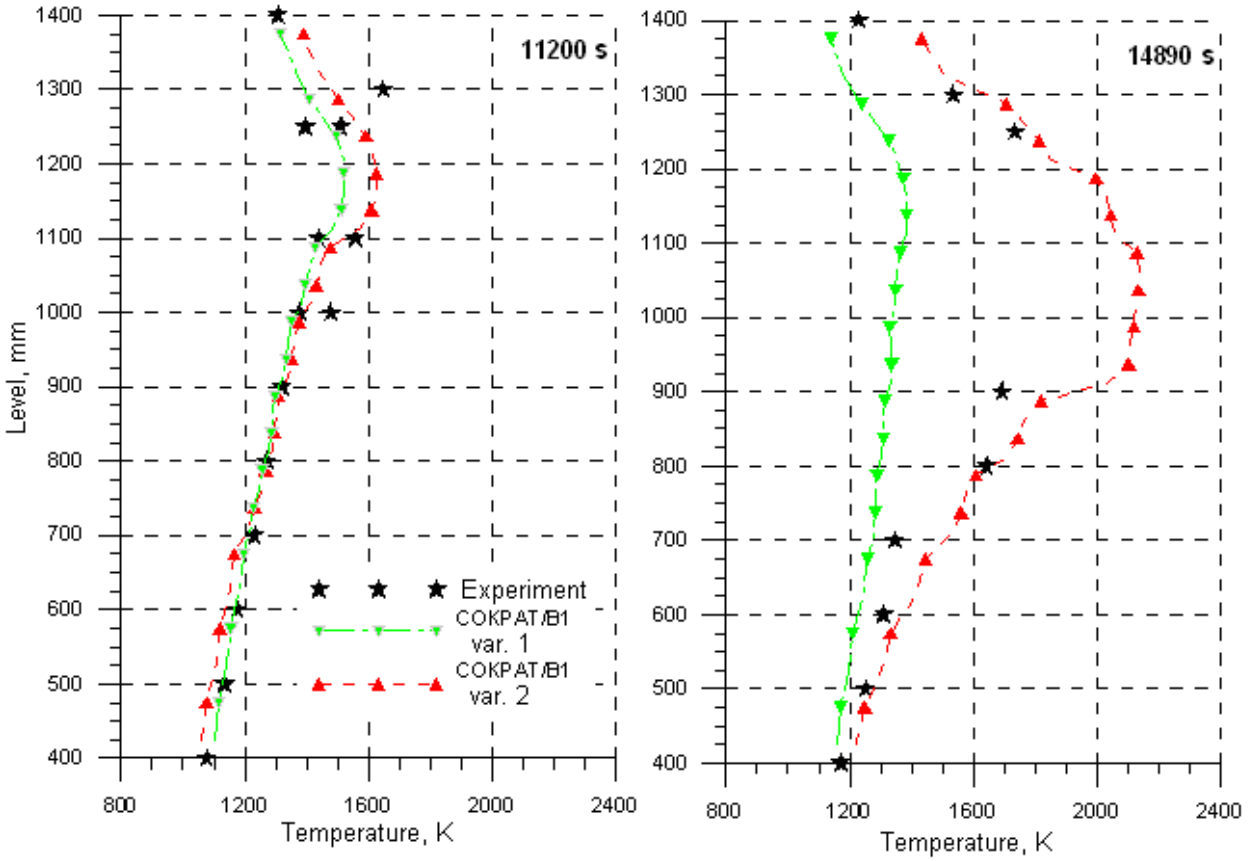

Figure 3.29 The 2nd row rods claddings temperature axial profile

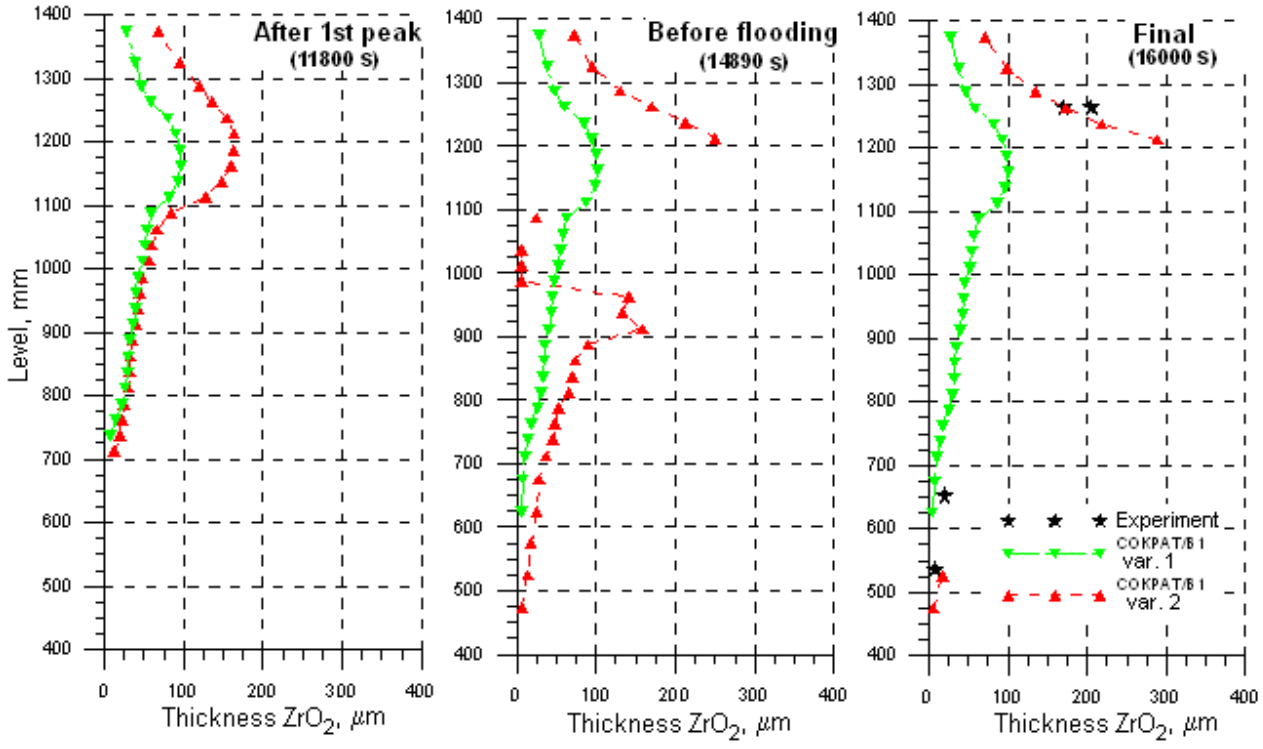

Figure 3.30 The 2nd row rods claddings oxide film thicknesses axial profile

In should be noted that in the assembly middle part a partial dissolution of fuel pellets was also observed. In calculations the temperature exceeded the zirconium melting point in this part of the assembly. It is known that molten zirconium will dissolve UO_2 and ZrO_2 intensively. The earlier performed experiments on dissolution of uranium dioxide show that the dissolution of uranium dioxide depends strongly on temperature and oxygen content in the melt. In the geometry of the intact rod the melting of the cladding inner surface occurs as soon as temperature reaches the zirconium melting point and simultaneous dissolution of fuel and oxide layers starts. In the case of rather thick oxide

layers the melt is saturated with oxygen quickly due to dissolution of the oxide film and the uranium dioxide dissolution is suppressed. In the case when the melt dissolves the cladding oxide layers the cladding damage occurs, and melt flows outside and downwards over fuel rod claddings, and with this, dissolves the fuel rod claddings on the below elevations. Hence it is seen that the uranium dioxide dissolution degree is governed by temperature, zirconium oxidation degree, moment of the protective oxide layer damage and by the rate of the melt relocation.

Fig. 3.31 presents a comparison of the calculated values of the degree of uranium dioxide dissolution with the results of measurements of uranium dioxide distribution over the assembly height (no direct measurements were made for the uranium dioxide dissolution). The analysis of the methods of uranium dioxide distribution shows that these experimental data (for 1100-700 mm elevations) can be used for comparison because considerable damage of fuel pellets due to fuel fragmentation was not revealed. Decrease in the uranium dioxide in fuel pellets above 1200 mm and below 700 mm elevations was caused by eutectic interactions of fuel pellets and zirconium claddings when they contact randomly. According to the basic assumptions of the models of computer code package SVECHA of the axial symmetry of the processes, the given phenomenon can not be self-consistently described by the code SOCRAT. It is seen from the comparison of calculated and experimental data that the code rather accurately predicts the fuel dissolution degree at the 800÷1100 mm elevations.

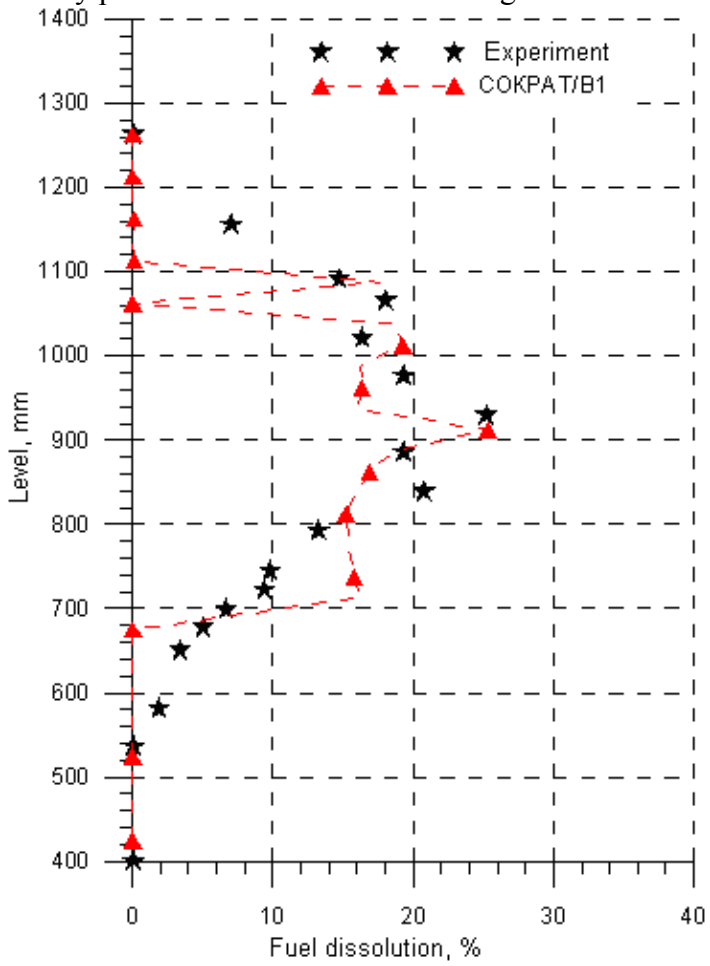

Figure 3.31 Dissolution of UO_2 pellets over the assembly height by the end of the experiment

The code correctly predicts bundle behaviour during the flooding stage. On the base of thermocouples reading one can conclude that at the 1300-1500 mm elevations FA was cooled in 3-5 s from the flooding onset. A delay in cooling was observed below 1300 mm elevations. The similar results were obtained by the numerical analysis. The main process governing water penetration into the assembly below 1300 mm was the process of water evaporation on the overheated fuel rod claddings. The generated steam flows upwards creating the counter flow for water streaming down. In general case at definite steam rate the conditions could be formed when the whole water, entering the assembly, will eject from the test section. The design of the test section was developed in such a way that to avoid the counter current flow phenomenon. The calculation shows that from 20 kg of water,

injected into the test section during flooding, about 3 kg is ejected by the counter steam flow into the condenser through the sleeve of steam-gas mixture outlet without reaching fuel rods. It can be noted a good agreement between the experimental and calculated data on ejection mass of steam and water into the condenser (see Fig. 3.32). The appropriate calculation of distribution of the injected water allowed to obtain the satisfactory agreement in the assembly cooling time and rate (se Fig. 3.33). The longer delay in cooling the assembly lower part (below 700 mm) in the experiment is caused, probably, by outflowing of a part of the top flooding water into thermal insulation through the shroud damage zone. In the given numerical analysis the shroud damage, observed in the experiment, is not described by the code because the test section components (shroud, thermal insulation, thermal insulation shroud, the test section body, the water cooling jacket) are not modelled in details.

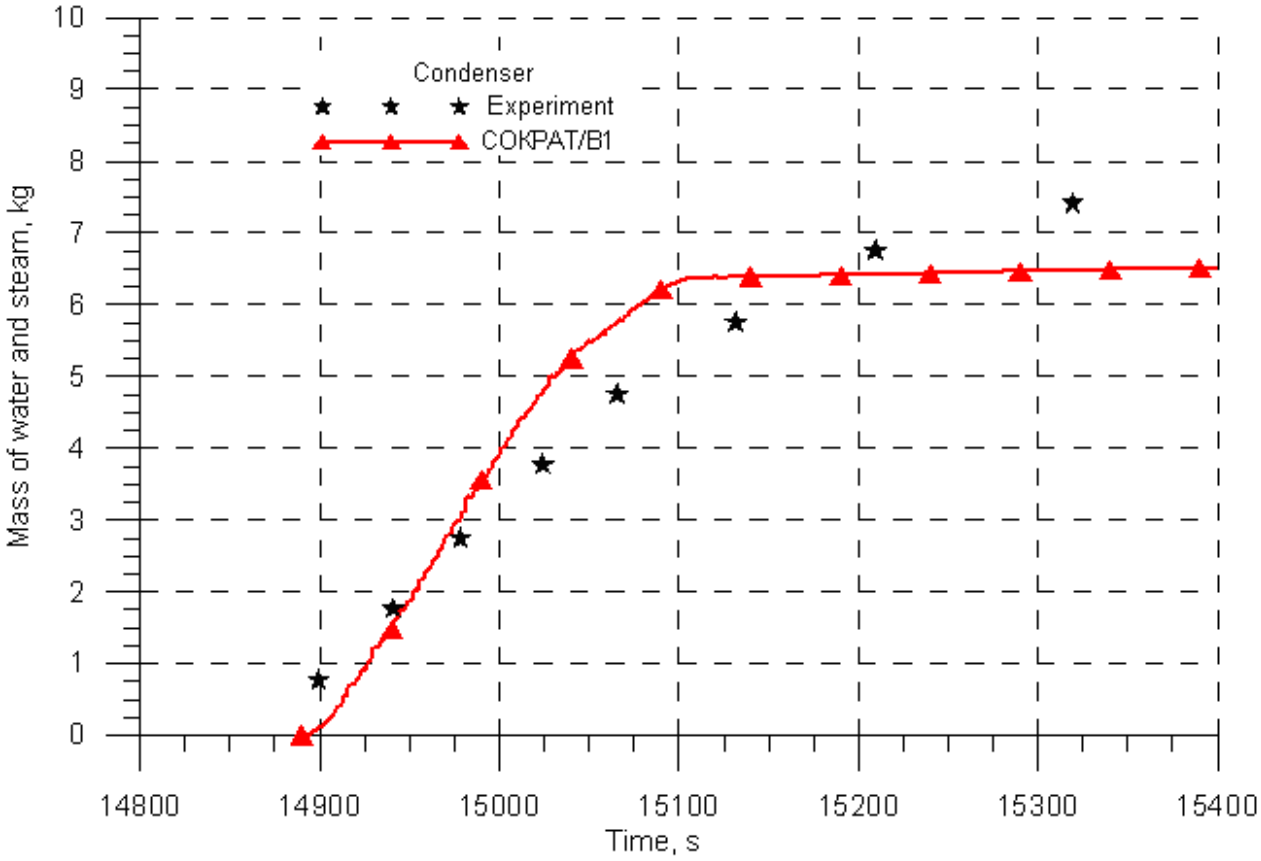

Figure 3.32 Total mass of water and steam ejected into the condenser during the flooding phase

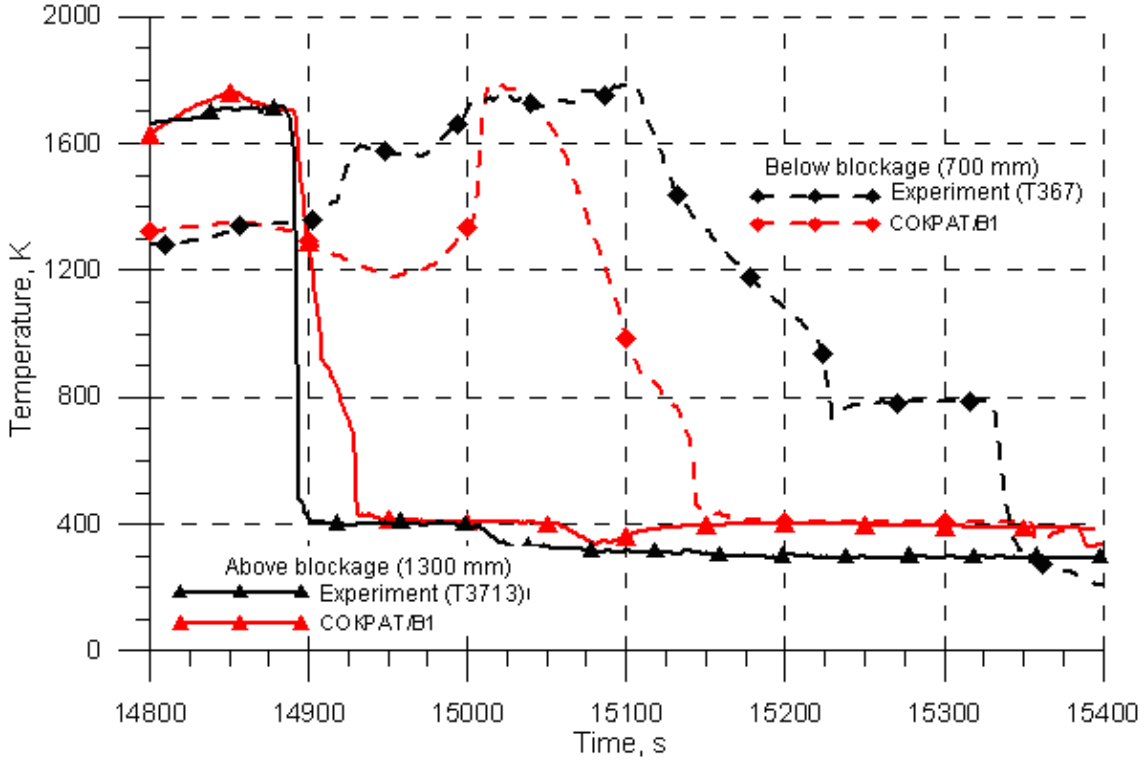

Figure 3.33 Rod claddings temperature history during flooding stage

One of the parameters, important for safety assurance, is the amount of hydrogen released as a result of zirconium oxidization. According to the calculational analysis the main contribution into the hydrogen release into the gaseous medium in the experiment SF1 is made by oxidation of zirconium elements during the pre-oxidization phase and the transient phase, as well as by the melt oxidation at the end of transient stage and during the flooding stage. The calculated data in comparison with readings of SOV-3 system are presented in Fig. 3.34. Both curves of hydrogen generation repeat the basic phases of the experiment.

At relatively low temperatures the oxidation process is sluggish. At the temperature above 1000°C the reaction is intensified. From the analysis of the calculated curve of hydrogen release it is seen that beginning from the time of ~10500 s, corresponding to the end of preliminary stage, the hydrogen starts to release slowly. From the comparison of the calculated data on hydrogen release and temperature it is seen that at that time the assembly reached the temperature of ~1000°C at the 1100-1300 mm elevations.

Approximately at 11000 s, corresponding to the beginning of the pre-oxidization phase, when the assembly was heated to temperature of 1200°C in the hottest zone the considerable rise in the rate of hydrogen release into the gas mixture is started. The code predicts that in 1000 s from the beginning of the pre-oxidization phase (approximately by 12000 s) about 10 g of hydrogen is released. With the rise of the oxide film, being the protective barrier for diffusion of oxygen ions to the surface of the cladding metal part, the oxidation process becomes less intensive, therefore by the end of the pre-oxidization phase, lasted for approximately 3450 s, about 11 g of hydrogen was released into steam-gas mixture.

Electric power increase at the transient stage leads to temperature increase, and, therefore, to intensification of oxidation. Amount of the released hydrogen begins to increase sharply. Stop of steam supply at 14858 second did not stop the assembly oxidation, it was continued due to steam remaining, though, evidently, the assembly components at the hottest upper zones were at that moment under the conditions of "oxygen starvation". Water flooding of the overheated assembly resulted in appearance of additional amount of steam that was mainly concentrated for a long time in the assembly upper part due to air slug at the 1250 mm elevation, preventing water moving downwards.

At the end of the transient phase a hot melt appears on surfaces of the assembly structural components and in the space between fuel rods. As known, at presence of steam the melt is oxidized

intensively, in this case the role of ZrO2 protective layer is not so significant, and transfer of oxygen in the melt is governed by the mechanisms of convective transfer. However in the experiment the melt oxidation was limited by the amount of steam accessible for oxidation: at the end of the transient phase - due to steam switching off approximately 40 s before the beginning of flooding, and during the flooding phase – due to delay of water entering into the assembly (the steam generated during water evaporation at the upper elevations rises upwards, and the melt flows downwards). Therefore the mass of hydrogen released during the flooding stage is not so high as it could be expected in case of complete melt oxidation. It is seen from Fig. 3.34 that the experimental and calculated data on hydrogen release at the stage of pre-oxidization and at the transient stage, as well as at the beginning of the flooding stage, are similar. At the same time there is a difference in the data at the end of flooding stage (total mass of the hydrogen released during the experiment is ~91g, the calculated value is about 60 g). Probably, the higher hydrogen release in the experiment is caused by the shroud damage and melt flowing out into thermal insulation; the corresponding processes can be described by the code only with more detailed modelling of the test section components.

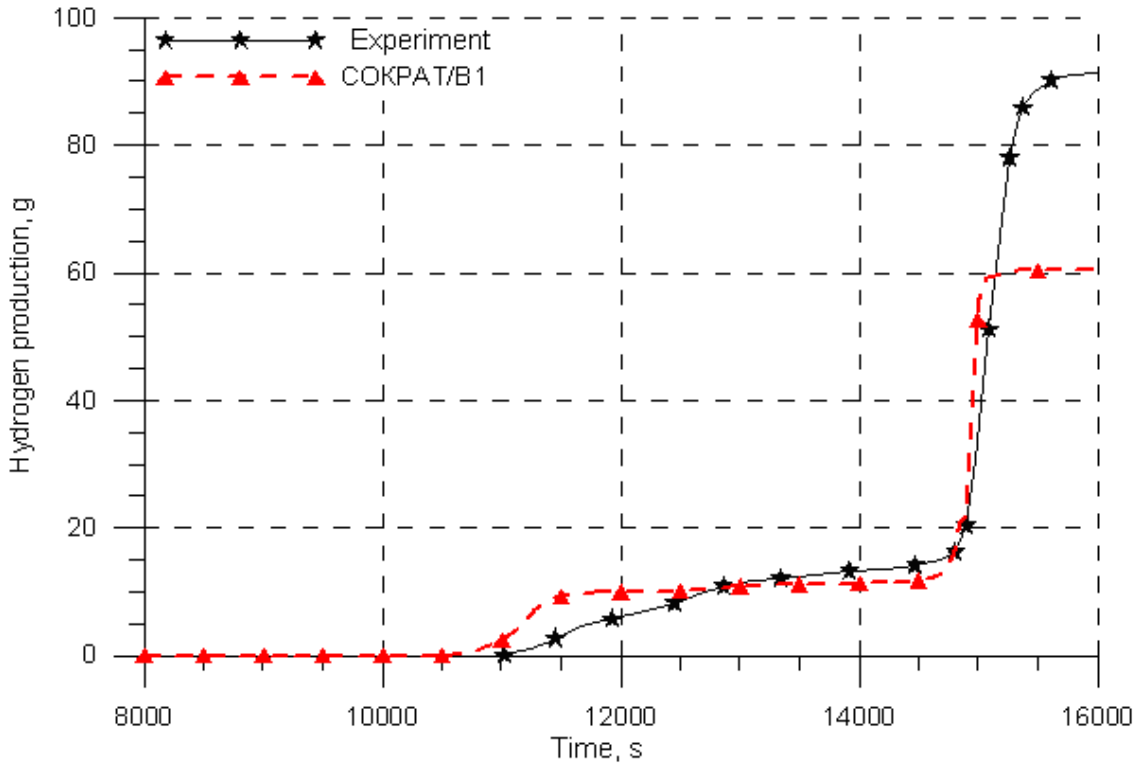

Figure 3.34. Total hydrogen production

3.4 Main conclusions derived from numerical analysis of the PARAMETER-SF1 experiment

For assessment of the degree of self-consistency of the results of the experiment SF1, on the basis of the developed nodalization of the test section at the PARAMETER facility a number of test calculations were made for assessment of the effect of uncertainties of possible ranges of parameters variation of the facility itself (insulation heat conduction, bypassing, cladding temperatures at the elevations where there are no reliable thermocouples readings, etc.) on the results of calculations; the through modelling was made by code SOCRAT for all phases of the experiment including the top flooding phase.

In spite of the uncertainty of experimental data (coolant flow rate through the assembly under fuel rods and the surrounding structure damage conditions; damage of the shroud and thermal insulation leading to reduction in cooling the melt nucleus, mass failure of thermocouples at high temperatures) typical for such kind of high-temperature experiments, it was managed to reproduce a set of experimental data.

For example, in the experiment the gradual displacement of the assembly hottest zone was observed from the elevation of ~1250 mm downwards to the elevation of ~1100 mm. The numerical analysis confirmed that such a displacement is caused by decrease in the steam flow rate through the assembly due to condensing and bypassing. It was demonstrated that the evolution of the temperature profile, observed in the experiment, is predicted with the sufficient accuracy. The appropriate modelling of the temperature profile allowed, in its turn, to give rather accurate description for the degree of fuel rod claddings oxidation: a good agreement was obtained as to oxide film thickness of the oxide film in the assembly upper and lower parts, and in the middle part – complete damage of fuel rod claddings.

In the assembly middle part a complete damage of fuel rod claddings and partial dissolution of fuel pellets was observed. It is known that the amount of uranium dioxide dissolved with melt zirconium depends strongly on the degree of zirconium pre-oxidization, the moment of damage of the protective oxide layer and the intensity of the melt relocation along the fuel rods. In SF1experiment the most intensive dissolution of UO_2 occurs in the assembly middle part (of the order of 20%), the code gives rather accurate prediction for the degree of fuel dissolution at the 800÷1100 mm elevations.

So, the qualitative and quantitative agreement of the calculated and experimental data has been obtained on the assembly temperature behaviour, distribution of oxide layers, dissolution of uranium dioxide. These results are indicative of the fact that the data of the experiment SF1 are self-consistency and is a valuable verification base for:

- studying the thermo-mechanical behaviour and cooling processes of 19-rod model FA of VVER-1000 under simulated conditions of severe accident including the stage of low rate cooling with top flooding;
- studying the thermo-mechanical behaviour of the assembly structural components (fuel pellets and claddings, shroud, spacing grids) under the conditions of top flooding of the model assembly overheated to high temperatures;
- studying the degree of oxidation of the assembly structural components;
- studying the interaction and structural-phase transformations in the model assembly materials (fuel pellets and claddings);
- studying the hydrogen release including the stage of low rate cooling with top flooding.

4 Pre-test calculations of the PARAMETER-SF2 experiment

The scenario of the PARAMETER-SF2 experiment (hereinafter referred to as the SF2) was designed p in such a way to obtain the valuable verification base for the SFD codes. With this aim the preliminary analysis of the thermo-hydraulic and physico-chemical models applied in the SOCRAT and ICARE codes had been performed and the two main tasks have been formulated – to assess the adequacy of modelling the flooding and oxidization processes by the codes and to obtain the data for improving the thermo-hydraulic models, and namely:

- Determination of the heat transfer coefficients in POST-CHF mode using the data on temperature evolution during quench phase.
- Evaluation of the components deformation after test and possible limitation of surface wetting due to decrease of flow area.
- Evaluation the engineering margins in designing the VVER equipment by measurement of water portion, ejected from the test section at the stage of flooding.
- Specification of the models parameters available in computer codes for POST-CHF heat transfer and flooding. Justification of the applicability of these parameters for simulation of the processes in the conditions similar to those observed in the experiment SF2.

In the course of the experiment SF1 the fuel rod simulator claddings were considerably damaged (up to 40%). A large number of the consistent processes, including zirconium melting, resulted in the assembly damage, makes the scope of possible verification material narrow (for instance, for verifying the oxidation models). Therefore a relatively low maximum temperature of fuel rod claddings before flooding was selected (to avoid zirconium melting) corresponding to the value of 1500C. Nevertheless, this temperature provides for rather long-term exposure of claddings under POST-CHF mode and allows on the base of thermocouples readings to study simulators heating/cooling during quenching phase. The rate of the top and bottom flooding corresponds to the prototype (as to water mass per one fuel rod) under the conditions of severe LOCA at VVER RP.

4.1 Brief description of nodalizations

The nodalization scheme for numerical analysis of the SF2 experiment by the code SOCRAT/B1 is based on the test section design and represented in Fig. 4.1.

The FA hydraulic channel is conventionally divided into three parts:

- the lower part of hydraulic channel (below the assembly heated part to the lower flange);
- the central part of hydraulic channel (the modelled length is 1275 mm – corresponds to the assembly heated part);
- the upper part of hydraulic channel (the modelled length is 400 mm – at the level of the upper molybdenum lead).

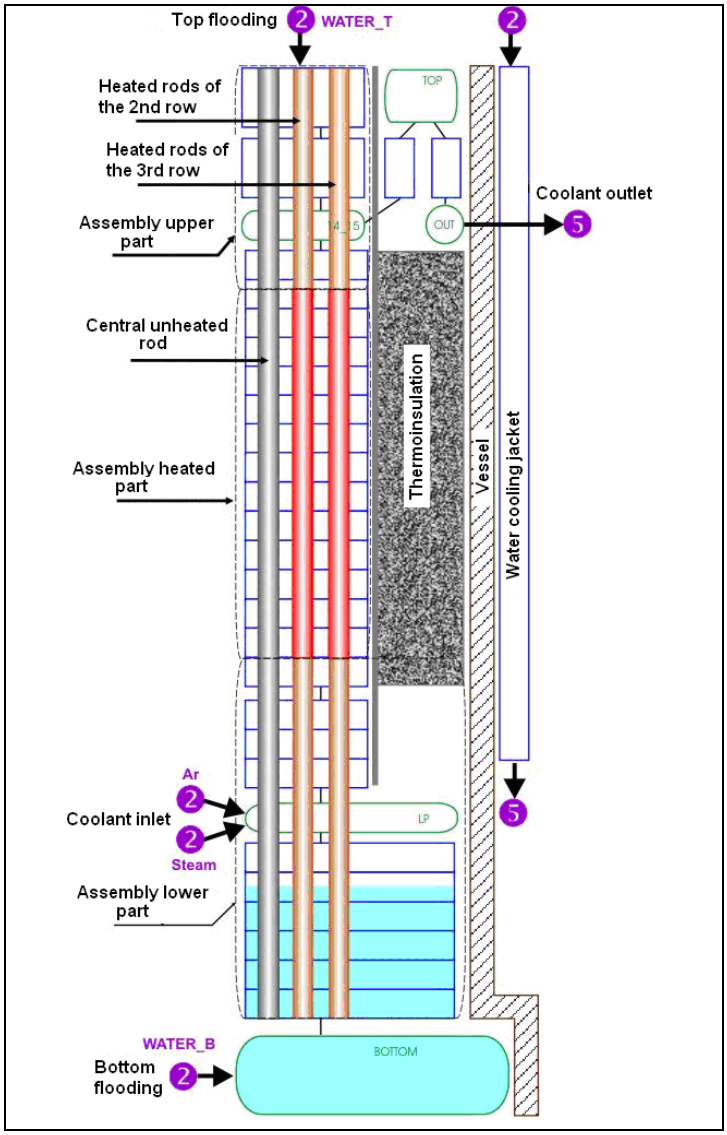

Figure 4.1 Nodalization of the test facility PARAMETER for the code SOCRAT

The FA itself is modelled with four heat elements:

– HEAT_1 - central rod;
– HEAT_2 - 6 heated fuel rod simulators of the inner (1st) row;
– HEAT_3 -12 heated fuel rod simulators of the outer (2nd) row;
– SHROUD – assembly shroud.

The shroud and surrounding structures nodalization is represented in Fig. 4.2

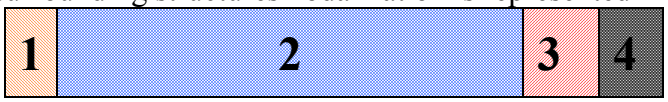

1 – shroud (zirconium tube); 2 – insulation; 3 - body (steel); 4 – water cooling.

Figure 4.2 Nodalization of the shroud and surrounding structures **for the code SOCRAT**

For evaluation of a contribution of different processes at "dry" stages of the experiment (before the flooding stage), as well as for specifying the supplied electric power mode, calculations were also performed using the thermo-hydraulic code PARAM-TG. Nodalization for the assembly shroud is presented in Table 4.1.

Table 4.1 Nodalization of the assembly shroud and surrounding structures **for the code PARAM-TG**

Layer No.	1	2	3	4	5	6
Layer thickness, mm	2	0,2	24,8	1	0,5	6
Material	Zr1%Nb	N_2	ZYFB-3	Steel	N_2	Steel

Nodalization scheme for the code PARAM-TG does not considerably differ from the nodalization used for the SF1 analysis of (Fig. 2.3). Description of changes: 1) In test section lower part there is a body of two diameters: 203x3 mm with length of 200 mm and 156x6 mm with length of 600 mm; 2) on the body of 156x6 there is an electric heater from the assembly bottom to the level of gases inlet; 3) tubular cooling jacket in the body middle and upper parts is replaced with the slot path; 4) there are no leakages between the outer shroud of thermal insulation and the body (16 and 6 Fig. 2.3); 5) steam and argon enter directly inside the body 156x6 mm and not inside the shroud (15).

4.2 Results of pre-test calculations

The multi-variant calculations were performed for evaluation of the contribution of physical processes and for specifying the experiment scenario with the assigned parameters (steam flow rate – 3,3 g/s, argon flow rate – 2 g/s, temperature of fuel rods at the pre-oxidization phase –1200 °C, thickness of oxide layer on fuel rod claddings at the and of the pre-oxidization phase –150-200 μm, heating up rate – 0,3 K/s, maximum temperature of fuel rod claddings – 1500 °C, water flow rate of top flooding – 40 g/s, of bottom flooding – 100 g/s). Joule heating power calculated by SOCRAT, ICARE and PARAM-TG codes accounting for SF1 pre- and post-test calculation results is in a rather good agreement (Fig. 4.3).

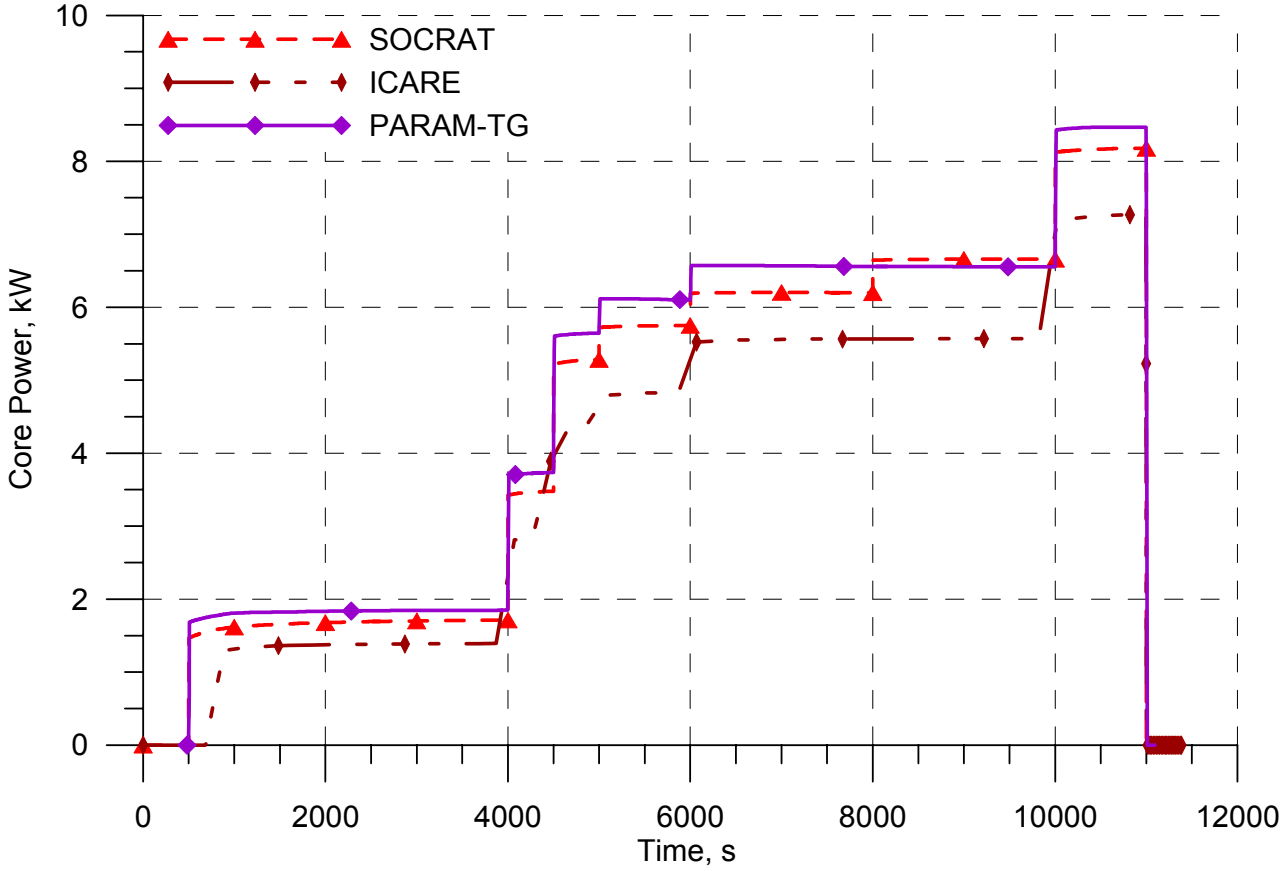

Figure 4.3 Joule heating power (0÷1275 mm elevations)

The differences in the Joule heating power are caused by differences in the radial heat loses: heat losses through the shroud depend on the applied nodalization, on thermal insulation properties and on the models of radiative and convective heat transfer in the assembly, applied in the codes. It is seen in Fig. 4.4 that differences in radial heat losses, predicted by the codes SOCRAT, ICARE and PARAM-TG at the pre-oxidization phase, reach 1,8 kW, at the transient phase - still more. Such the uncertainty indicates that experimenters should increase electric power gradually taking account thermocouples readings.. It is also necessary to account for changing in the geometry of the heat

insulator and the cooling jacket in comparison with the experiment SF1, and this could lead the additional uncertainty in heat losses in radial direction.

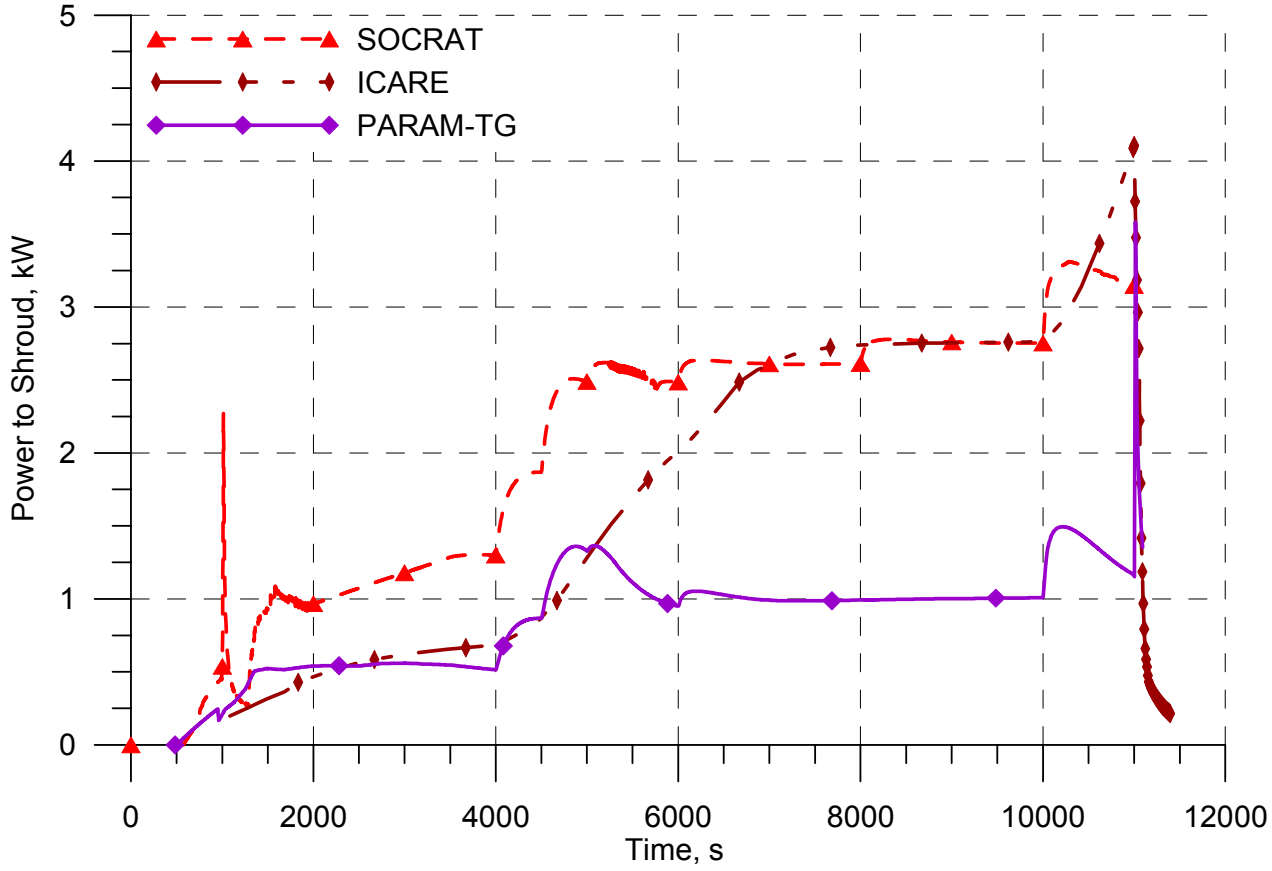

Fig. 4.4 Power of heat losses to shroud

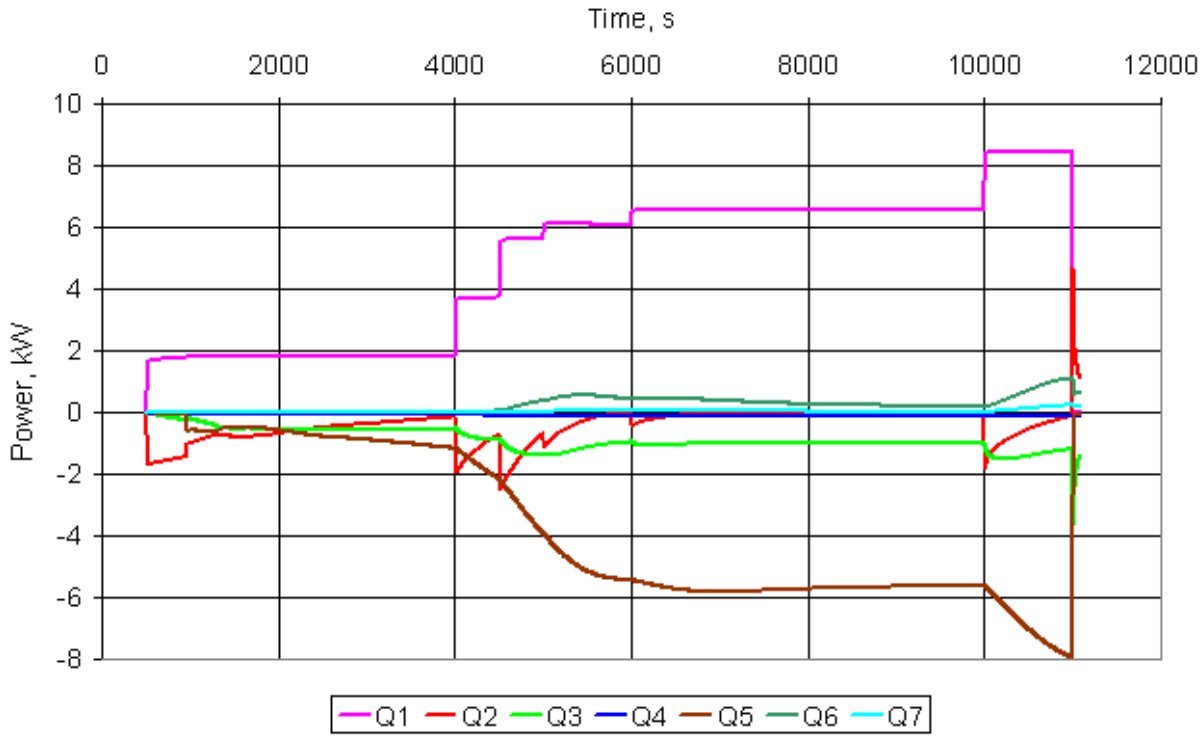

Q1 – Joule heating power, Q2 – the heat stored in fuel rods (in time unit), Q3 – power of heat losses to insulation, Q4- axial heat flux over fuel rods, Q5- heat flux to coolant, Q6- power of steam-zirconium reaction, Q7 – power balance.

Figure 4.5 Balance of powers in the assembly heated part – PARAM-TG

Fig. 4.5 gives a power balance calculated by PARAM-TG code for all heat supply and loss processes. Heat supply is positive and heat loss is negative. A small disbalance at high temperatures (not more than 2.5%) is caused by an error in consideration of steam-zirconium reaction due to large time step (3-5 s).

It should be noted that small experimental deviations in the steam flow rate within the range of 10-20% of the design value shall not result in the threshold effects (temperature escalation) the pre-oxidization phase (with the correctly chosen power) because the fuel rods cooling is governed by several mechanisms simultaneously (in the codes SOCRAT and ICARE a loss power to steam is ~50% of the Joule heating power , in the code PARAM-TG it is ~ 85%).

The analysis by SOCRAT code shows that the maximum temperatures in the assembly should be expected at 1250 mm elevation (see Fig. 4.6), thickness of the oxide layer of fuel rod claddings at the 1200 mm elevation is 150 μm at the end of the pre-oxidization phase and about 250 μm at the end of the experiment (see Fig. 4.7). The proposed electric power supply mode (see Fig. 4.15) leads to heating-up the assembly to the temperature of 1500°C, the heating up rate in the hottest zone at the beginning of the transient phase is governed by the electric power, it being 0,3 K/s.

To choose the scheme of water apply (of sequence and time delays in switching the top and bottom flooding) the multi-variant calculations were performed. The numerical analysis shows that when the bottom flooding water reaches -300 mm elevation, where the temperature of body and fuel rod claddings is high enough (~750K), the intensive water boiling is started. In Fig. 4.8 it is seen that at the time moment of ~11070 s the claddings at the 1250 mm elevation, having already cooled with the top flooding water to the temperature of ~400K, begin to be heated-up again. Evidently, this phenomenon is caused by the top flooding water displacing with the steam generated as a result of the bottom flooding.

Taking into account the fact that one of the main tasks of the experiment is development of thermohydraulic models, and that the calculated data presented in Fig. 4.8 are preliminary, it is reasonable to develop such a scheme of the combined flooding that will allow to obtain the experimental data applicable for design aims. It should be acceptable to start the bottom flooding after the top flooding water has entered into the assembly to the1250 mm elevation (to the upper spacer grid) and cooled the fuel rod claddings to the temperature of 900K or below (close to the threshold of wetting).

Pre-test calculations by the SOCRAT code show that the scheme of the combined flooding with a delay of bottom flooding of ~50 s allows obtaining acceptable experimental data.. Numerical analysis predicts that for this time the fuel rod claddings cooling off with the top flooding water occurs in the hottest elevation of 1250 mm to the temperature of 900K (see Fig. 4.8). In Fig. 4.9 it can be seen that the steam generation calculated does not depend practically on the rate of water flow rate, it being ~14 g/s during the flooding phase. The calculated collapsed water level in the assembly is given in Fig. 4.10. Pre-test calculation shows that the total mass of the generated hydrogen is 23 s, and 3 g of them – during the flooding phase (Fig. 4.11).

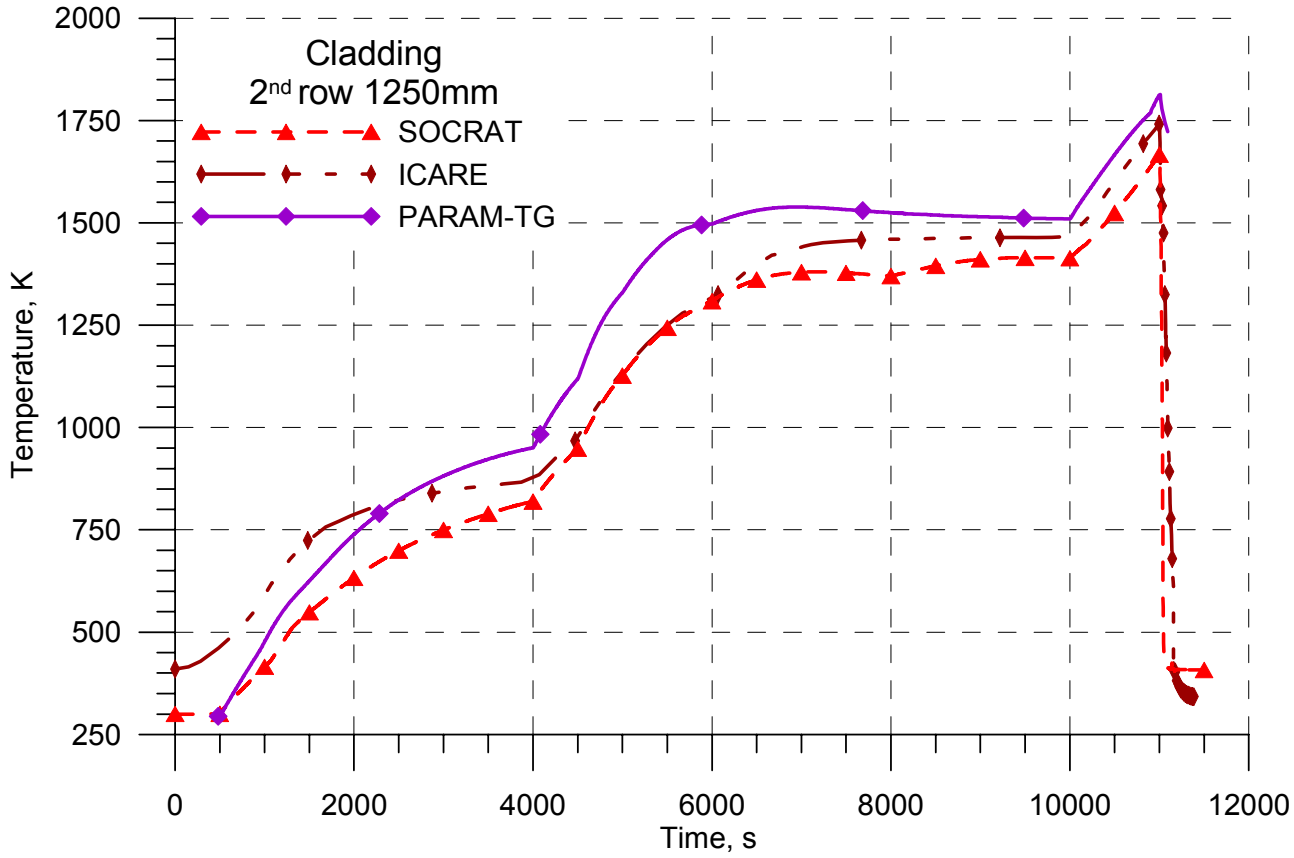

Figure 4.6 The 2nd row rods claddings temperature at the elevation of 1250 mm

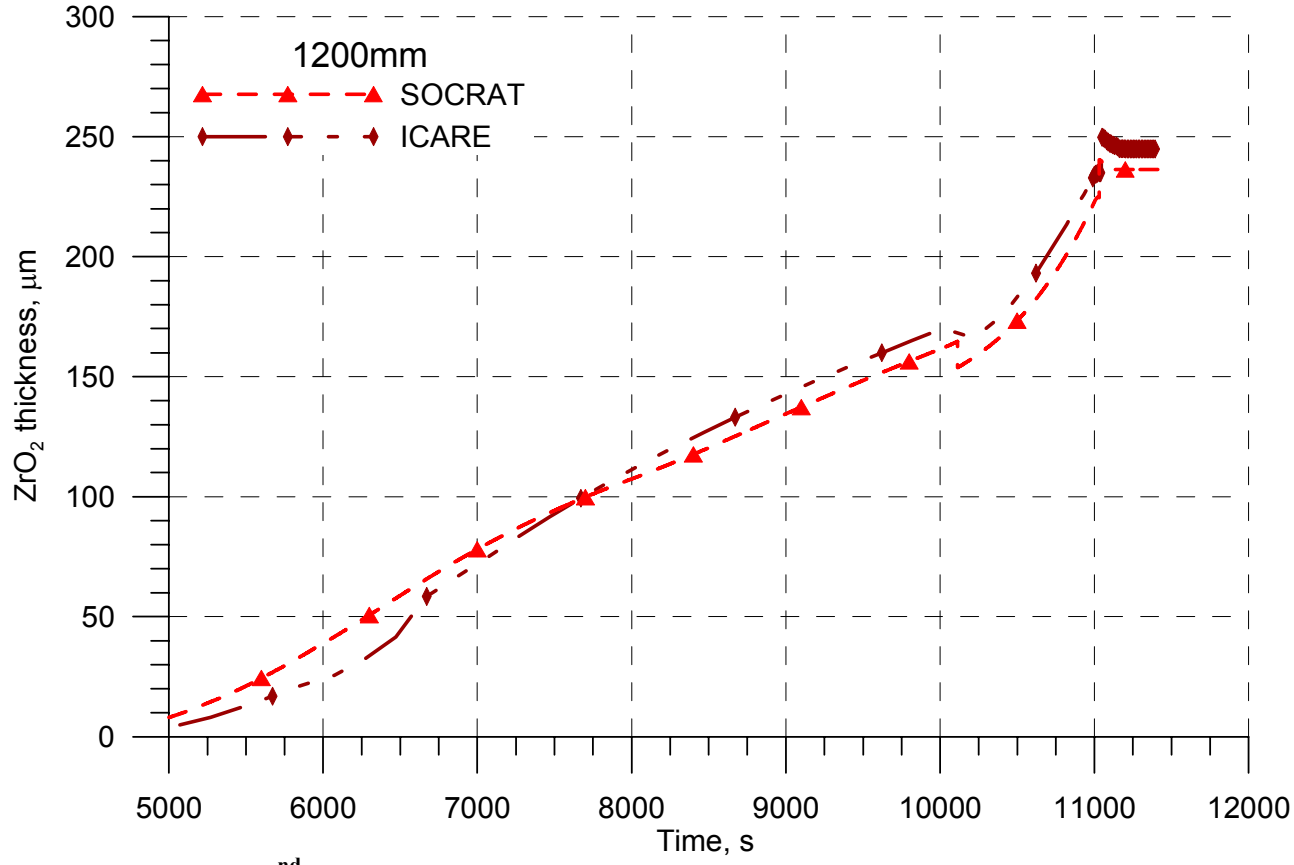

Figure 4.7 The 2nd row rods claddings oxide scale thickness at the elevation of 1200 mm

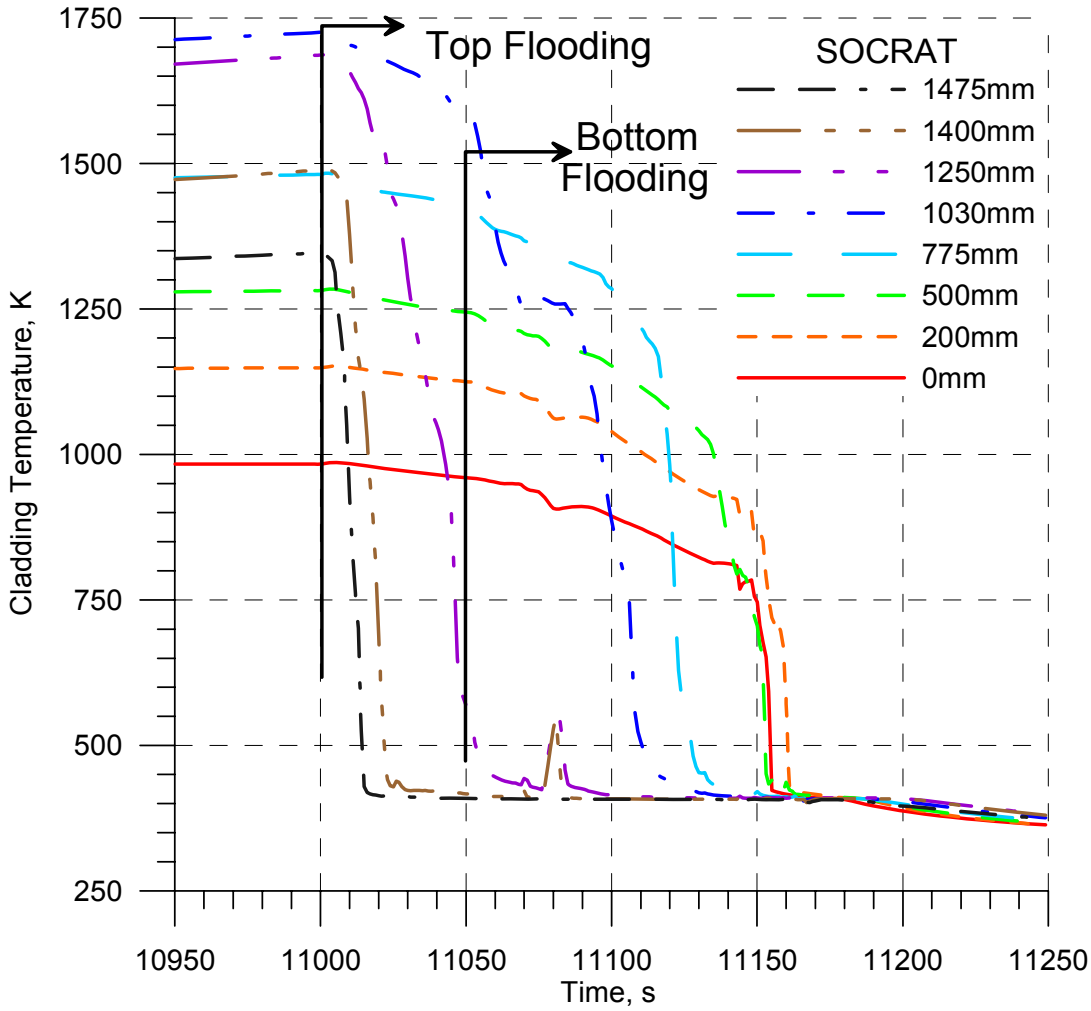

Figure 4.8 Rod claddings temperature during the flooding stage

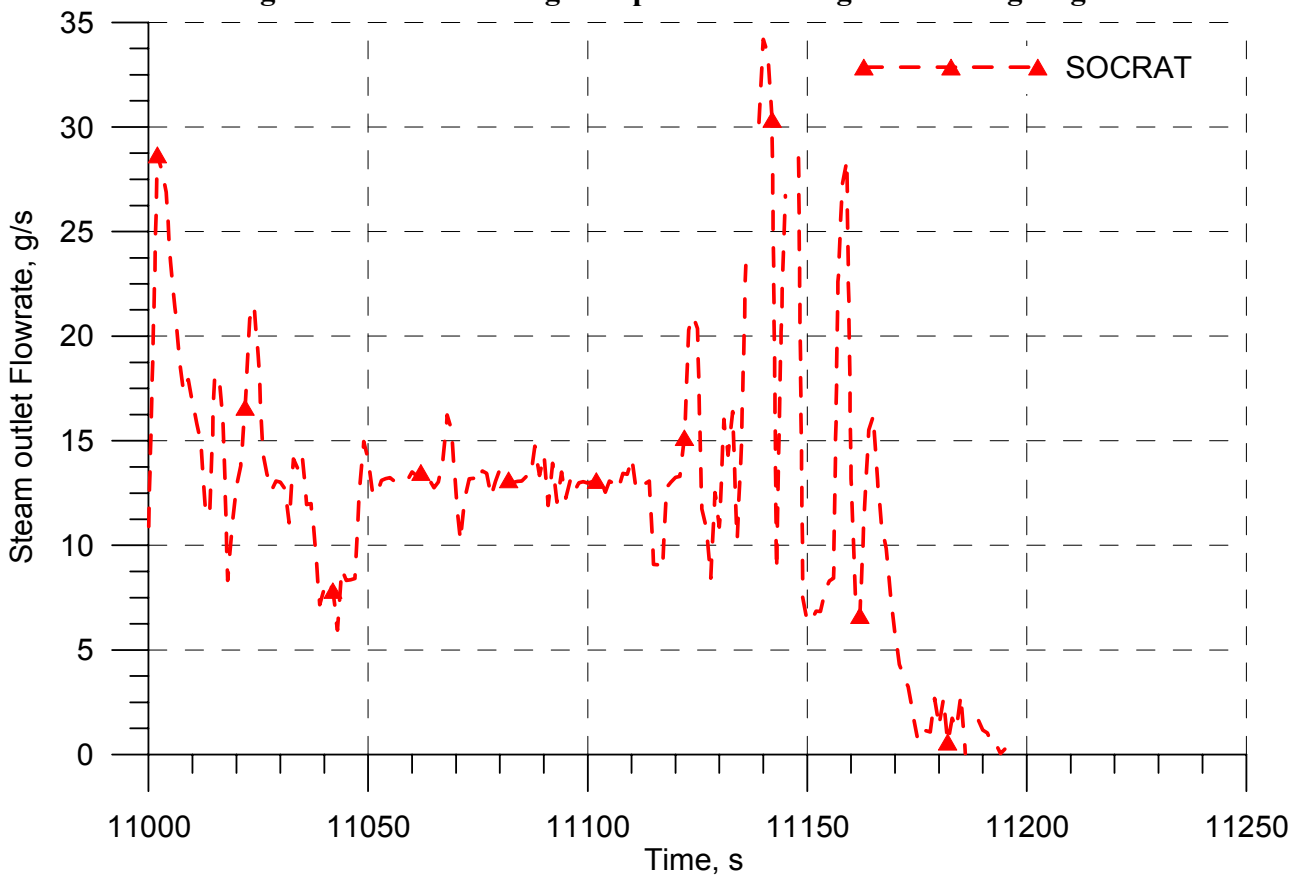

Figure 4.9 Steam generation during flooding phase

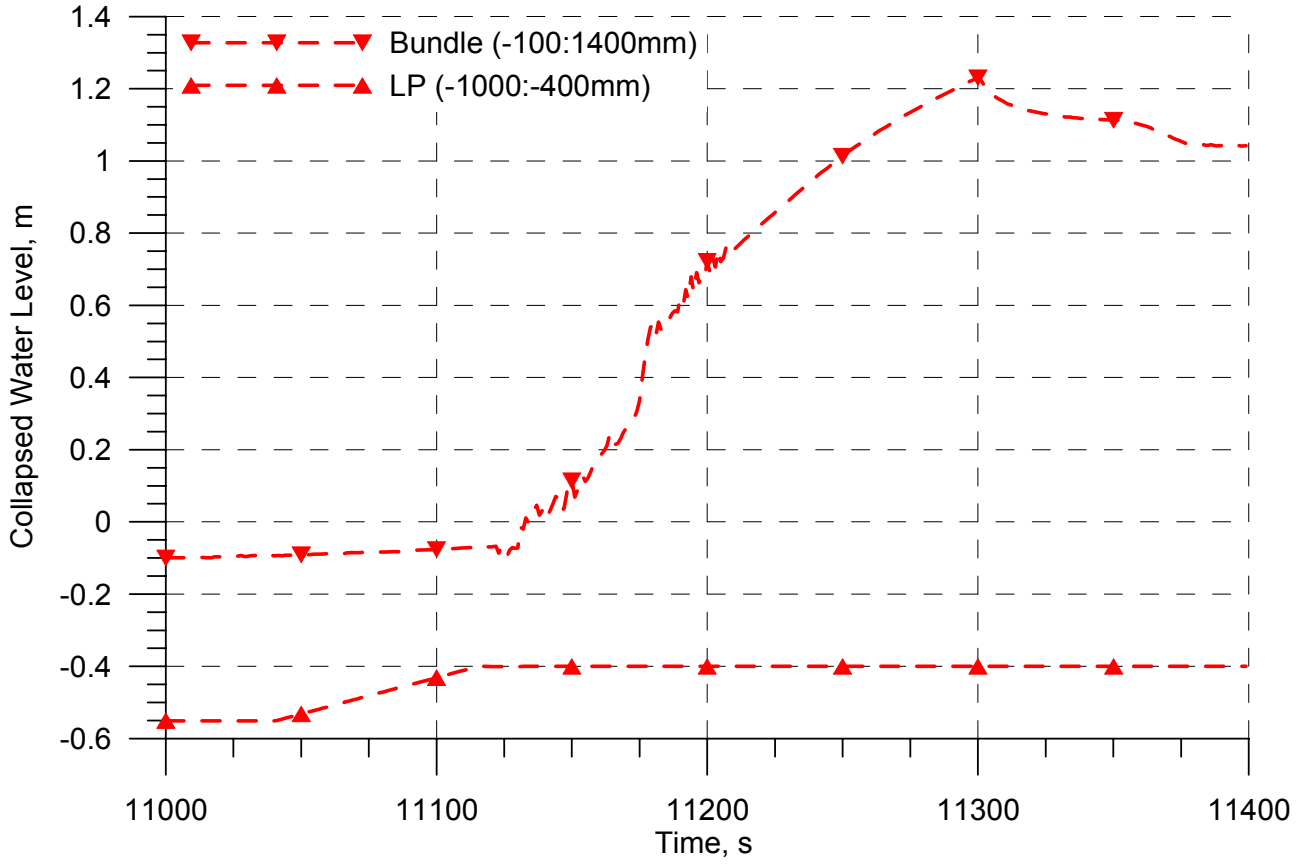

Figure 4.10 Collapsed water level in the assembly

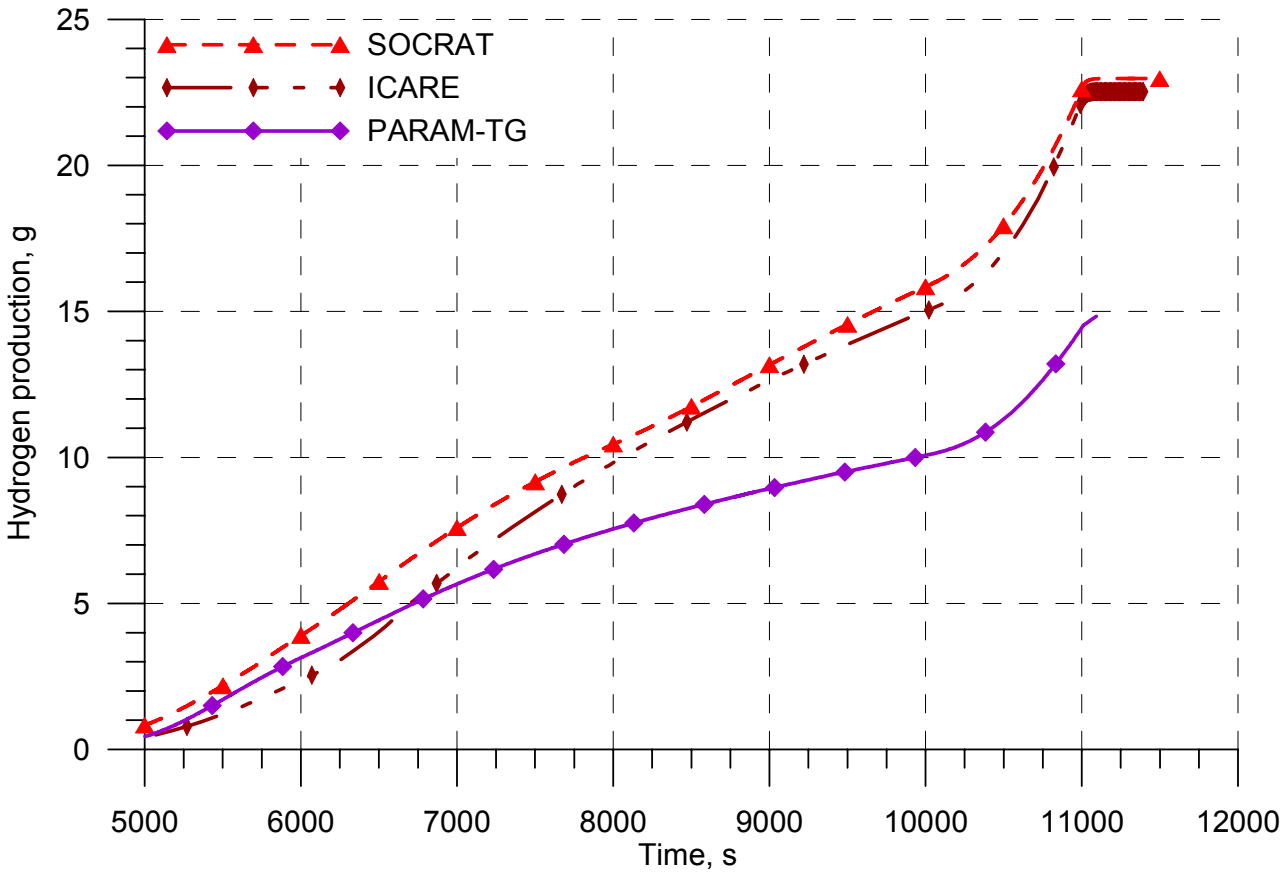

Figure 4.11 Total hydrogen release

4.3 The proposed scenario of the experiment

On the basis of the analysis of results of the variant calculations the scenario of experiment SF2 is proposed (see Table 4.2). Temperature of the steam-gas mixture injected in the test section is shown in Fig. 4.12, the flow rate of steam and argon – in Fig. 4.13, pressure in the assembly – in Fig. 4.14, the electric power supply mode - in Fig.4.15.

Table 4.2 Scenario of the experiment

No.	Stage	Main parameters			
		FA temperature, K	Medium	Heating rate	Time, s
1	FA heating-up with argon flow	~300-350	Argon flow at temperature to 670K (argon flow rate - 2 g/s)	-	0-1000
2	Joule heating of FA in the flow of steam-argon mixture	~770	Steam-argon mixture (argon/steam flow rate - 2/3,3 g/s, at temperature of 670/770K)	-	1000-4000
3	FA heating to 1200°C	~ 770→1470	Steam-argon mixture (argon/steam flow rate - 2/3,3 g/s, at temperature of 670/770K)	0,3 K/s	4000-6000
4	FA pre-oxidation	~ 1473	Steam-argon mixture (argon/steam flow rate - 2/3,3 g/s, at temperature of 670/770K)	-	6000-10000
5	Assembly heating-up to maximum temperature (transient phase)	1470→1770	Steam-argon mixture (argon/steam flow rate - 2/3 g/s)	0,3 K/s	10000-11000
6	Assembly top flooding (when FA reaches Tmax=1770 K)	To complete assembly cooling	Water (flow rate 40 g/s, water temperature ~ 330K)	-	~150 (duration)
7	Assembly bottom flooding (in 50 s after the beginning of the top flooding or when FA cooling down below 900 K at the 1250 mm elevation)	To complete assembly cooling	Water (flow rate 100 g/s, water temperature ~ 330K)	-	~100 (duration)

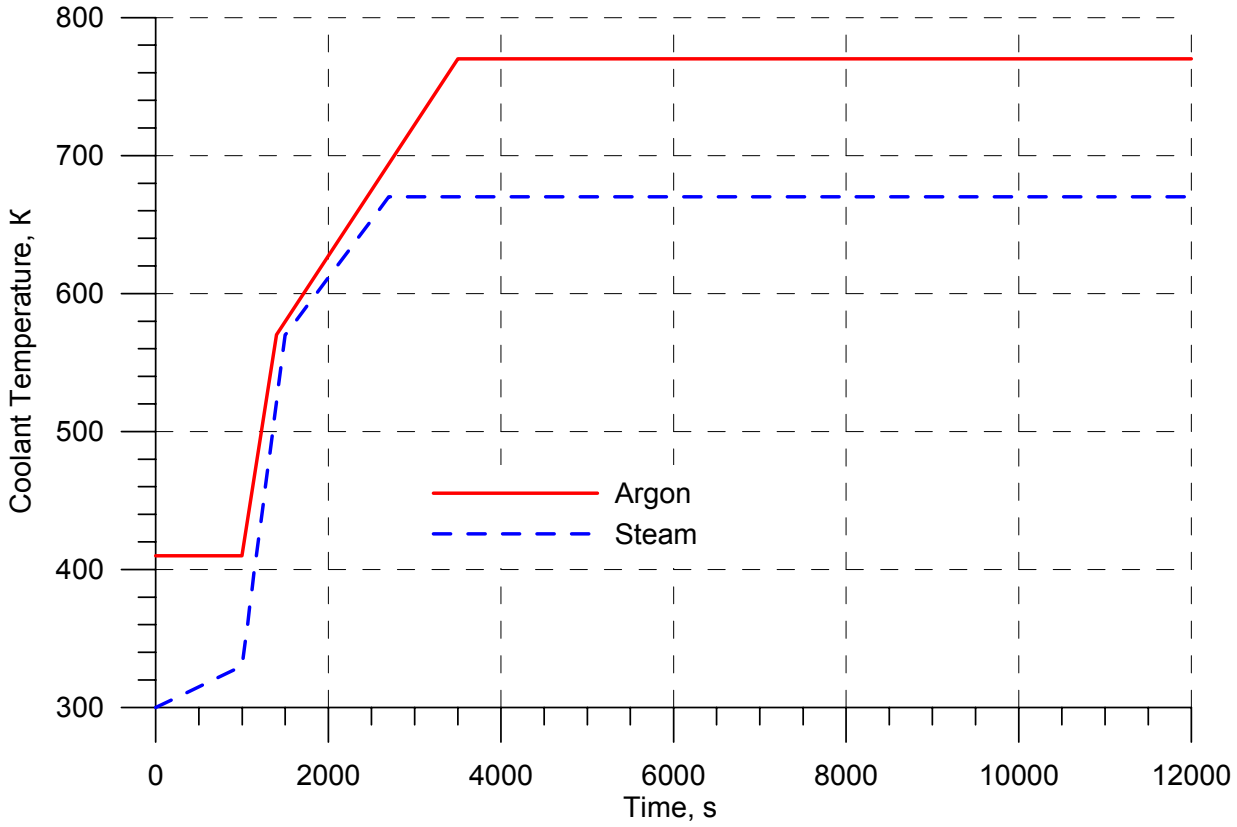

Figure 4.12 Steam-gas mixture temperature

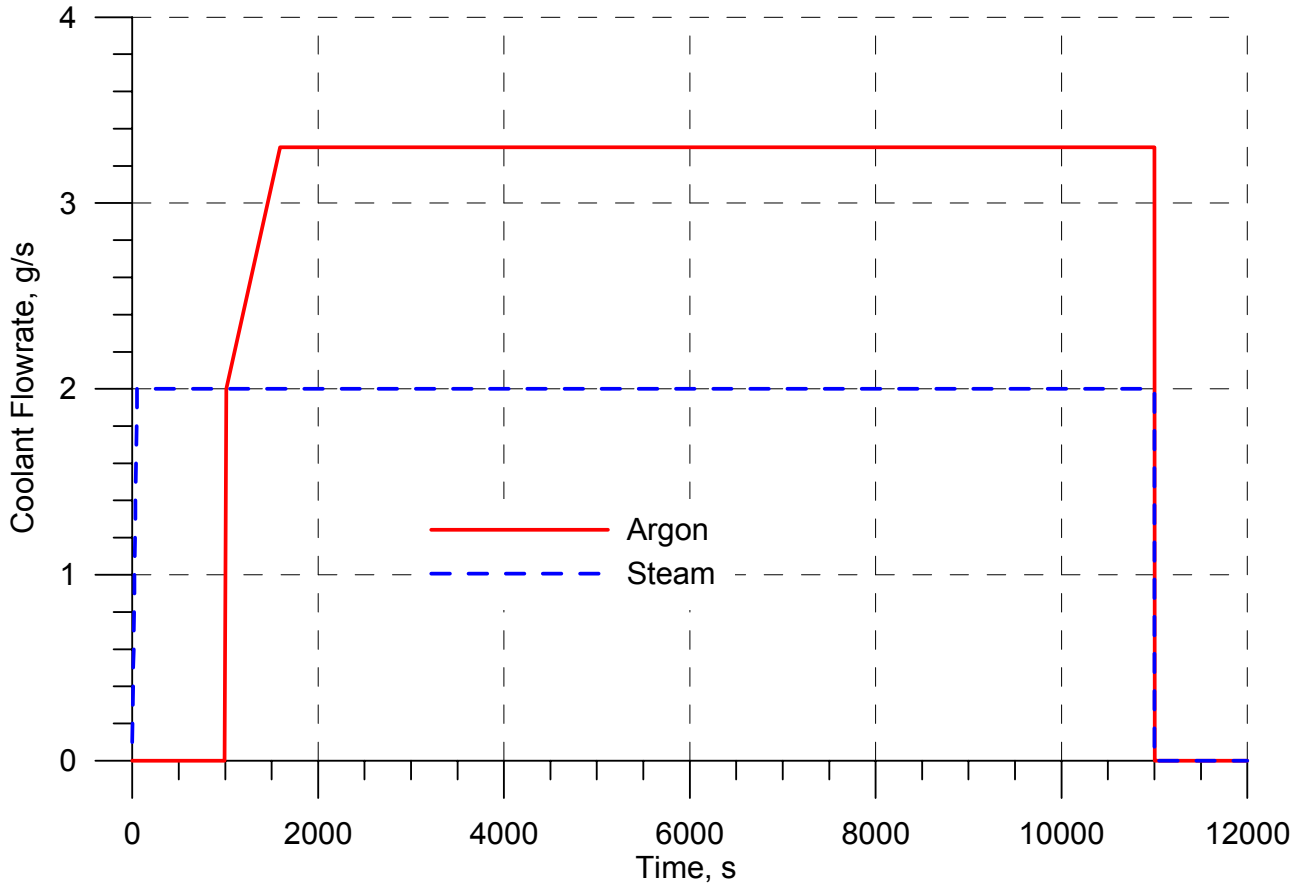

Figure 4.13 Steam and argon flow rate

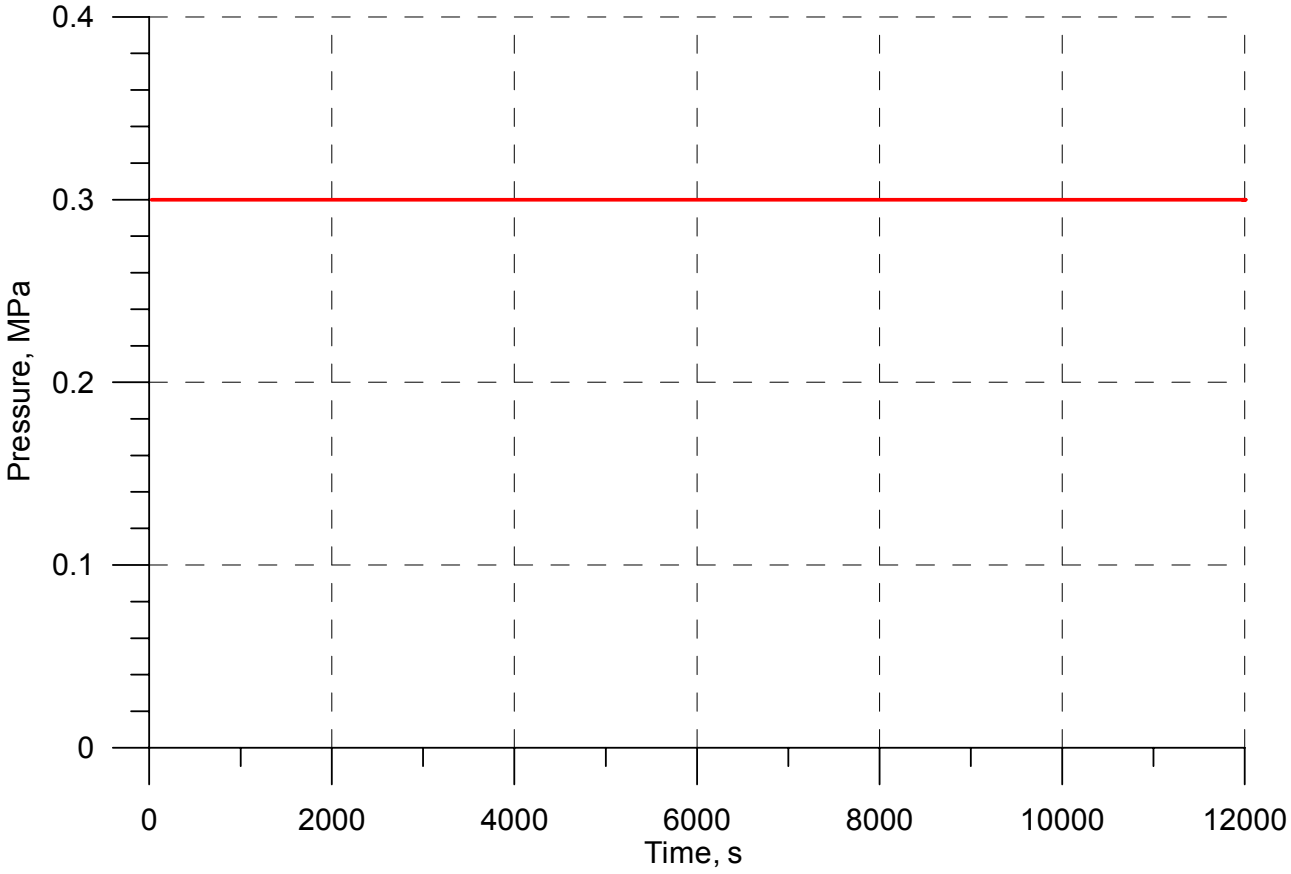

Figure 4.14 Pressure in the assembly

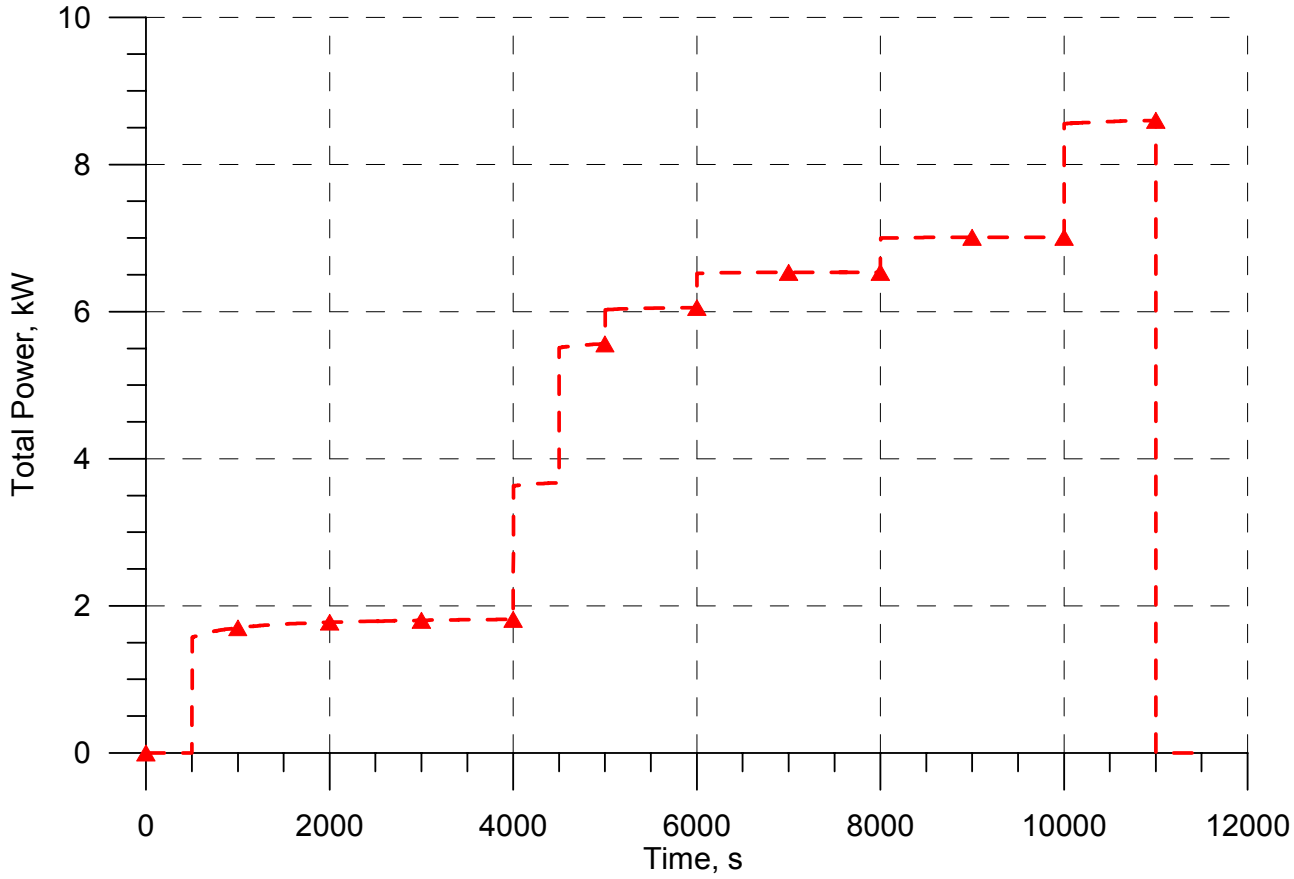

Figure 4.15 Electric power supply mode

Conclusion

On the whole in the course of performing the pre-test and post-test calculations of the SF1 experiment by various computer codes the qualitative and quantitative agreement between the calculated and experimental data on temperature, oxide layers distribution, dissolution of uranium dioxide was obtained, .

A number of calculations was performed for sensitivities evaluation (insulation heat conductivity, bypassing, cladding temperatures at the elevation where no reliable indications of thermocouples are available, etc). Through modelling by SOCRAT code was performed including the top flooding phase:

- heating-up the fuel rod simulators in the flow of argon and steam-gas mixture by Joule heating power;
- steam condensation on the test section body;
- convective and radiative heat transfer between coolant, fuel rod simulators and shroud, heat transfer by heat conduction from the shroud to thermal insulation;
- bypassing;
- wetting of thermal insulation;
- oxidation of fuel rods and shroud;
- zirconium melting;
- fuel dissolution with the melt;
- dissolution of oxide films;
- limitation of the cooling water entering during top flooding due to counter steam flow (flooding);
- melt relocation;
- melt oxidation;
- solidification of the melt, formation of blockage.

The evaluation of a contribution of various physical processes in heat balance and their influence on bundle heating up/cooling was made by various computer codes.

In spite of the uncertainty in experimental data typical for such high-temperature experiments (decrease of coolant flow rate through the assembly under the conditions of damage of fuel rods and the surrounding structures; damage of the shroud and thermal insulation, failures of thermocouples at high temperatures) the set of experimental data was reproduced numerically.

By SOCRAT code it was also possible qualitatively describe the flooding phase. The calculation shows that from 20 kg of water injected into the test section during flooding about 3 kg is ejected with the counter steam flow into the condenser through the sleeve for outlet of steam-gas mixture. It should be noted that there is a good agreement on steam and water mass ejected into the condenser. The appropriate calculation of the injected water distribution allowed obtaining the satisfactory agreement on time and the rate of the assembly cooling.

So, the qualitative and quantitative agreement of calculated and experimental data on many consisted processes and phenomena confirms the reliability of the SF1 experimental data and allows applying them for verification of the computer codes.

Pre-test calculations of the SF2 experiment by SOCRAT, ICARE, PARAM-TG codes show that maximum temperatures in the assembly should be expected at 1250 mm elevation (see Fig. 4.5). Thickness of the oxide layer on the fuel rod claddings at the elevation of 1200 mm is 150 μm at the end of the pre-oxidization phase and about 250 μm at the end of the experiment.

By numerical analysis using SOCRAT code it was shown that the scheme of the combined flooding with a delay of bottom flooding of ~50 s allows obtaining acceptable experimental data. As well it was recommended to start the bottom flooding after the top flooding water will arrive to the 1250 mm elevation (the position of upper spacer grid) and when the fuel rod claddings will be cooled down to the temperature of 900K or below. With this, the average rate of steam generation under the combined flooding is expected to be ~14 g/s, and the total steam mass ~2450 g. Pre-test analysis predicts the total hydrogen mass of 23 g, from which 3 g is released during the flooding phase.

References

[1] Estelle Brunet-Thibault, Serge Marguet. «Top Flooding Modeling with MAAP4 Code», Proceedings of the International Conference Nuclear Energy for New Europe 2006, Portoroz, Slovenia, September 18-21, 2006.

[2] W.Erdmann. «Short information on the results of calculations with ATHLET-CD», Technical Note, ERD-TN-01/06-RS 1155, revised version, May 2006.

[3] Воронова О.А., Гатилова Р.Я., Ивченко Т.Г., Самигулин М.С. «Программа РАТЕГ для численного моделирования нестационарной термогидравлики ядерных реакторов», 4-ая Ежегодная Научно-Техническая Конференция Ядерного Общества "Ядерная энергия и безопасность человека", Нижний Новгород, 28.06-2.07, 1993. Рефераты конференции. ч.2, 719-721.

[4] Воронова О.А., Гатилова Р.Я., Ивченко Т.Г., Самигулин М.С. «Программа РАТЕГ для численного моделирования нестационарной термогидравлики сетей с двухфазным теплоносителем. Математическая модель и метод численного решения», Вопросы атомной науки и техники, сер. Математическое моделирование физических процессов. 1994, вып. 4.

[5] A.M. Volchek, A.E.Kisselev, M.S.Veshchunov, «Modelling of the Pellet/Cladding/Steam Interactions in the framework of the Oxygen Diffusion Theory (T<2273 K)», Preprint NSI-SAAR-03-94, Moscow, 1994.

[6] A.V.Palagin. «SVECHA Project Candling Model: Description of Melt Relocation During Core Degradation», Proceedings of the 31-th National Heat Transfer Conference, Severe Accidents Fundamentals Session, Houston, USA, Vol.1, 1996.

[7] Allison C.M. et al. «RELAP5/MOD3 Code Manual. Volume 1: Code Structure, System Models, and Solution Methods», NUREG/GR-5535, 1995.

[8] R.O.Goountt, R.K.Cole, S.A. Hodge, et al. MELCOR Computer Code Manuals, Version 1.8.5, NUREG/CR-6119, Sandia National Laboratories, Albuquerque, NM, 1998

[9] Gonzalez R., Chatelard P. and Jacq F. ICARE2: «A computer program for severe core damage analysis in LWRs», Note Technique SEMAR 93/33, IPSN, France, May 1993. -1993.

[10] Yu.K.Bibilashvily, N.B.Sokolov, L.N.Andreyeva-Andrievskaya, A.V.Salatov, A.M.Morozov. «High-temperature Interaction of Fuel Rod Cladding Material (Zrl%Nb alloy) with Oxygen-containing Mediums», Proceedings of IAEA Technical Committee on Behaviour of LWR Core Materials under Accident Conditions, held in Dimitrovgrad, Russia, on 9-13 October 1995. IAEA-TECDOC-92 I.Vienna, 1996, pp.117-128.